PhD Thesis

INCREASING THE RESOLUTION AT THE NANOBIOINTERFACE WITH ENGINEERING INORGANIC NANOPARTICLES

Memoria presentada por **Sofía Rubio Ponce**
Para optar al grado de
Doctor por la Universidad Autónoma de Barcelona, UAB.
Programa de Estudios de Doctorado en Bioquímica, Biología Molecular y Biomedicina.

Tesis realizada bajo la dirección del Profesor Víctor Franco Puntes del Grupo de Nanopartículas Inorgánicas del Instituto Catalán de Nanociencia y Nanotecnología (ICN2), y con la tutoría de la Dra. Ester Boix Borràs del Departamento de Bioquímica y Biología Molecular de la Facultad de Ciencias de la Universidad Autónoma de Barcelona (UAB).

Departamento de Bioquímica y Biología Molecular.
Facultad de Ciencias en la Universidad Autónoma de Barcelona (UAB).

Cerdanyola del Vallès, Julio 2016

Prof. Víctor F. Puntes

Sofía Rubio Ponce

CHAPTER 3: DESIGN

The importance of mixing sequence on NPs conjugation

3.1. Introduction

The supreme importance of nanoparticle functionalization, without it there will be no control of nanoparticle colloidal stability and there would be no possibility to use NPs in the myriad of proposed applications. In recent years, nanoparticles have been conjugated to all imaginable molecules of interest: drugs, catalysts, biomolecules, proteins, antibodies, fluorophores, sugars, detergents, etc with a poor conformational control what is fundamental in biointerations.

It is know that colloidal systems are out of equilibrium. Nanoparticle surfaces have a very high surface energy to dissipate, in a highly degenerated energy states landscape leading to unprecedented versatility, plasticity and, concomitantly, lack of reproducibility. Therefore, precise and careful design is needed. The system is so high in energy that functionalization is mainly based on the simple incubation of the nanoparticle with the targeting molecule. Note that studies of this phenomenon with particular molecules, as serum proteins, have created a whole field of research around the Protein Corona (PC) formation[1-3].

Changes in the NP-Biomolecule organization is supremely important[4, 5] since they will determine the nature of the conjugates and their maintenance and stability in media. The conformation of molecules onto AuNPs will be critical in vitro as well as in vivo assays and will compromise the biodistribution of the NPs and their interaction with the body[6-8].

It has been observed that changes on the conformation of macromolecules as PEG[9-11] or the degree of ordering of the peptide sequences, may change dramatically the immune response towards nanoparticles from tolerance to anaphylaxis.

Here we want to know how far different conformations and arrangements may affect nanoparticle behavior. As a model, we choose 11-mercaptoundecanoic acid (MUA) to

cap gold nanoparticles (AuNPs). Alkanethiolates, such as MUA, have been largely used to obtain Self-Assembled Monolayers (SAM) onto gold surfaces[12]. The ability to organize SAM onto the NP surfaces is due to the presence of a thiol group and a hydrophobic chain in the MUA molecule structures which allow a very compact packing of the layer. Thiol-gold (SH-Au) bond is the most widely exploited due to its pseudo-covalent character (≈45 Kcal/mol)[13]. This high bond strength allows the exchange with other ligands which bind gold more weakly such as citrate, amines, or phosphates. In addition, the high strength makes the bond very stable over the time. Thus, the use of thiolated molecules is a common strategy to functionalize AuNPs allowing us to unveil all the metastability of the conjugation process.

Interestingly, if we repeat the conjugation many times we observe differences in the basic characterization of the conjugates. Due to the lack of reproducibility, the kinetics of the conjugation procedure was in the point of interest to be explored. Until now, conjugation was considered as a simple, fast and univocal process. The way in which kinetics conditions were changed was maintaining the formulation of the conjugation procedure but changing the order of addition of components.

In this chapter we perform a very simple study of the formation of gold nanoparticle-MUA (AuNP-MUA) conjugates by inverting the addition of the two conjugating moieties. Despite having the same composition and to give similar responses to analytical characterization, when we challenge the two different obtained conjugates in different situations we clearly observe different behavior. This allows us to determine a lower energy conjugation state and to design an optimal mixing strategy for obtaining highly stable and reproducible nanoparticle conjugates. We also extend this study to Protein Corona (PC) formation onto functionalized inorganic nanoparticles.

The first evidence about the nature of the conjugation process is irreproducibility. As we could not really discriminate between different conjugation states with the standard characterization we submited the MUA-conjugated AuNPs to a serie of challenges to study their dynamic responses. It is well known that the response to a stimulus allows to better study intrinsic differences than static measurements. The

derivative of a function measures the sensitivity to change of a quantity determined by another quantity.

The first challenge is colloidal stability. Electrostatic stabilization is based on the adsorption of ions to the surface of NPs creating an electrical double layer which results in a Coulombic repulsion force between individual particles. The general mechanism for stabilization of colloidal materials in water has been described in the Derjaguin-Landau-Verwey-Overbeek (DLVO) theory, which combines the effects of van der Waals attraction and electrostatic repulsion due to the so called double layer of counterions[14, 15]. This electrical double layer can be altered while exposing the conjugates to a media of high ionic strength that can induce the compression of the layer and the subsequent aggregation of the NPs[16].

The SAM of MUA onto the AuNP surface is deprotonated at the working pH (pH=7, pKa_{MUA}=4.8). The electrostatic stability mechanism of the conjugates was evaluated by studing the aggregation of MUA-conjugated AuNPs over a range of ionic strengths (by NaCl addition) [17]. The conformation of MUA molecules onto the AuNPs surface will be critical in avoiding aggregation of conjugates, which is a key point not only for in vitro applications but also for in vivo ones, since effective size strongly influences the way in which organisms deal with nanosystems[11].

The stabilitity of MUA-conjugated AuNPs was further evaluated by the exposure of conjugates to Sodium Cyanide (NaCN) digestion[18]. Cyanide groups are able to dissolve the AuNPs, so then conjugates can be studied by their ligand´s ability to protect the NPs against NaCN digestion. Additional information about the conformation states of conjugates, such as density and packing of the capping SAM, could be determined by the MUA molecules's ability to shield the inorganic core against strongly etching CN^- anions[19, 20]. These CN^- anions come into contact with the inorganic core, progressively etching the nanoparticle surface and creating complexes with the gold atoms. This converts the reddish AuNPs sample into a colorless solution of $Au(CN)^{2-}$ ions. Special care has to be taken when working with cyanide to avoid its transformation into hydrogen cyanide gas (HCN) if lowering the pH[21].

Finally, complex physiological environments, such as complete cell culture medium, contain a large amount and variety of molecules. Nanoparticles (NPs) are sensitive to these biological fluids and can suffer alterations such as the rapid absorption of proteins onto their inorganic surface generating the Protein Corona (PC) formation onto the nanoparticles[1, 3, 6].

Pioneered by Leo Vroman back in 1962 [15] and revised later by other authors [14], it has been established that the adsorption of proteins to inorganic surfaces follows the so-called "Vroman Effect": the highest mobility proteins arrive first and are later replaced by less motile proteins that have a higher affinity for the surface.

Nowadays, scientific literature shows an increasing awareness of the importance of this spontaneous coating process when takes place onto nanoparticles[22]. Natural albuminization is on the basis of the research in the improvement of the biocompatibility of some nanomaterials. Protein Corona could render the nanoparticles less toxic and improve their biocompatibility and solubility [6].

The proteins that build the Protein Corona in a spontaneous coating, confer a biological identity to the composite NP-PC that would critically determine their biodistribution and further reactivity inside living systems (affecting immunological and biological responses). In this context, the surface coating in the case of study: sodium citrate and negatively charged mercaptoundecanoic acid gold nanoparticles, resulted into different developments of stable coronas[23].

We hypothesize that there are important kinetic considerations in the bioconjugation procedure, where degenerated states could favor the conformation of conjugates. Therefore results will depend on initial very short times. However, it has been observed the time evolution of conjugates exposed to protein resulting in bioconjugates that would present a different nature.

3.2. Synthesis of gold nanoparticles

EXPERIMENTAL SECTION

All chemicals used were of highest available purity, and were supplied by Sigma-Aldrich. The Millipore water had a resistance of 18.2 MΩcm. All reagents were prepared following the manufacturer's recommendations.

Monodisperse citrate-stabilized gold nanoparticles (Au NPs) with an uniform quasi-spherical shape of ~12 nm and a narrow size distribution were synthesized following a kinetically controlled strategy via the reduction of $HAuCl_4$ by sodium citrate[24]. A solution of 2.2mM sodium citrate in milli-Q water (150 mL) was heated with a heating mantle in a 250mL three-necked round-bottomed flask for 15 min under vigorous stirring. A condenser was utilized to prevent the evaporation of the solvent. After boiling had commenced, 1 mL of $HAuCl_4$ (25 mM) was injected. The color of the solution changed from yellow to bluish gray and then to red in 10 min. The resulting particles (~12 nm, ~$3 \cdot 10^{12}$ NPs/mL) are coated with negatively charged citrate ions and hence are well suspended in H_2O.

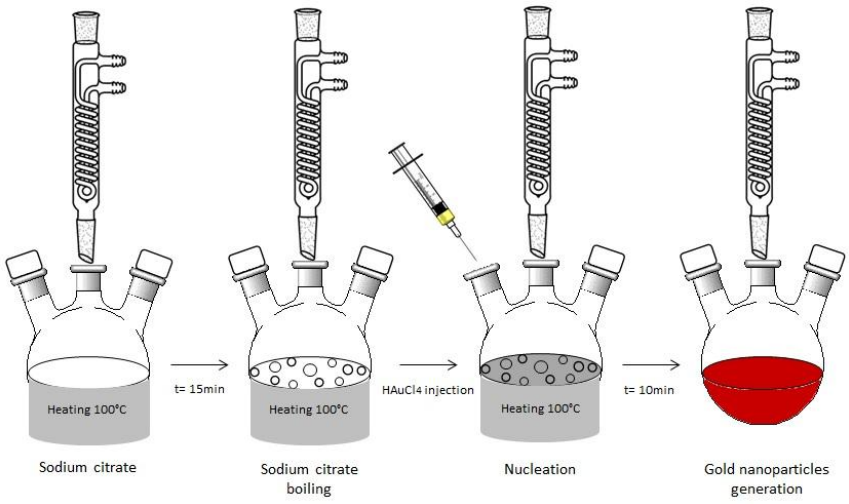

Figure 3.1.: Escheme of the gold nanoparticles synthesis procedure. Sodium citrate solution is heated for 15min, time in which the solution starts to boil. Subsequently, $HAuCl_4$ gold precursor is injected to the boiling solution. A change of colour in the boiling solution is experienced varying from transparent to yellow and immediately to dark grey colour indicating that nucleation of gold nanoparticles is taking place. The solution is maintained under heating for 10min until it reaches the characteristic red colour of gold nanoparticles solution. All the process takes place under stirring conditions.

RESULTS AND DISCUSSION

Gold nanoparticles (~12 nm) were synthesized based on the reversed classical Turkevitch method (Figure 3.1.) where $HAuCl_4$ gold precursor was injected into a boiling 2.2mM sodium citrate aqueous solution. Through this method, a well size controlled gold nanoparticles solution can be achieved with a high monodispersity. Gold nanoparticles synthesized can be analysed by Transmission Electron Microscope (TEM) to determine the real size of the particles and the monodispersity of the sample (Figure 3.2.).

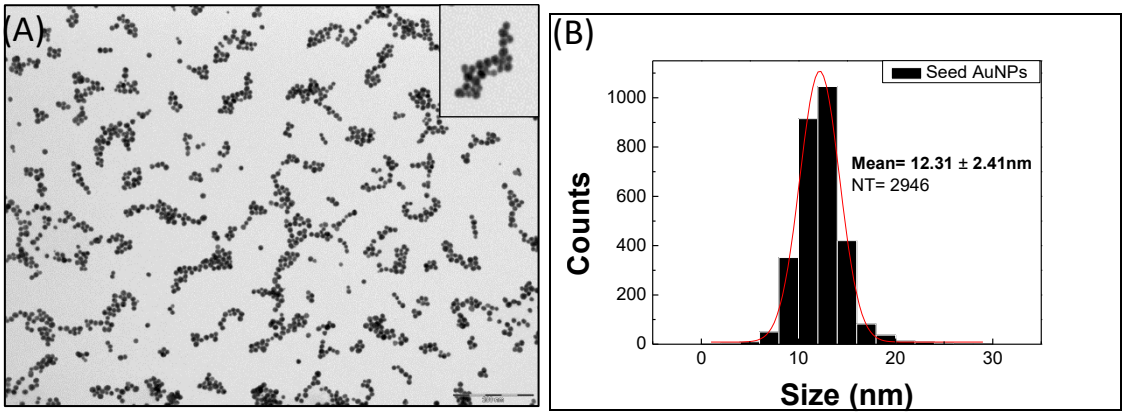

Figure 3.2.: Transmission electron microscopy (TEM) images (A) and Size distribution (B) of monodispersed citrate-stabilized ~12 nm Au NPs prepared by the sodium citrate reduction of hydrogen tetrachloroaurate. The colloid ($3 \cdot 10^{12}$ NP/mL) was dropcasted onto a Formvar carbon-coated copper grid for microscopy observation. The bar in TEM image indicates 200nm.

3.3. Conjugation of gold nanoparticles

EXPERIMENTAL SECTION

Once gold nanoparticles are synthesized, a process of conjugation between gold nanoparticles solution and an aqueous solution of 11-Mercaptoundecanoic acid 98% (MUA) molecules was carried out.

The conjugation process was performed by mixing through the two procedures, the gold nanoparticles with an excess of MUA up to 10 times the theoretical value ($3 \cdot 10^{12}$ NP/mL; 0.21 nm^2 Au NP surface/molecule), leads to a final 0.1mM molecule concentration of the MUA molecule in an aqueous solution for 1 hour to ensure rapid and full coverage (Figure 3.5.). Previous studies[(22)] showed that in these conditions conjugation of thiolated molecules to AuNPs takes place in few minutes.

Exploring conjugation methods

For this purpose, two different methods of conjugation have been explored:

The first one, called Low Pressure (LP) understanding that concentration translates into a *pressure* or collision rate in the process of conjugation, in which 2 mL of an aqueous solution of MUA (0.35mM) was added dropwise to 5 mL of gold nanoparticle solution ($\sim 3 \cdot 10^{12}$ NPs/mL). The second one, called High Pressure (HP), in which the order of admixture in the conjugation procedure was inverted. So then the process followed the drop by drop addition of 5 mL of gold nanoparticle solution ($\sim 3 \cdot 10^{12}$ NPs/mL) onto the 2 mL of the aqueous solution of MUA (0.35mM).

The final formulation of the two different aliquots was exactly the same, but the mixing way was different. In one case, drops of AuNPs enter into a saturated (regarding AuNP available surface) MUA solution and in the other case, AuNPs surfaces compete to absorb the incoming molecules. It is important to note that NP surface are high in energy and tend to agglomerate or absorb molecules from the environment.

The final concentration of MUA in each gold nanoparticle solution was 0.1mM. Both methods of conjugation were stirred for 1 hour at room temperature (Figure 3.5.).

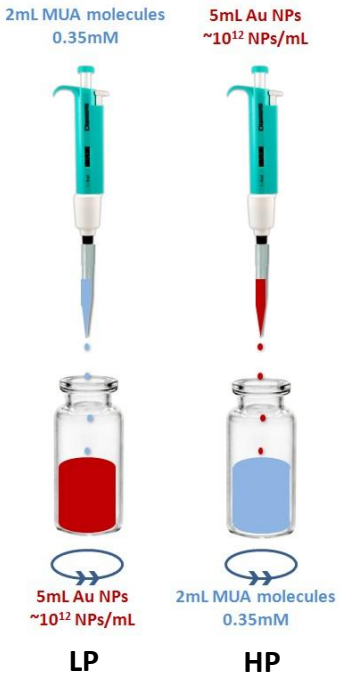

Scheme of Conjugation methods of Au NPs with MUA molecules. Both types of Low Pressure (LP) and High Pressure (HP) methods used for the generation of MUA-conjugated gold nanoparticles are shown. Graph is not drawn at scale.

RESULTS AND DISCUSSION

Gold nanoaparticles (Au NPs) are stabilized by sodium citrate ions that are coating the nanoparticle surface. These ions can be replaced by MUA molecules that can strongly bind to the nanoparticle surface through a pseudo-covalent bond. This binding between gold nanoparticles and MUA molecules is possible due to the thiol terminal group that MUA molecules present in their structure (Figure 3.3.). Consequently, the conjugation procedure of gold nanoparticles with an excess of MUA molecules can be simply carried out (Figure 3.4.) by mixing both solutions.

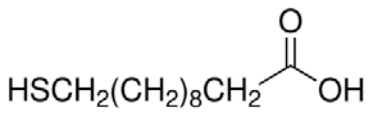

Figure 3.3.: Structure of MUA molecule. The molecule contains a terminal thiol group that will make possible the conjugation procedure with gold nanoparticles.

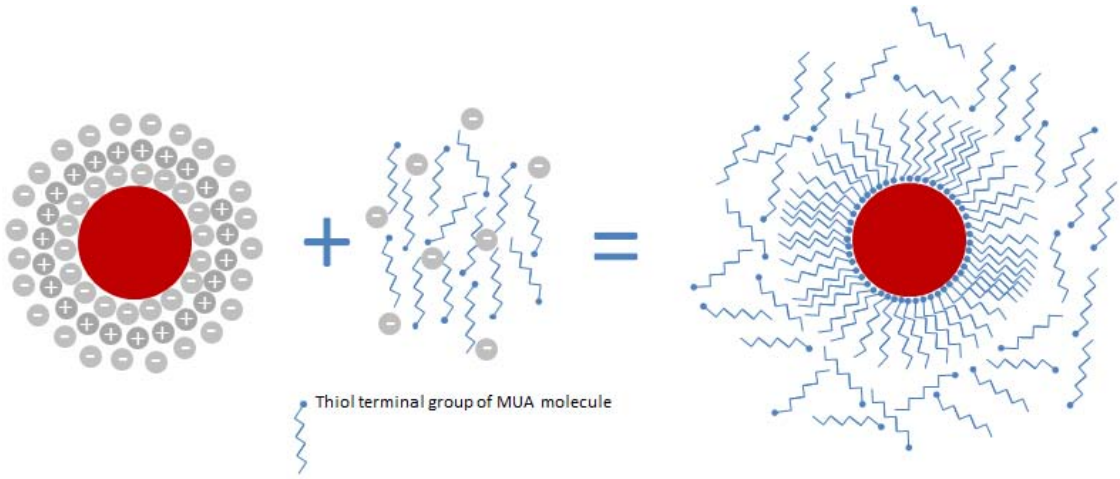

Figure 3.4.: Conjugation procedure of MUA molecule onto gold nanoparticles.

The selected nomenclature of Low Presusre (LP) and High Presusre (HP) corresponds to the expected environment that gold nanoparticles could find in the encounter with MUA molecule solution. At short time, the [MUA]/[Au][(25)] can be much higher or much smaller than 1 depending in the order of mixing (A+B or B+A). This is when the conjugation is done drop by drop. Besides, rapid conjugation produced similar results but higher variability.

We hypothesize that at LP, when MUA is added on top of AuNPs solution, there is more time for Self Assembled Monolayer (SAM) to form. Whereas, at HP a caotic formation of SAM would be expected.

In the case of HP method, the process of conjugation is thought to generate a *high pressure* system in which the gold nanoparticle solution is added drop by drop to the aqueous solution of MUA molecules. Therefore, each drop of gold nanoparticle solution will be exposed to a higher concentration of MUA molecules than in the case of adding the MUA on the top of the nanoparticles. Hence, this process of conjugation is considered *low pressure*.

Thus, in the LP method a large number of NPs have to share the slow coming MUA molecules. While in the HP method, the entering AuNPs encounter an overwhelming excess of MUA molecules.

Techniques

UV-Visible spectra were acquired with a Shimadzu UV-2400 spectrophotometer, recording UV-Visible absorption spectra in the wavelength range of 300-800 nm. Dynamic light scattering (DLS) measures were made with a Malvern ZetaSizer Nano ZS instrument operating at a light source wavelength of 532 nm and a fixed scattering angle of 173°. ζ-Potential was determined using a Malvern ZetaSizer analyzer.

Static Characterization

Nanobioconjugates were characterized immediately after conjugation, considering this point time as the so-called time zero. After 1 hour of conjugation, it is assumed that the complete conjugation process of gold nanoparticles with MUA molecules was completely finished[(22)].

As it is shown in Figure 3.5., the SPR band position of MUA-conjugated gold nanoparticles during the process of conjugation can be analyzed. This characterization through the absorbance spectrum provides information about how the conjugation process is being developed and enables to determine the time at which the conjugation is completely finished.

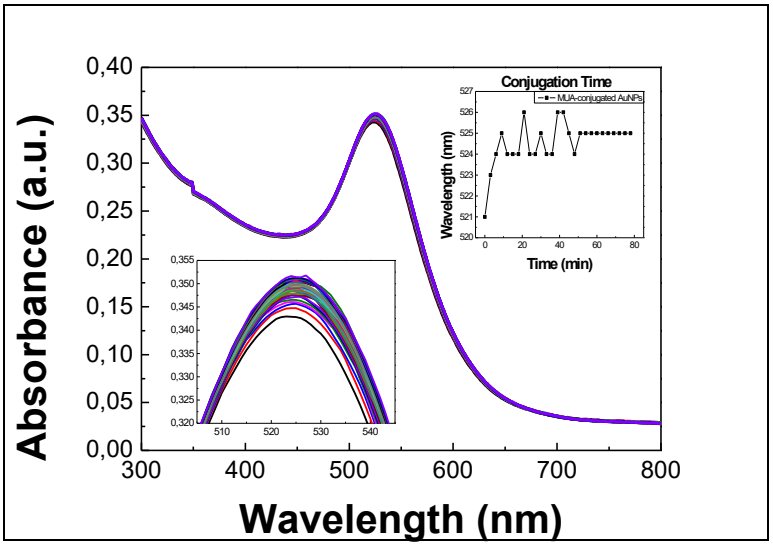

Figure 3.5.: Time of conjugation analysis through monitoring the peak position (nm) of the SPR band of conjugates along the time. Conjugation procedure seems to be completed at 48 min were the peak position maintains stable along the time. As a consequence, the conjugation time were fixed at 1 hour to ensure that the conjugation process is completed.

Citrate-stabilized gold nanoparticles are stable in aqueous media and display the characteristic UV-Vis absorption spectrum with a plasmon band at 520.5 nm. The absorption spectrum is sensitive to the nanoparticle environment and an observable red-shift of the surface plasmon resonance (SPR) band of about 4 nm appears once MUA molecules are attached (Figure 3.6. - A). The shift occurs within a few minutes, suggesting that the conjugation process is quick (as it is shown in Figure 3.5.).

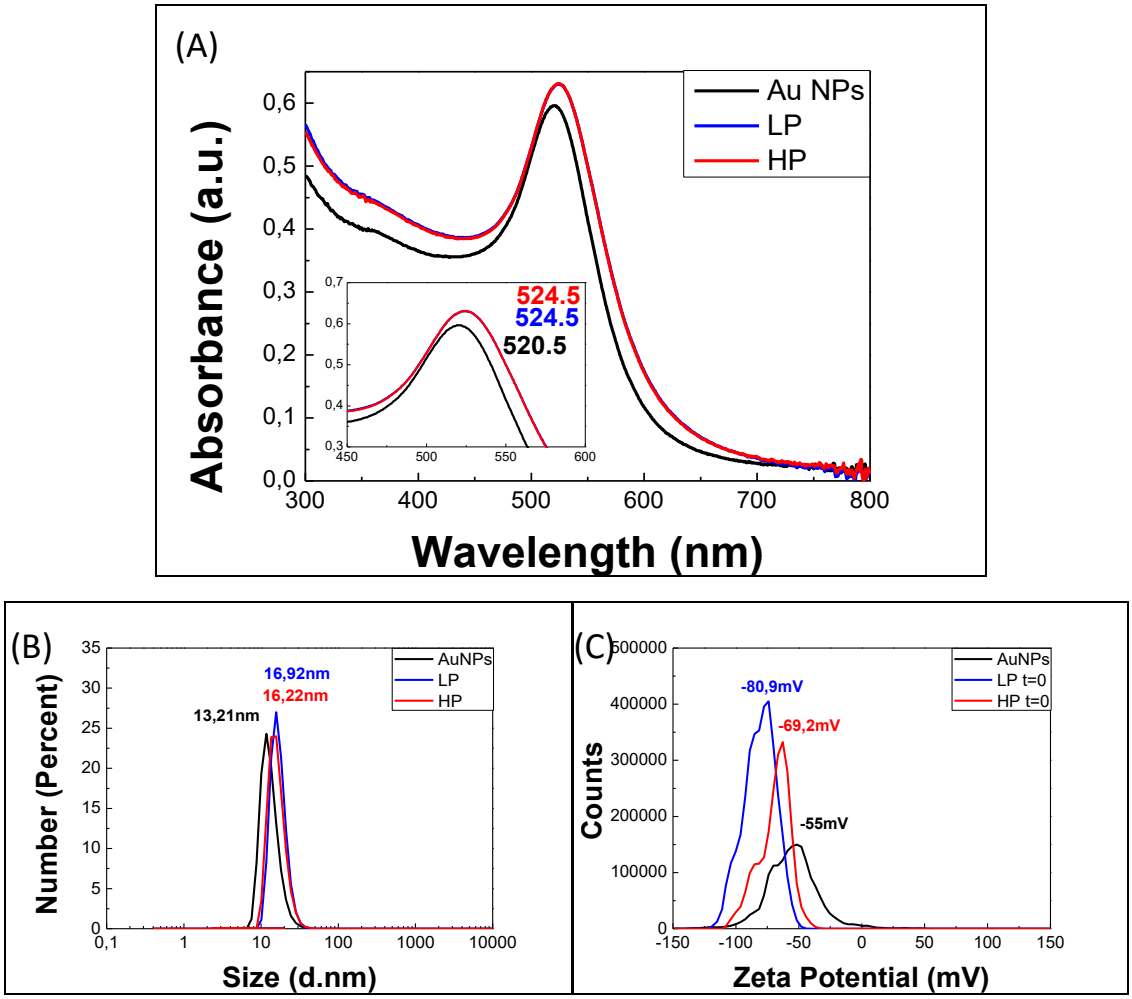

Figure 3.6.: (A) UV-Vis spectra characterization of MUA-conjugated gold nanoparticles. The red-shift in the position of the SPR band of 4nm in both types of conjugates. **(B) DLS and (C) ζ-Potential characterization of MUA-conjugated Au NPs**. **(B)** The increase in the hydrodynamic radius from 13.21nm to 16.92nm and 16.22nm in the case of LP and HP conjugates respectively; and **(C)** the increase of charge intensity of MUA-conjugated Au NPs from -55mV to -80.9mV and -69.2mV (LP and HP conjugates respectively).

However, although the UV-Vis spectra characterization (Figure 3.6. -A) was able to detect changes in the gold nanoparticle absorption before and after conjugation with MUA molecules, the absorbance spectrum were not sensitive enough to distinguish between the different methods of gold nanoparticles conjugation. The peak position of both MUA-conjugated gold nanoparticles, LP and HP types, was localized at the exact same position: 524.5nm.

The conjugation process was also followed by dynamic light scattering (DLS) where a clear increase in hydrodynamic size around 3nm of the Au NPs occurred at time zero after conjugation: From 13.21nm (non-conjugated Au NPs) to 16.92nm and 16.22 nm (in the case of MUA-conjugated Au NPs LP type and HP type, respectively) as it is shown in Figure 3.6. - B. Even though conjugates seem to be slightly different on size by DLS, the change is not very significant considering the DLS low accuracy.

Simultaneously, the surface charge assessed by ζ-Potential measurements confirms the conjugation process to be successful (Figure 3.6. - C). The ζ-Potential values increase in surface charge intensity once deprotonated MUA molecules are conjugated onto gold nanoparticles surface.

In detail, significant variations are observed in the two conjugation procedures: A change from -55mV (non-conjugated Au NPs) to -80.9mV in the case of MUA-conjugated Au NPs LP type; and a change from -55mV to -69.2 mV in the case of MUA-conjugated Au NPs HP type.

Contrary to UV-Vis spectra characterization, ζ-Potential measurements show differences between both types of conjugates LP and HP types. In particular, MUA-conjugated Au NPs of LP type at time zero present higher increase in surface charge intensity (around 25mV) than MUA-conjugated Au NPs of HP type (around 15mV). Note that the organization of charges around a nanoparticle is very sensitive to local molecular arrangements. It can be correlated to hydrodynamic radius when thiol groups binding to gold surfaces.

Curiously, despite through UV-Vis and DLS characterizations was difficult to distinguish different types of MUA-conjugated Au NPs (LP and HP) at time zero, ζ-Potential

characterization suggests that LP and HP MUA-conjugated Au NPs are two different objects despite having the same formulation.

In order to explore differences between both conjugates types, a large batch of MUA-conjugated (LP and HP) Au NPs was prepared. For this purpose, the conjugation of 20 independent replicas of MUA-conjugated Au NPs samples by LP method and 20 replicas of MUA-conjugated Au NPs samples by HP method were carried out. If there is degeneracy, this will be manifested as lack of reproducibility. Thus, we analyzed the UV-Vis spectra of all the 40 samples (Figure 3.7.).

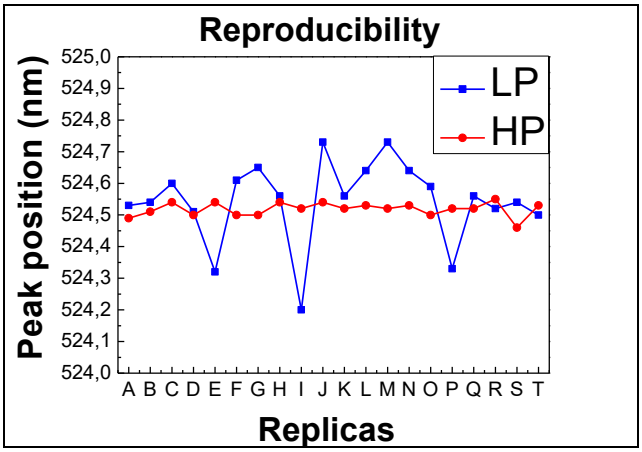

Figure 3.7.: Reproducibility of conjugation methods (LP and HP) after 20 replicas of conjugates analyzed.

A difference in the final conjugates was observed analyzing the peak position (nm) of the SPR band of each conjugated sample (from A to T) by UV-Vis spectroscopy. The conjugation procedure used in method HP results in less variability of conjugates (this method present a maximum difference of 0.09nm between peak position of conjugates) respect to the method LP (which results in conjugates that differ in 0.53nm of variation in peak position between conjugates, which corresponds to around 6 times more variability and it is considered to be significant). The method of conjugation seems to be crucial in the nature of the final conjugates.

3.4. Reactive characterization

As it is difficult to discriminate both objects, we study their response to different challenges in order to determine their nature. Thus, we look for differences in response to colloidal, chemical and biological environmental changes.

It is well known, especially at the nanoscale, that subtle morphological alterations have big impacts on performance and behavior, as the SAR paradox and paradigms in biological macromolecules (nature's nanoparticles).

EXPERIMENTAL SECTION

Colloidal Stability Characterization

Conjugates samples (1mL) were treated with Sodium Chloride (NaCl) at different concentrations (from 0 to 0.5M) testing their colloidal stability in the presence of an excess of salts. Due to the conformation of molecules onto the Au NP, conjugates are thought to show different behavior against salt solution. As a consequence of their stability against salt, different types of MUA-conjugated Au NPs (corresponding to LP and HP types of conjugates) can be characterized.[17]

Chemical Characterization

Conjugates samples were also analyzed by their resistance to Sodium Cyanide (NaCN)-induced digestion. The more dense coating should work as a better barrier. For this purpose, 1mL of MUA-conjugated Au NPs of each type of conjugates (LP and HP types) was exposed against NaCN (with a final concentration of 45mM in solution[).[18]

Biological Characterization

In order to explore the behavior of conjugates in biological conditions and the consequent Protein Corona (PC) formation, samples were exposed to complete cell cuture medium (c-CCM) consisting in 90% of Dulbecco's Modified Eagle Medium (DMEM) and 10% of Fetal Bovine Serum (FBS). For this purpose, 1mL of each sample was added to 9mL of c-CCM, followed by incubation at 37°C for 1 and 2 days.

Afterwards, samples were purified by centrifugation at 13rpm for 5 minutes and resuspension in sodium citrate (2,2mM) for further characterization by UV-Visible spectrophotometer, DLS and ζ-Potential.

RESULTS AND DISCUSSION

Colloidal Stability Characterization

In nanoparticle conjugation, the order determines the product. Changing the order of conjugation does change the product.

After the conjugation procedure took place, both types of MUA-conjugated AuNPs (LP and HP types) were studied by characterizing their colloidal stability. These are electrostatically stabilized nanoparticles, so they are subject to DVLO theory.

For the physical colloidal stability characterization, conjugates samples were treated with Sodium Chloride (NaCl) at different concentrations (from 0 to 0.5M of NaCl) proving their stability in the presence of an excess of salts. MUA confers no steric repulsion, only electrostatic repulsion. So, its negative changes can be screened or protonated. LP conjugated samples seem to be more stable against NaCl than HP conjugates at time zero (Figure 3.8.). This can be correlated with the higher charge intensity in the surface of LP MUA-conjugated Au NPs (-80.9mV) against the charge intensity of HP conjugates (-69.2mV) at time zero plotted in Figure 3.5. As higher is the charge intensity, greater is the difficulty for conjugates to lose stability.

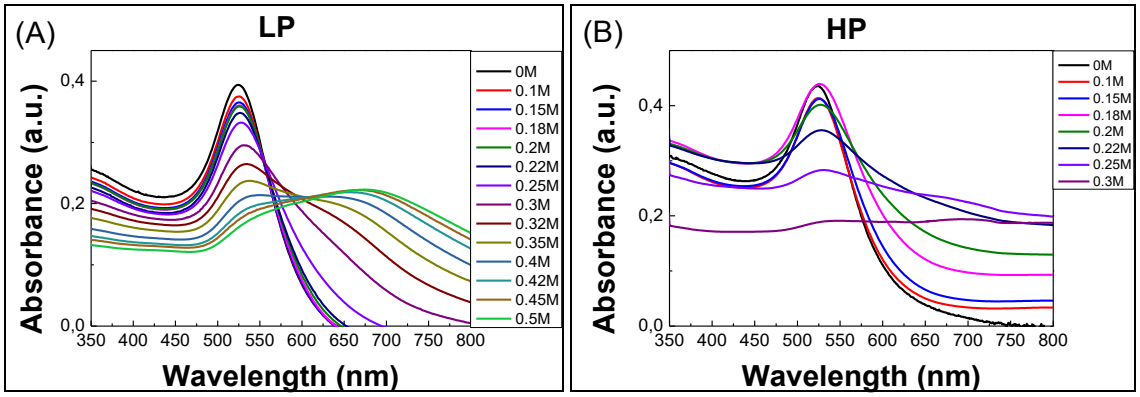

Figure 3.8.: Colloidal stability of MUA-conjugated Au NPs at time zero by UV-Vis spectra: MUA-conjugated Au NPs LP type **(A)** present higher stability against NaCl than MUA-conjugated Au NPs HP type **(B)**. The latter suffer a higher red-shift in the position of the SPR band against NaCl concentrations and experienced a loss of the SPR characteristic peak at lower values of NaCl concentrations than in the case of LP conjugates. This fact corresponds to the aggregation of the samples, so it can be said that HP conjugates type are less resistant to NaCl than LP conjugates type at time zero.

Conjugated samples were also compared to Au NPs. A lower colloidal stability against NaCl is presented in the case of non-conjugated Au NPs (Figure 3.9.) since their surface is less protected than the conjugated samples covered with MUA molecules. Au NPs were seen to be completed aggregated at values of 0.1M of NaCl where conjugates maintained their colloidal stability.

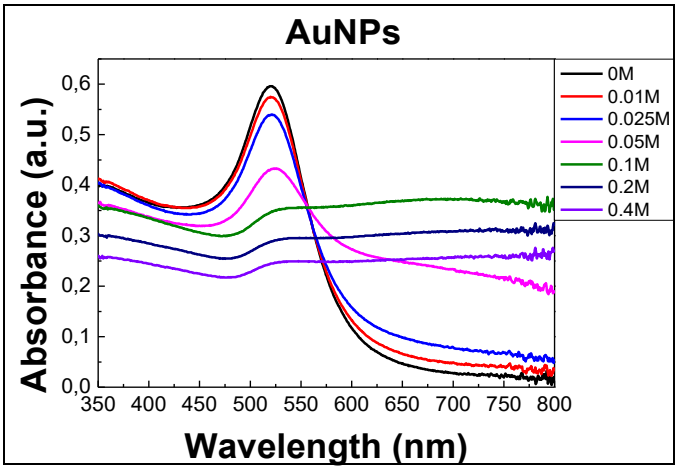

Figure 3.9.: Colloidal stability of Au NPs at time zero by UV-Vis spectroscopy. Samples were treated against different concentrations of NaCl (from 0 to 0.4M).

Chemical Characterization

Additionally, MUA-conjugated samples were chemically characterized by their resistance to Sodium Cyanide (NaCN)-induced digestion. CN^- has a strong affinity for metals and can dissolve AuNPs. A more dense coating should result in a less reactive nanoparticle' surface. The chemical reaction involved in the digestion is:

$$4Au + 8NaCN + O_2 + 2H_2O \rightarrow 4NaAu(CN)_2 + 4NaOH$$

In which NaCN can capture gold ions generating a gold-cyanide complex and reducing the gold core of the conjugated nanoparticles. Carefull has to be taken since cyanide salts are among the most rapidly acting of all known poisons.

This NaCN digestive reaction can be followed by UV-Vis spectroscopy, where a clear decrease in the absorption spectrum occurs with time. A new feature also appear in the spectrum with a well-defined peak around 240 nm (signature of $Au(CN)_2^-$ formation)[18] that become increasingly visible with time (Figure 3.10.).

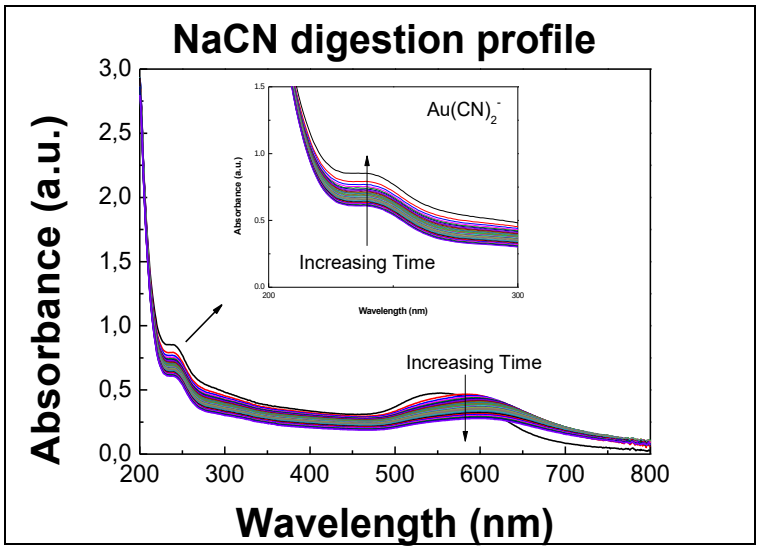

Figure 3.10.: Representative progression of the absorption spectra of MUA-conjugated Au NPs collected in the presence of Sodium Cyanide: The surface plasmon band decreases while the absorption peaks of $Au(CN)_2^-$ (expanded in the inset) increase along time; both features reflect a progressive digestion of the MUA-conjugated Au NPs'core by added NaCN. The data showed belongs to LP type of MUA-conjugates AuNPs after 7 days of conjugation in 45 mM NaCN solution over the course of 2 hours and 30 minutes.

MUA-conjugated Au NPs were exposed to 45mM of NaCN and UV-Vis spectra were collected for 2 hours and 30 minutes to determine the reaction process in each type of conjugate (LP and HP) at time zero after the conjugation (Figure 3.11.). Note that NPs digestion induces aggregation and Ostwald ripening.

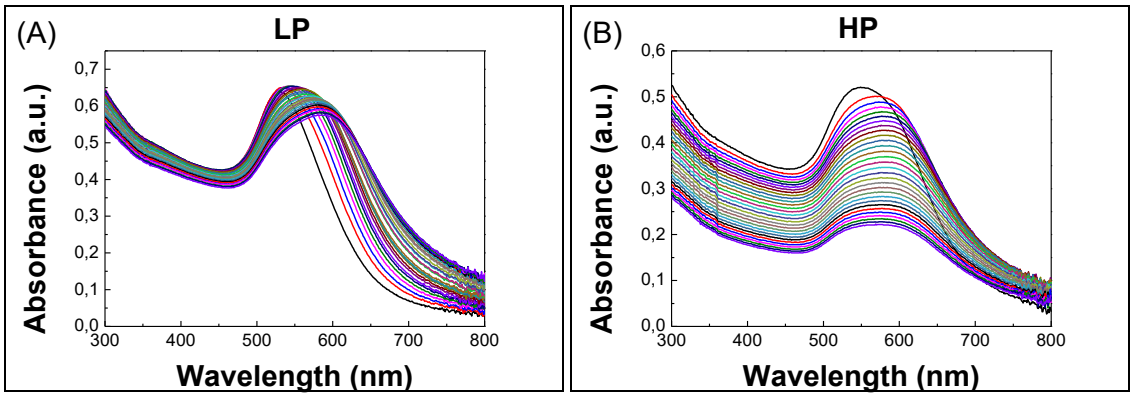

Figure 3.11.: Chemical characterization of MUA-conjugated AuNPs by UV-Vis spectra at time zero: LP conjugates type **(A)** show a lower decrease in absorbance vs HP conjugates type **(B)**. For this reason, LP conjugates are considered to present a higher resistance to NaCN than HP conjugates type at time zero. It can be considered that the coverage of MUA molecules onto the AuNPs surface at time zero is more robust at LP conjugates type than at HP conjugates type.

The rate of decomposition of MUA-conjugated gold nanoparticles at time zero can be determined (Figure 3.12.) by measuring the time-dependent decrease of the surface plasmon band absorbance.

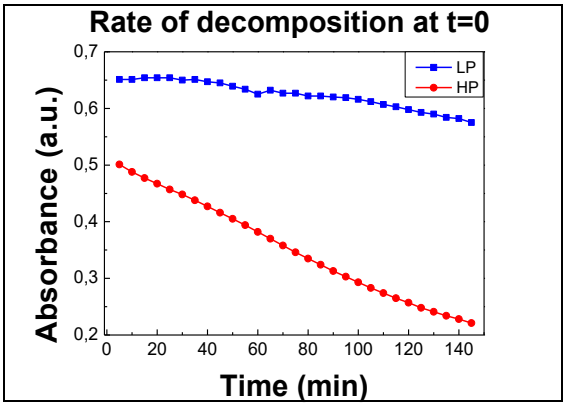

Figure 3.12.: Rate of decomposition of MUA-conjugated AuNPs at time zero by measuring the digestion time of conjugates against NaCN: LP conjugates seem to be more stable than HP conjugates (that have a faster rate of decomposition). Results can be correlated with the UV-Vis spectra of MUA-conjugated Au NPs against NaCN-induces digestion. It can be said that LP conjugates present a higher robustness against NaCN digestion than HP conjugates at time zero.

To conclude with the reactive characterization of MUA-conjugated Au NPs at time zero after conjugation, it can be said that LP conjugates type demonstrated to be more stable than HP conjugates type, not only against an excess of salt but also against NaCN-induced digestion of the nanoparticle's core.

In addition, this stability behavior showed by LP conjugates can be correlated to the higher surface charge that LP conjugates presented while analyzing ζ-Potential of conjugates at time zero.

More surface charge means more COO^- per unit area that can be translated into more stable states against NaCl and NaCN. A more dense coating of MUA conjugated molecules should result in a less reactive NPs surface.

As a consequence, MUA-conjugated Au NPs developed by LP method seem to present a more robust conformation of MUA molecules onto the surface of gold nanoparticles at time zero than MUA-conjugated Au NPs generated by HP method of conjugation. Interestingly, as we will see later, LP conjugated Au NPs evolve to HP conjugates conformation.

Biological Characterization

The formation of a Protein Corona onto AuNPs and MUA-conjugated AuNPs is due to the absorption of proteins from the c-CCM where samples are exposed. Incubation of samples in c-CCM was carried out for 48h.

The corresponding Protein Corona generation onto gold nanoparticles surfaces can be detected by UV-Vis spectroscopy (Figure 3.13.). An increase in absorbance and red-shift in peak position of the SPR spectra determine the absorption of proteins onto nanoparticles.

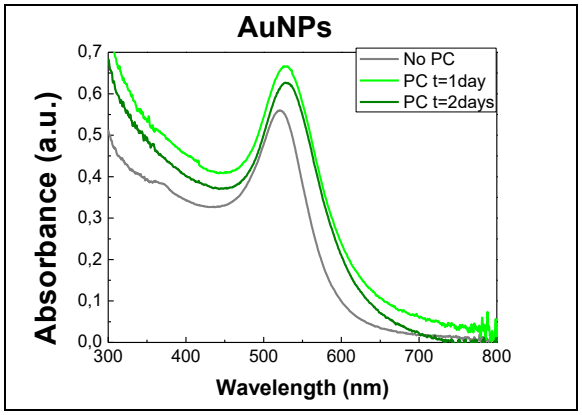

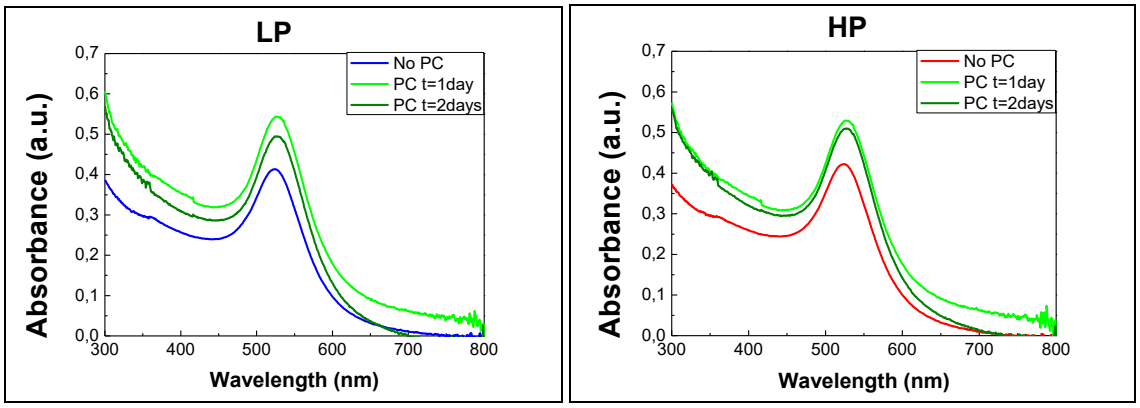

Figure 3.13.: UV-Vis characterization of the Protein Corona (PC) formation onto AuNPs and MUA-conjugated AuNPs (LP and HP conjugate types) at time zero and after time evolution.

As it can be seen in SPR spectra, absorbance increases after Protein Corona formation both in gold nanoparticles and conjugates. Related to peak position, naked gold nanoparticles experienced a higher red-shift after incubation in c-CCM than MUA-conjugated gold nanoparticles. These differences can be explored in detail as Figure 3.14. shows.

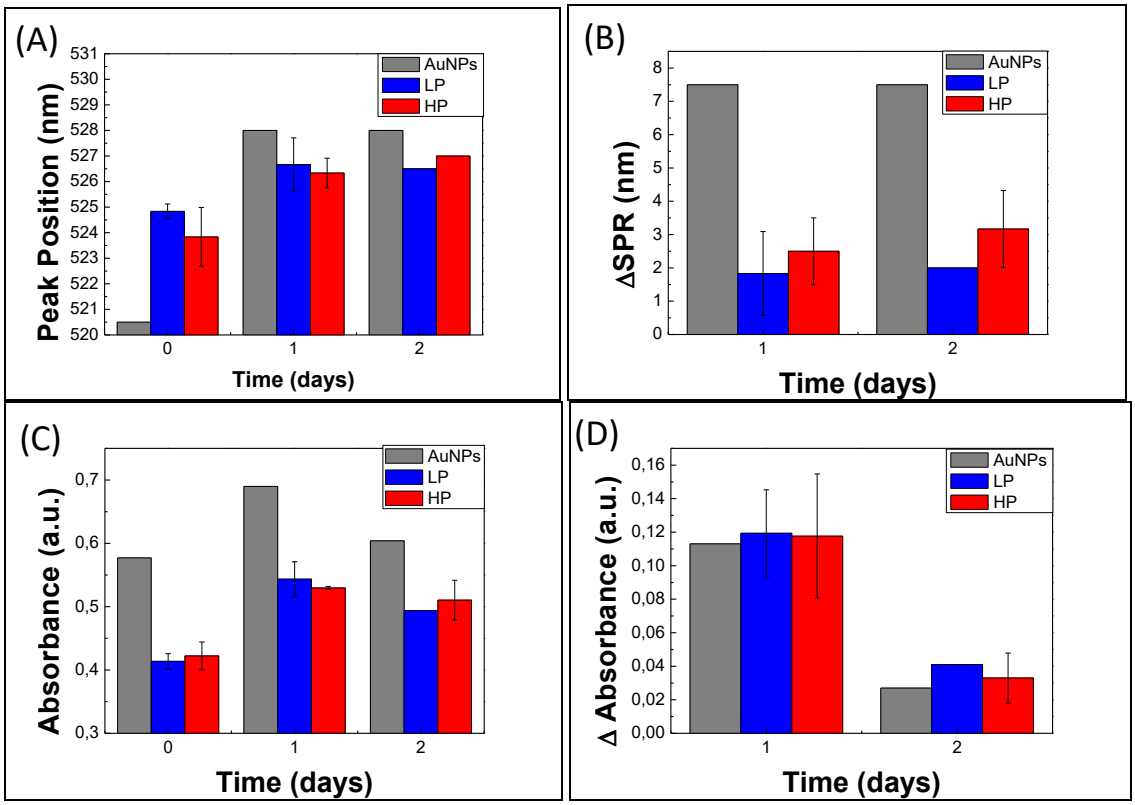

Figure 3.14.: (A and B) Peak position determination and Increment of the **Surface Plasmon Resonance (SPR) peak** after incubation and Protein Corona formation characterized by UV-Vis spectroscopy. **(C and D) Changes in absorbance** values during PC formation were also determined. Time zero corresponds to gold nanoparticles and conjugates before exposure to complete cell culture medium.

Related to conjugates, the PC formation differences seem to be not as evident as in the case of Au NPs, since less red-shift of the SPR peak (2-3nm) is observed after PC formation onto conjugated samples. PC generation onto naked Au NPs (with a red-shift of 7.5nm) is higher than onto conjugates. Proteins would have a stronger affinity to get absorbed onto bare Au NPs than onto conjugates samples presenting a SAM of MUA molecules on their surfaces that would electrostatically interact against proteins (also, metal surfaces show a higher affinity for organic molecules).

Regarding differences between conjugates, the SPR spectra suffered a higher red-shift in the peak position of HP conjugates compared to LP conjugates. It can be correlated to the less negative surface charge present in HP conjugates compared to LP conjugates that could let a higher absorption of proteins onto their surfaces.

The absorbance also increases after Protein Corona formation onto gold nanoparticles and conjugates, being the increment of absorbance in SPR spectra almost the same in both cases. It can be observed that 1 day of incubation of samples in c-CCM generates a higher absorbance increment than 2 days of incubation that could be related with the hardening of the nanoparticle Protein Corona[25].

The PC formation can be further analyzed by exploring the Size and ζ-Potential evolution of naked and conjugated nanoparticles after incubation in c-CCM, as Figure 3.15., Figure 3.16. and Table 3.1. show.

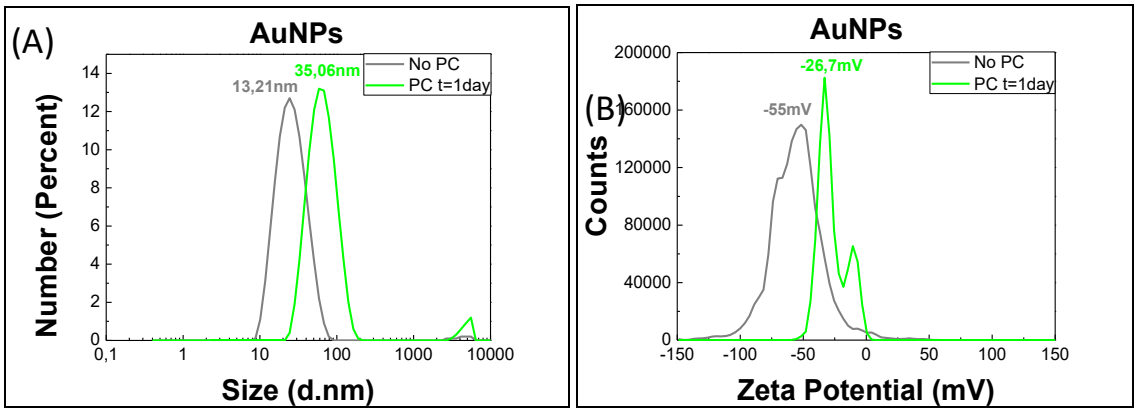

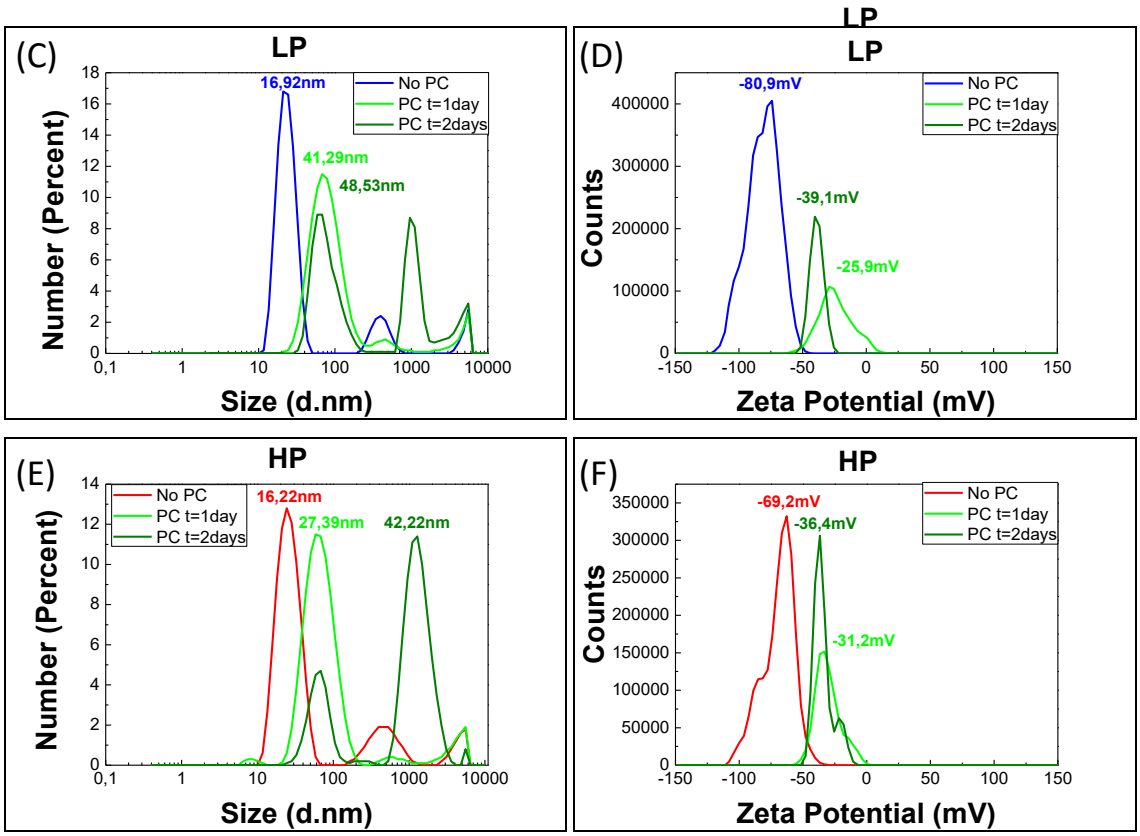

Figure 3.15.: DLS and ζ-Potential characterization of Seed AuNPs (A and B), LP conjugates (C and D) and HP conjugates (E and F) before and after Protein Corona (PC) formation at 37°C in c-CCM for 1 and 2 days.

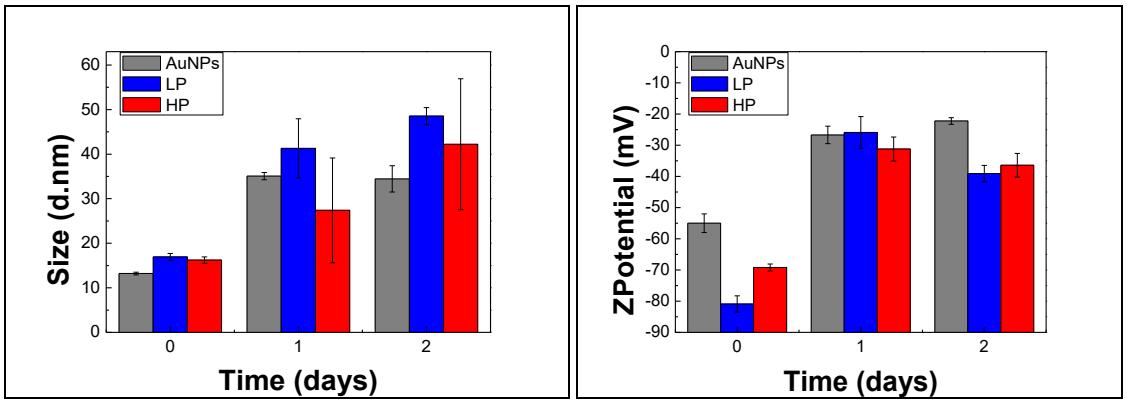

Figure 3.16.: DLS and ζ-Potential evolution of Protein Corona formation onto AuNPs, LP and HP conjugates. Time zero corresponds to gold nanoparticles and conjugates before exposure to complete cell culture medium.

Type	Time	Number (d.nm)	S.D.	ζ- Potential (mV)	S.D.
Au NPs	0	13.21	0.3122	-55	2.97
AuNPs-PC	1 day	35.06	0.8102	-26.7	2.80
AuNPs-PC	2 days	34.45	2.941	-22.2	1.06

LP	0	16.92	0.8007	-80.9	2.61
LP-PC	1 day	41.29	6.645	-25.9	5.08
LP-PC	2 days	48.53	1.917	-39.1	2.63
HP	0	16.22	0.7123	-69.2	1.14
HP-PC	1 day	27.39	11.75	-31.2	3.83
HP-PC	2 days	42.22	14.69	-36.4	3.78

Table 3.1.: Average values of DLS and ζ-Potential of Seed AuNPs and MUA-conjugated AuNPs (LP and HP types) after incubation in CCM and formation of PC.

NOTE: Values of DLS and ζ-Potential of AuNPs-PC at 2 days corresponds to a different batch of sample.

In the case of Au NPs, an increment in the hydrodynamic size of 21.24nm is experienced due to the formation of PC changing from 13.21nm before PC to 34.45 nm after PC formation at 1 day. Additionally, an increase of 33mV to less negative value of ζ-Potential is also seen after PC, changing from -55mV to -22mV. Both measurements correspond to 2 days of incubation of Au NPs in c-CCM.

In the case of LP type MUA-conjugated AuNPs, an increase in the hydrodynamic size of 24.37nm is experienced due to the formation of PC at 1 day of incubation. The value increases 7.24nm after 2 days of incubation. Samples suffered a total increment of 31.61nm in size, ending with a hydrodynamic size of 48.53nm after 2 days (original size value before PC formation was 16.92nm). Additionally, an increase of 55mV to less negative value of ζ-Potential is seen after PC of LP conjugates at 1 day of incubation and an increase of 13.2mV to more negative value of ζ-Potential from 1 day to 2 days of incubation. Samples suffered a total decrease of negative charge surface of 41.8mV ending with a ζ-Potential of -39.1mV after 2 days of PC (original ζ-Potential value before PC formation was -80.9mV).

In the case of HP type MUA-conjugated AuNPs, an increase in the hydrodynamic size of 11.17nm is observed due to the formation of PC at 1 day of incubation. Additionally, an increase of 14.83nm occurred from 1 day to 2 days of incubation. Samples suffered a total increment of 26nm in size, ending with a hydrodynamic size of 42.22nm after 2 days of PC (original size value before PC formation was 16.22nm). Related to ζ-Potential, a decrease of 38mV to less negative value of ζ-Potential is seen after PC of

HP conjugates at 1 day of incubation and an increase of 5.2mV to more negative value of ζ-Potential is experienced from 1 day to 2 days of incubation. Samples suffered a total increment of 32.8mV ending with a ζ-Potential of -36.4mV after 48h of PC (original ζ-Potential value before PC formation was -69.2mV).

Although HP conjugates seem to present a final ζ-Potential value slightly less negative than LP conjugates that could be correlates with a higher load of proteins in the PC formation onto HP than LP, no significant differences can be observed in the physicochemical properties between conjugates when exposed to proteins. The question about different biological behavior is still open. Simple in vitro experiments should clarify this issue.

3.5. Time evolution

EXPERIMENTAL SECTION

Static Characterization

The observed differences in reproducibility should be correlated with a different stability and temporal evolution. The stability of samples that can be determined by their evolution through time. For this purpose, as prepared samples were stored in the same excess of MUA molecules (0.1mM) used for the conjugation during 14 days. In this environment, MUA-conjugated Au NPs could maybe evolve to different states through the exchange of MUA molecules attached to the Au NPs surface and those non-attached MUA molecules in the surrounding of the Au NPs in an excess concentration.

Colloidal Stability Characterization

As it was previously done after conjugation of gold nanoparticles with MUA molecules, aged conjugates samples (1mL) at 7 and 14 days after conjugation procedure were treated with Sodium Chloride (NaCl) at different concentrations (from 0 to 0.4M) proving their colloidal stability in the presence of an excess of salts.

Chemical Characterization

Furthermore, conjugates samples were also also analyzed by their resistance to Sodium Cyanide (NaCN)-induced digestion. The more dense coating should work as a better barrier. For this purpose, 1mL of MUA-conjugated Au NPs of each type of 7 days aged conjugates (LP and HP types) was exposed against NaCN (with a final concentration of 45mM in solution).

Biological Characterization

The evolution of conjugates was analyzed by the study of protein absorption onto the surfaces of evolved 7 days conjugated AuNPs. For the generation of Protein Corona, 1mL of conjugates were exposed to 9mL of complete cell culture medium (c-CCM) containing 90% of DMEM and 10% of FBS. Samples were incubated at 37°C for 48h and

further purified by centrifugation at 13rpm for 5 minutes and resuspension in sodium citrate (2,2mM) for characterization by UV-Visible spectrophotometer.

RESULTS AND DISCUSSION

Static Characterization

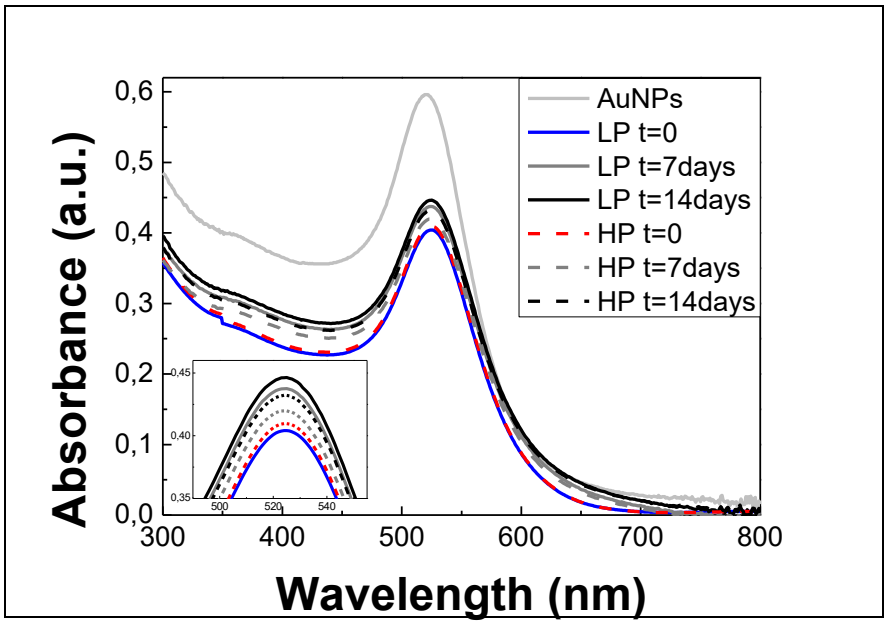

Figure 3.17.: UV-Vis characterization of the time evolution of MUA-conjugated Au NPs.

As it can be seen in the UV-Vis spectra characterization (Figure 3.17.), LP conjugates evolve more than HP conjugates presenting the former higher absorbance intensity in peak through time.

Samples were also analyzed by DLS. Results showed that all conjugated NPs (either LP or HP type) maintained the same size along time. Whereas, the surface charge intensity of the conjugates decrease from time zero to 14 days after conjugation, changing around 15mV from -80.9mV to -66.1mV (in the case of LP conjugates) and around 4,5mV from -69.2mV to -64.7mV (in the case of HP conjugates). (Figure 3.18., Figure 3.19. and Table 3.2.) Note that vials were closed and no evaporation or gas absorption (mass exchange) ocurred.

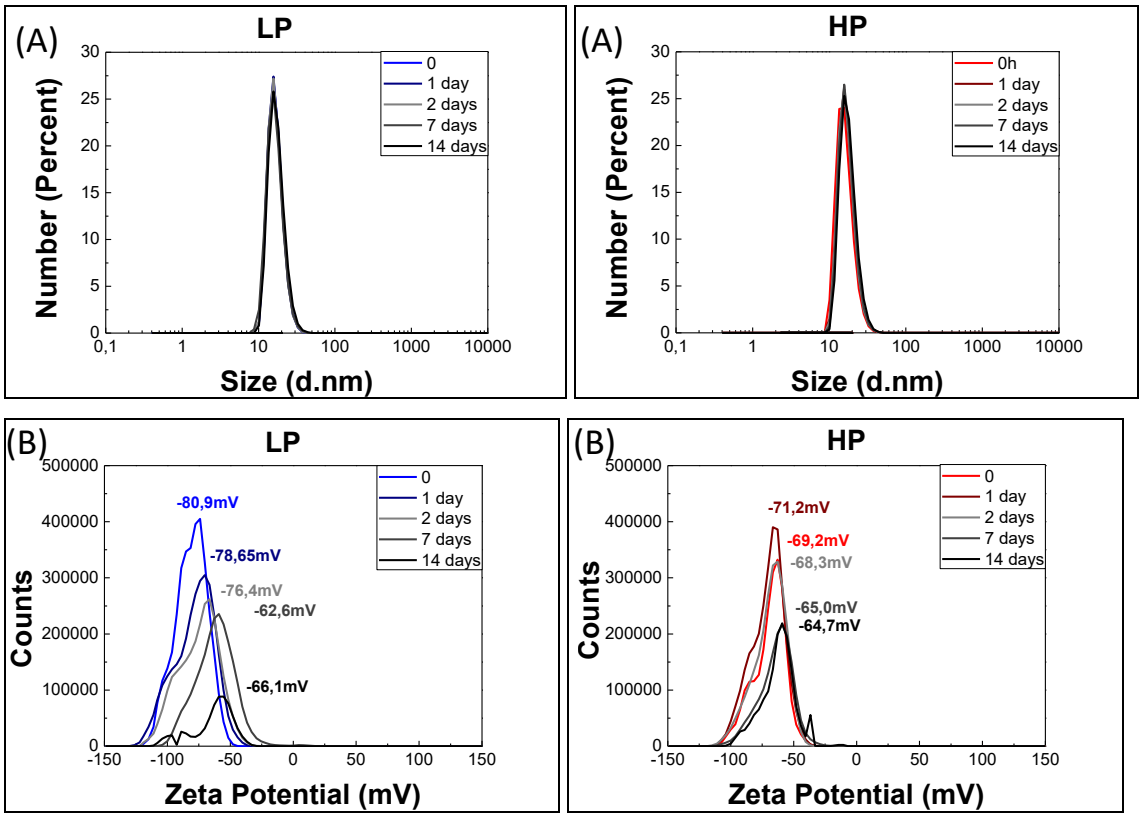

Figure 3.18.: DLS and ζ-Potential characterization of the time evolution of MUA-conjugated Au NPs. **(A)** The hydrodynamic radius of both LP and HP types of conjugates maintain stable ~17nm over time from time zero to 14 days. **(B)** However, the surface charge intensities of conjugates (both LP and HP types) decrease, from time zero to 14 days after conjugation.

Type	Time	Number (d.nm)	S.D.	ζ- Potential (mV)	S.D.
LP	0	16.92	0.8007	-80.9	2.61
LP	1 day	16.79	0.3707	-78.65	3.08
LP	2 days	16.75	0.5453	-76.4	5.64
LP	7 days	16.61	0.78	-62.6	4.8
LP	14 days	17.45	1.309	-66.1	6.79
HP	0	16.22	0.7123	-69.2	1.14
HP	1 day	16.94	0.4388	-71.2	3.24
HP	2 days	16.97	0.3696	-68.3	2.6
HP	7 days	17.30	0.45	-65.0	2.71
HP	14 days	17.95	1.017	-64.7	2.23

Table 3.2.: Average values of DLS and ζ-Potential of the time evolution of conjugates.

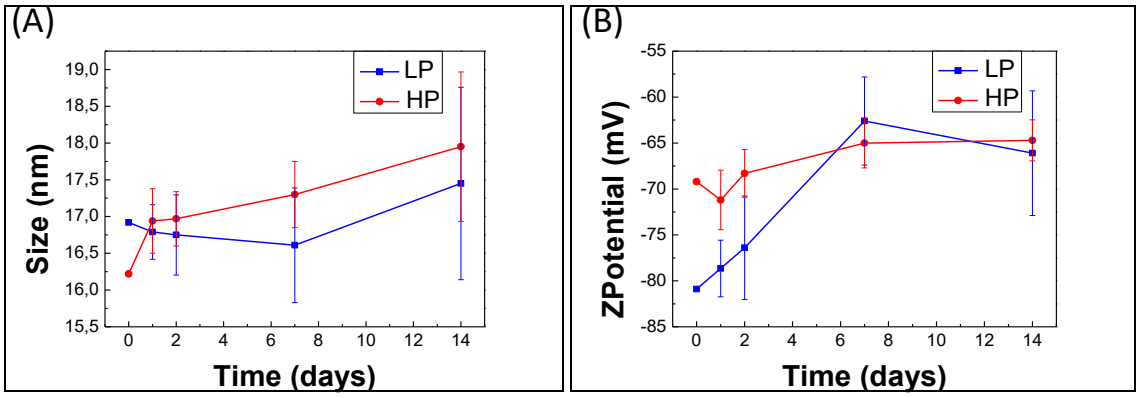

Figure 3.19.: Size (A) and ζ-Potential (B) evolution through time of LP and HP types MUA-conjugated Au NPs.

After time evolution, both types of MUA-conjugated Au NPs reduced their charge intensity (Table 3.2.). LP conjugates experienced a higher surface charge reduction (18.3%) than HP conjugates (6.5%).

Notwithstanding that both types of MUA-conjugated Au NPs were characterized to be different at time zero, it seems that after 14 days of time evolution both types of conjugates evolved to a similar conformation. In both cases (LP and HP), a similar value of around -65mV was reached in ζ-Potential. This value is more similar to the surface charge intensity that HP conjugates showed at time zero (-69.2mV), as it was previously indicated in Figure 3.5. - C.

For this reason, MUA-conjugated Au NPs generated by HP method could be considered objects with a lower energy state than MUA-conjugated Au NPs generated by LP method. As a consequence, since objects would prefer a low energy state to maintain stability, the system could evolve along time towards the state of lower energy (Figure 3.20.). This is consistent with what the surface charge intensity of LP conjugates experienced after 14 days evolution, changing to a similar surface charge intensity value of the one presented in HP conjugates state.

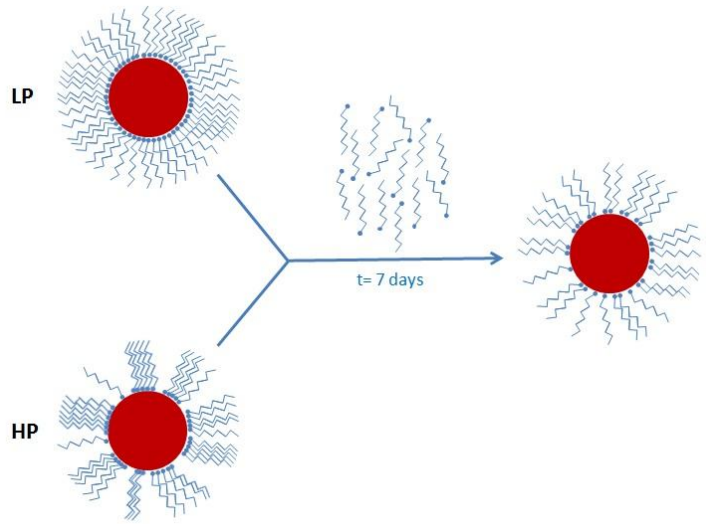

Figure 3.20.: Schematic picture of coating density states onto MUA-conjugated Au NPs after 7 days of evolution in conditions of excess of MUA molecules.

If there are differences in the energy state, one would expect time evolution of samples. Indeed, it was already observed, now we study it in detail.

Samples were further characterized after 7 and 14 days of time evolution. Conjugated Au NPs have been kept in the excess of MUA molecules used for the conjugation procedure in the fridge at 4°C. It was previously determined by static characterization that MUA-conjugated Au NPs experienced an evolution of surface charge analyzed by ζ-Potential values from conjugate state at time zero to conjugate state after time evolution in the excess of MUA molecules (Figure 3.18. - B, Figure 3.19. – B and Table 3.2.).

Colloidal Stability Characterization

Analyzing the colloidal stability of conjugates after time evolution of the samples it could be detected that UV-Vis spectra showed less aggregation of samples against salt at high concentrations of NaCl (0.4M) than the ones that MUA-conjugated Au NPs, either LP or HP, experienced at time zero after conjugation (previously showed in Figure 3.8.) even if HP conjugation led to higher ζ-Potential values.

Focusing on the evolution of conjugates from time zero to 7 days after conjugation, both MUA-conjugated AuNPs (LP and HP types) seem to have evolved along time towards higher stable conformations of MUA molecules onto conjugates that are able

to resist against higher concentration of NaCl. (Figure 3.21.). Similar behavior has been observed for both aged LP and HP samples, as should correspond to the similar surface charge of both conjugates.

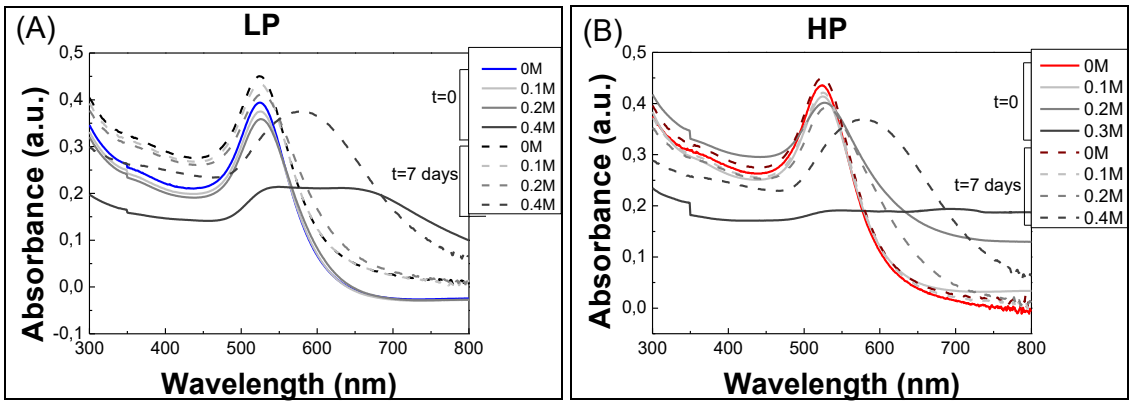

Figure 3.21.: Colloidal stability of MUA-conjugated AuNPs by UV-Vis spectra at time zero and 7 days after the conjugation: Both LP **(A)** and HP **(B)** conjugates present higher stability against 0.4M NaCl at 7 days after conjugation than at time zero. Nevertheless, it doesn't occur at lower concentrations of salt (from 0M to 0.2M) where each conjugate type behaves different:

For low concentrations of salt, LP conjugates (A) seem to be quite more resistant against NaCl at time zero than conjugates after 7 days of conjugation. Since the SPR band of LP conjugates after 7 days evolution experienced an increase in absorbance in the region of 600-700nm of wavelength that indicates aggregation of samples.

On the contrary, HP conjugates (B) present similar UV-Vis spectra against 0M and 0.1M of NaCl at time zero and 7 days after conjugation. Whereas, particularly against 0.2M of NaCl, HP conjugates become slightly more stable at 7 days than at time zero (considering the absorbance values of SPR band in the region of 600-700nm of wavelength). It also happens against 0.4M of NaCl, where HP conjugates at 7 days present spectra that show less aggregation against salt than HP conjugates at time zero. In this case, the maximum concentration of salt tested at time zero did not reach 0.4M of NaCl but 0.3M since, at this concentration, the sample was totally aggregated.

Consequently, LP conjugates present higher stability at the highest NaCl concentration tested (0.4M) in the state of evolved conjugate after 7 days evolution than in the state of the conjugate at time zero. Similarly, HP conjugates better resist against aggregation due to salt addition to samples at the evolved state of 7 days after conjugation rather

than at the time zero conjugate state not only for the highest concentration of salt tested, but also in the case of intermediate salt concentration (0.2M and 0.4M of NaCl).

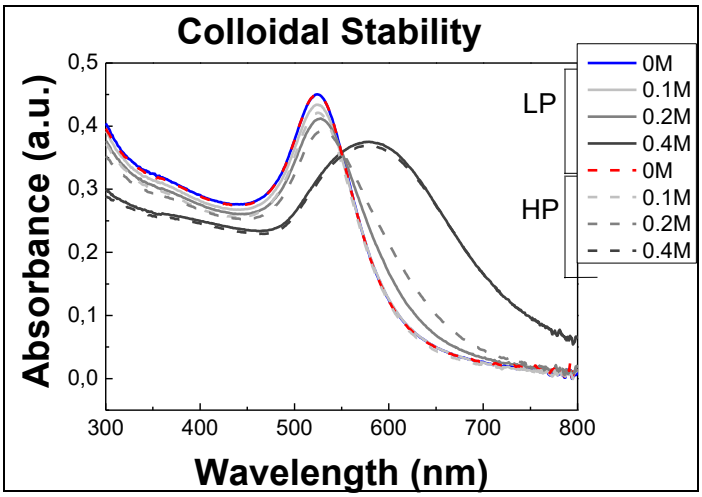

Figure 3.22.: Physiological characterization of MUA-conjugated AuNPs by UV-Vis spectra at 7 days after the conjugation: Both LP and HP conjugates present similar UV-Vis spectra at 0M and 0.1M of NaCl. However, when the conjugates are exposed against 0.2M of NaCl, HP conjugates type seem to be less stable than LP conjugates type due to the higher red-shift in the position of the SPR band and the increase in absorbance in the range of 600-700nm. Nevertheless, both types of conjugates show almost the same UV-Vis spectra at 0.4M exposure of NaCl. This can be correlated with the final structure of MUA molecules onto the AuNPs surface that seems to generate similar type of conjugate states.

Exploring the state of two types of MUA-conjugated Au NPs after 7 days evolution from the conjugation procedure (Figure 3.22.), HP conjugates type seem to be less stable than LP conjugates type against the concentration of 0.2M of NaCl at 7 days of evolution. however this difference is minute. Beside this, at the highest concentration of salt tested (0.4M of NaCl) both types of conjugates (LP and HP types) present after 7 days evolution almost equal stability against salt solution.

Chemical Characterization

In order to evaluate the evolution of MUA-conjugated Au NPs in an excess of MUA molecules at 7 days after conjugation, samples were not only physically but also chemically characterized.

For this purpose, conjugates were treated with 45mM of NaCN and UV-Vis spectra were collected for 2 hours and 30 minutes. This assay could determine the reaction process of the gold nanoparticles core digestion in each type of conjugate (LP and HP) at 7 days after conjugation (Figure 3.23.). Corrosion of the NPs is associated with Ostwald Ripening and the size distribution increases leading to a decrease and broadening of the peak rather than a blue shift.

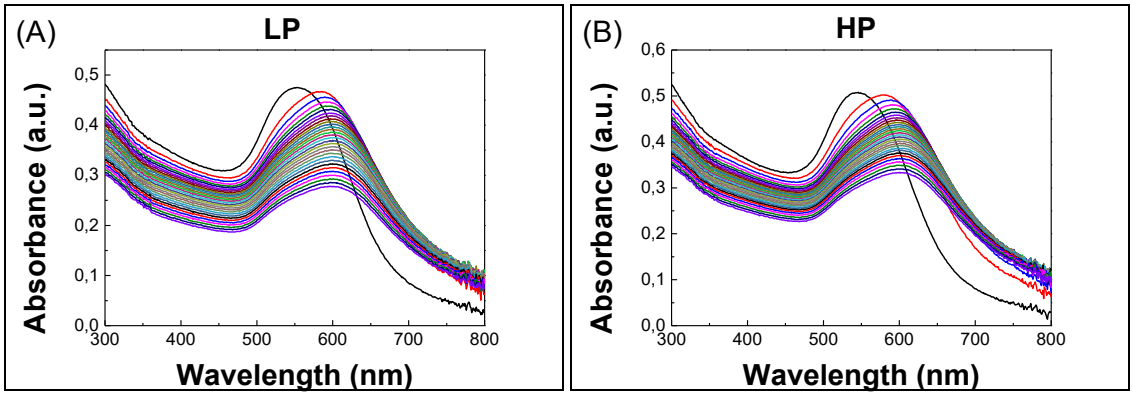

Figure 3.23.: Chemical characterization of MUA-conjugated AuNPs by UV-Vis spectra at 7 days after conjugation: LP conjugates type **(A)** show similar spectra than HP conjugates **(B)** against NaCN digestion for 2hours 30minutes at 7 days after conjugation.

Based on the chemical characterization of Figure 3.23., a similar behavior against NaCN-induced digestion of conjugates (LP and HP types) at 7 days of evolution time after conjugation can be considered.

However, HP conjugates present a slightly higher absorbance of the peak at 2 hours and 30 minutes of NaCN digestion than LP conjugates. It can be said that, although both conjugates are almost equal on resistance against NaCN digestion, HP conjugates can present a slightly higher stable conformation than LP conjugates at 7 days after conjugation. However, these differences may be irrelevant.

On the other hand, LP conjugates (A) seem to have evolved to a less stable conformation through time but to a similar HP conjugate conformation. This can be

correlated with the decrease in absorbance that the UV-Vis spectra of LP conjugates show at 7 days after conjugation in comparison with the one showed at time zero (Figure 3.11. - A).

In the case of HP conjugates (B), a lower decrease of absorbance can also be seen at 7 days after conjugation in contrast with HP conjugates at time zero (Figure 3.11. - B). Consequently, it can be said that HP conjugates also evolve to a more stable conformation through time.

As it was analyzed at time zero, the rate of decomposition of MUA-conjugated Au NPs at 7 days after conjugation can be also quantified (Figure 3.24. and Figure 3.25.) by measuring the time-dependent decrease of the surface plasmon band absorbance.

Studying time evolution, both types of conjugates (LP and HP) evolve towards similar rates of decomposition at 7 days after conjugation compared to the ones presented at time zero (Figure 3.12.).

However, LP conjugates present a faster digestion time with a difference in absorbance of around 0.05a.u. at 2 hours and 30 minutes of NaCN digestion. Therefore, LP conjugates seem to be less stable against NaCN digestion than HP conjugates at 7 days after conjugation.

Although being the DLS and ζ-Potential measurements not so much accurate, higher size and higher surface charge could indicate higher density of molecules onto HP conjugates. This could be related to the slightly higher stability of HP conjugates against NaCN digestion.

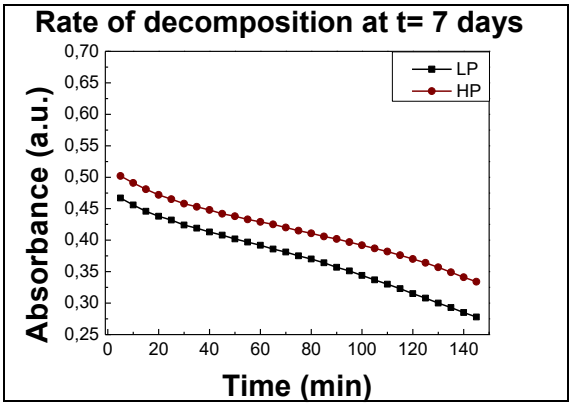

Figure 3.24.: Rate of decomposition of MUA-conjugated AuNPs at 7 days after conjugation by measuring the digestion time of conjugates against NaCN.

To conclude with the chemical characterization, the rate of decomposition of each type of MUA-conjugated Au NPs can be analyzed before and after time evolution. As it was shown in Figure 3.24., both conjugate types presented a similar rate of decomposition after time evolution. However, the time evolution of each conjugate type can be also analyzed independently as it can be observed in the following image (Figure 3.25.).

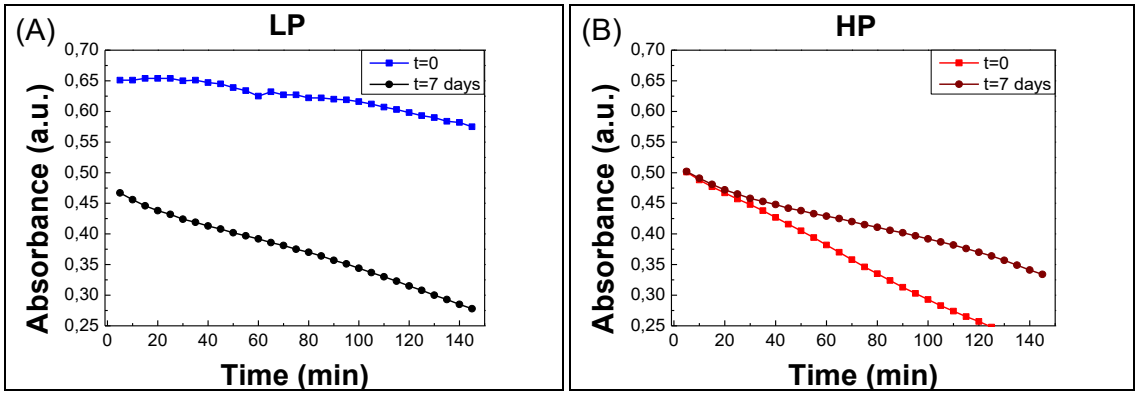

Figure 3.25.: Time evolution of the digestion of MUA-conjugated AuNPs by NaCN: Comparison of the rate of decomposition of LP conjugates **(A)** and HP conjugates **(B)** from time zero to 7 days after conjugation.

The rate of decomposition of LP conjugates at 7 days after conjugation is much faster than at time zero. Therefore, LP conjugates evolve to a conformation that is less stable than their conformation at time zero but similar to HP conjugates at 7 days after conjugation.

On the contrary, HP conjugates present the opposite behavior as LP conjugates: At time zero, HP conjugates present a faster rate of decomposition than at 7 days after conjugation.

As a consequence, HP conjugates are considered to evolve to a more stable conformation through time that leads to a more protected Au NPs surface and therefore a higher stability against NaCN-induced digestion.

Biological Characterization

The absorption of proteins onto gold nanoparticles and aged conjugates surfaces was explored to determine time evolution of the conjugates. As it can be seen in Figure 3.27., an increment of absorbance and red-shift of the SPR band is observed after Protein Corona formation at day 1 and day 2 of incubation of 7 days aged conjugates in complete cell culture medium.

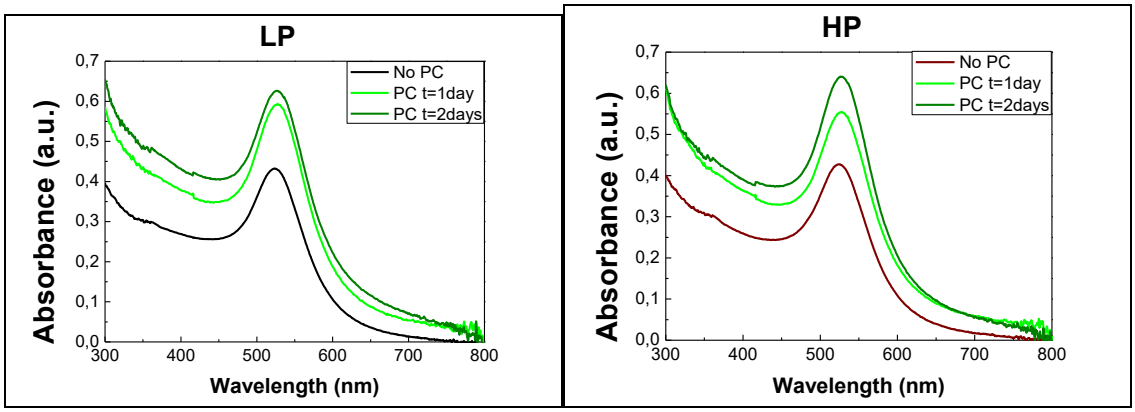

Figure 3.27.: UV-Vis characterization of the Protein Corona (PC) formation onto MUA-conjugated AuNPs (LP and HP conjugate types) after 7 days of time evolution of conjugates.

Differences of aged conjugates (LP and HP types) by UV-Vis spectroscopy can be analyzed by the determination of the peak position of the SPR band (Figure 3.28.) in the formation of Protein Corona onto conjugates surfaces.

As previously observed, the red-shift of SPR band that Au NPs experienced is higher (7.5nm) than the one observed in aged conjugates, where both LP and HP types presented a 3nm red-shift at 2 days of incubation in complete cell culture medium. So then, no detectable differences between conjugates types can be identified by UV-Vis spectroscopy characterization of the Protein Corona.

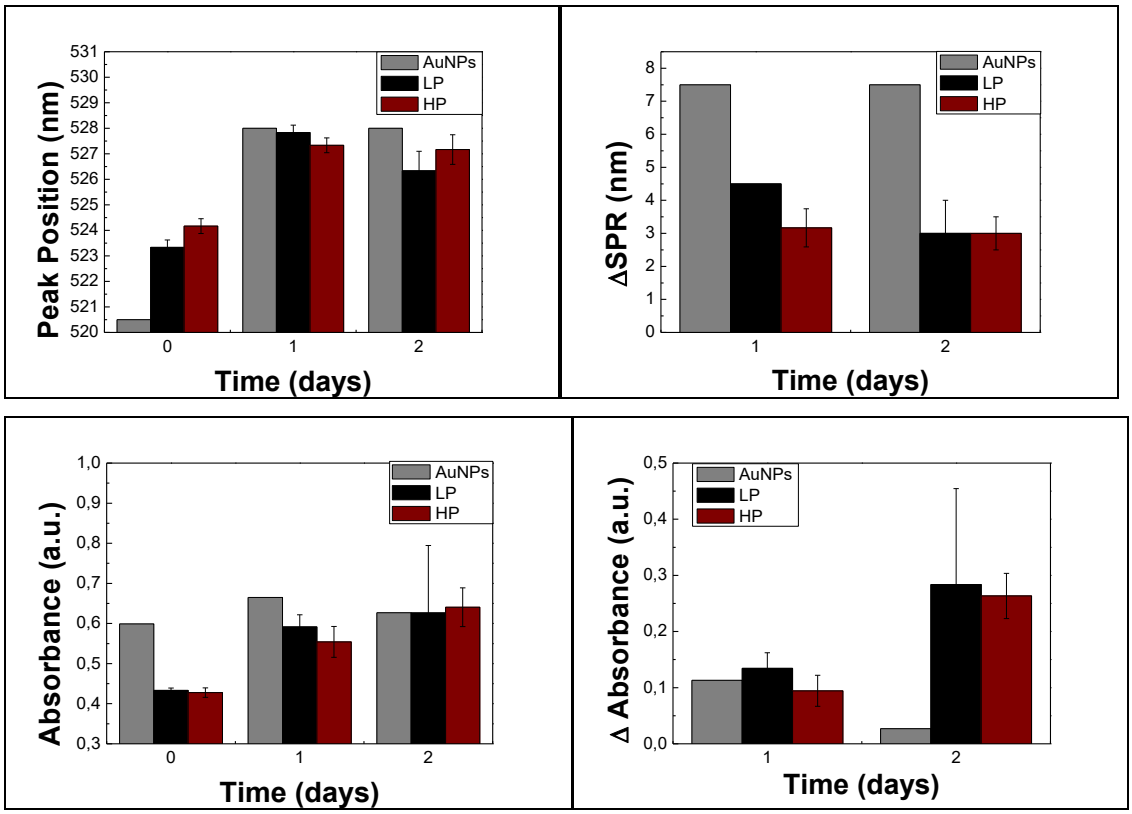

Figure 3.28.: Evolution of the Protein Corona (PC) formation onto AuNPs and MUA-conjugated AuNPs (LP and HP conjugate types) after 7 days of time evolution of conjugates.

Interestingly, differences between conjugates are bigger at time zero than at 7 days of time evolution in the case of aged conjugates (Figure 3.29.). These results correlate with the reactive characterization of conjugates evolving to similar states through time.

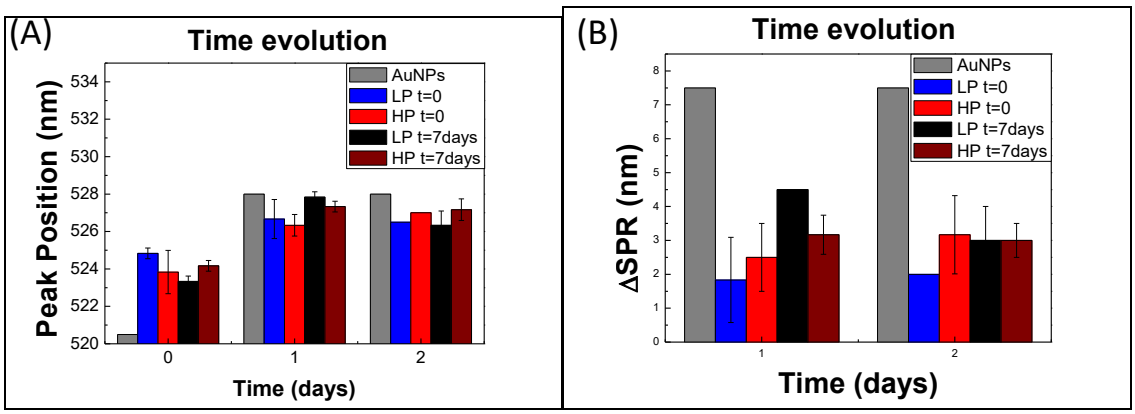

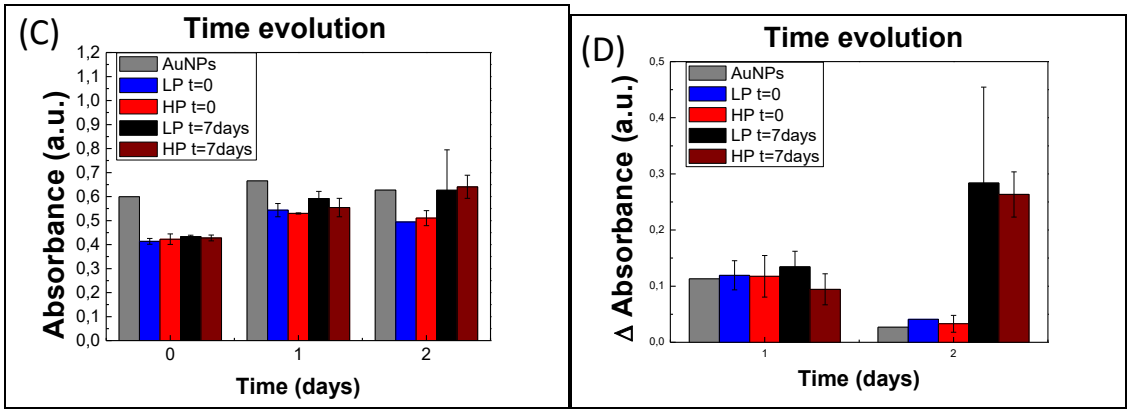

Figure 3.29.: Analysis of Protein Corona formation onto AuNPs and MUA-conjugated AuNPs (LP and HP conjugate types) at fresh (t=0) and aged (t= 7 days) conjugates states.

It can be observed in Figure 3.29. how differences in conjugates LP and HP type are higher at time zero than after 7 days of time evolution of conjugates.

The increment in absorbance could be related due to the aging of the samples in the case of aged conjugates.

Related to the increment of the SPR peak, bare gold nanoparticles are the one to present a higher increment due to PC formation. This behavoiur indicates the favourable PC formation onto naked nanoparticles respect to conjugates.

In the case of conjugated nanoparticles, dissimilarities of SPR increment were observed in conjugates LP and HP at time zero. However, aged conjugates (after 7 days of time evolution) seem to present the same increment of SPR for both types (LP and HP) of conjugates. This, again, is consistent with the hypothesis that conjugates evolve towards a similar conformation states with time.

3.6. Design exploration with peptide

The influence of the conjugation method (either LP or HP) was found to be also determinant for the functionalization of gold nanoparticles with peptides, such as CLPFFD-NH_2. This is a biomedically significant peptide that can be conjugated to gold nanoparticles towards the thiol of the N-terminal cysteine[(5)].

The peptide of interest H_2N-CLPFFD-$CONH_2$ presents hydrophobic groups such as the Leucine (L) and Phenylalanine (F) groups that enable the activation of the immune system. The aspartic acid (D) was functionalized with an amide group that gives neutral charge instead of the negative charge that corresponds to the aspartic acid group.

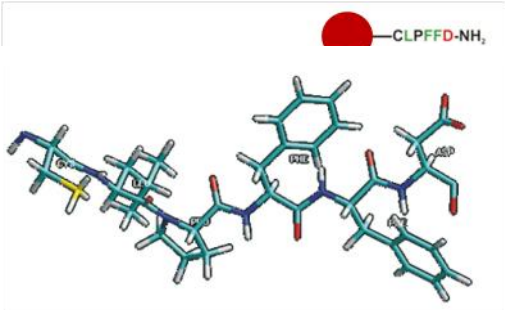

Eschematic representatio of Peptide molecular conformation and its interaction with gold nanoparticles (yellow sphere). The peptide was synthesized by the Peptide Scientific Technical Service of University of Barcelona.

The CLPFFD-NH_2 peptide corresponds to an amyloid growth inhibitor peptide that compromises amino acids 11 through 16 of the $A\beta_{1-42}$ protein. This amyloid beta protein is related to Alzheimer disease and peptide recognizes a particular hydrophobic domain of the β-sheet structure and enables the selective attachment of Au NPs to β-amyloid fibers[(26)].

3.6.1. The influence of the conjugation method

The design of conjugation was studied by proving the conjugation methods LP and HP types, which were already explored with MUA molecules, by testing them with CLPFFD-NH_2 peptide. In this case, the conjugation will be carried out with a peptide of interest in medicine related with Alzheimer disease.

EXPERIMENTAL SECTION

Conjugation

For the conjugation of gold nanoparticles with CLPFFD-NH_2 peptide, the two different methods of conjugation previously explored were carried out.

The LP conjugation method follows a procedure in which 2 mL of an aqueous solution of CLPFFD-NH_2 peptide (70µM) was added dropwise to 5 mL of gold nanoparticle solution ($\sim 3 \cdot 10^{12}$ NPs/mL).

The HP conjugation method follows the inverse admixture with the addition of 5 mL of gold nanoparticle solution ($\sim 3 \cdot 10^{12}$ NPs/mL) onto the 2 mL of the aqueous solution of CLPFFD-NH_2 peptide (70µM).

The final concentration of peptide in each gold nanoparticle solution was 20µM. Both methods of conjugation were stirred for 1 hour at room temperature.

Chemical Characterization

Conjugates samples were also analyzed by their resistance to Sodium Cyanide (NaCN)-induced digestion. The more dense coating should work as a better barrier. For this purpose, 1mL of Peptide-conjugated Au NPs of each type of conjugates (LP and HP types) was exposed against NaCN (with a final concentration of 45mM in solution).[*18*]

Biological Characterization

In order to explore the behavior of conjugates in biological conditions and the consequent Protein Corona (PC) formation, samples were exposed to complete cell

cuture medium (c-CCM) consisting in 90% of Dulbecco's Modified Eagle Medium (DMEM) and 10% of Fetal Bovine Serum (FBS). For this purpose, 1mL of each sample was added to 9mL of c-CCM, followed by incubation at 37°C for 1 and 2 days and 7 days. Afterwards, samples were purified by centrifugation at 13rpm for 5 minutes and resuspension in sodium citrate (2,2mM) for further characterization by UV-Visible spectrophotometer, DLS and ζ-Potential.

RESULTS AND DISCUSSION

Conjugation

In order to explore reproducibility of conjugation methods, six replicas of each conjugation method (LP and HP type) were carried out. As it can be observed in Figure 3.30., samples were analyzed by UV-Vis spectroscopy and Peak Positions of the SPR bands were determined. Based on peak position, HP conjugation method presents higher reproducibility than LP conjugation method. The HP replicas generate a maximum variation of 1.5nm in peak position, whereas the LP replicas give a maximum variability of 3.5nm in peak position.

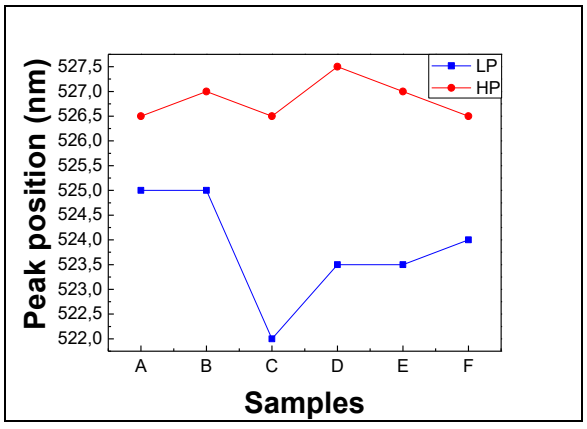

Figure 3.30.: Reproducibility of conjugation methods (LP and HP) at 6 replicas of conjugates analyzed.

In order to evaluate the conjugation procedure, SPR band spectra of samples before and after conjugation were analyzed as well as their size through DLS and their surface charge by ζ-Potential (Figure 3.31.).

Samples experienced a red-shift of the SPR band spectra of 3.5nm after conjugation, varying from 523.5nm in the case of gold nanoparticles to 527nm in the case of

Peptide-conjugated gold nanoparticles. Differences between LP and HP method of conjugation were not detectable by UV-Vis spectroscopy.

Regarding DLS analysis, a difference in size could be detected between conjugates, presenting HP conjugates a slightly higher size than LP conjugates after gold nanoparticles functionalization. LP conjugates presented a final size of 20.3nm, increasing 1nm respect the gold nanoparticles (19.3nm) and HP conjugates increased 2.2nm with a final size of 21.5nm.

In the case of ζ-Potential, LP conjugates experienced an increment of negative surface charge of 6.7mV changing from -46.1mV in the case of gold nanoparticles to -52.8mV in the case of LP conjugates. This change is related with a decrease in the conductivity of the media, which generates an increase in the surface charge. In contrary, HP conjugates suffered a decrease of negative surface charge varying 8.9mV from -46.1mV to -37.2mV. This could be related with a higher loading of peptides, which would contribute with neutral charge, onto the gold nanoparticles surfaces.

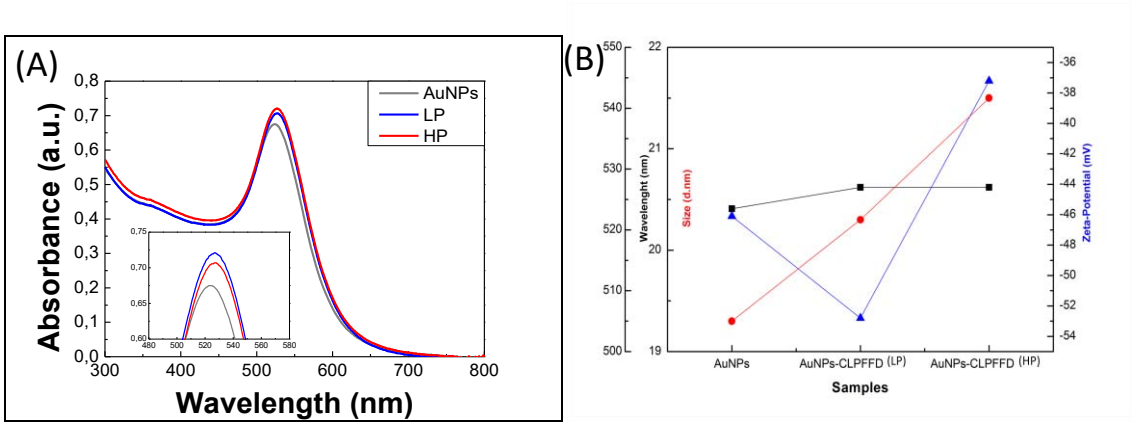

Figure 3.31.: (A) UV-Vis spectra characterization of Au NPs and Peptide-conjugated gold nanoparticles. **(B) Peak Position, DLS and ζ-Potential characterization** of Au NPs and Peptide-conjugated Au NPs (LP and HP conjugate types).

Chemical characterization

Peptide-conjugated gold nanoparticles can be also chemically characterized while exposing them against NaCN-induced digestion. The digestion time of the gold nanoparticles will be determined by the peptide coverage onto their surfaces.

Depending on their final conformation, conjugates will present different rate of decomposition against NaCN digestion.

In this sense, both types of conjugates (LP and HP) present similar behavior against NaCN digestion (Figure 3.32.). A slightly higher resistance against digestion was observed in the case of HP conjugates, presenting a digestion time curve against NaCN with higher absorbance values in the first 50 minutes of reaction. This behavior of HP conjugates against NaCN could be correlated with a more dense coating of peptides onto the gold nanoparticles surfaces.

The rate of decomposition can be quantified by measuring the time-dependent decrease of the SPR absorbance band and fitting it to a first-order exponential decay function where t_D is the decay time and y_0 is the absorbance value at t=0.

$$y = y_0 \times \exp\left(-\frac{t}{t_D}\right)$$

LP conjugates present a faster rate of decomposition against NaCN digestion (0.8 minutes) than HP conjugates (11.5) minutes.

Changes seem not to be as critical as in the case of MUA-conjugated gold nanoparticles where differences in digestion between LP and HP conjugates were more evident, likely due to the inhabillity of the peptide to make high dense self assembled monolayers (SAMs) .

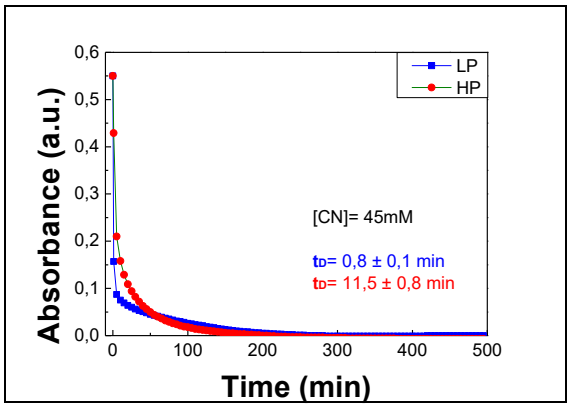

Figure 3.32.: Rate of decomposition of Peptide-conjugated Au NPs by measuring the digestion time of conjugates against NaCN.

Biological Characterization

Samples were exposed to complete cell culture medium (c-CCM) in order to generate a Protein Corona onto the gold and Peptide-conjugated gold nanoparticles surfaces. Differences in protein absorption onto conjugates surface, LP and HP types, were explored.

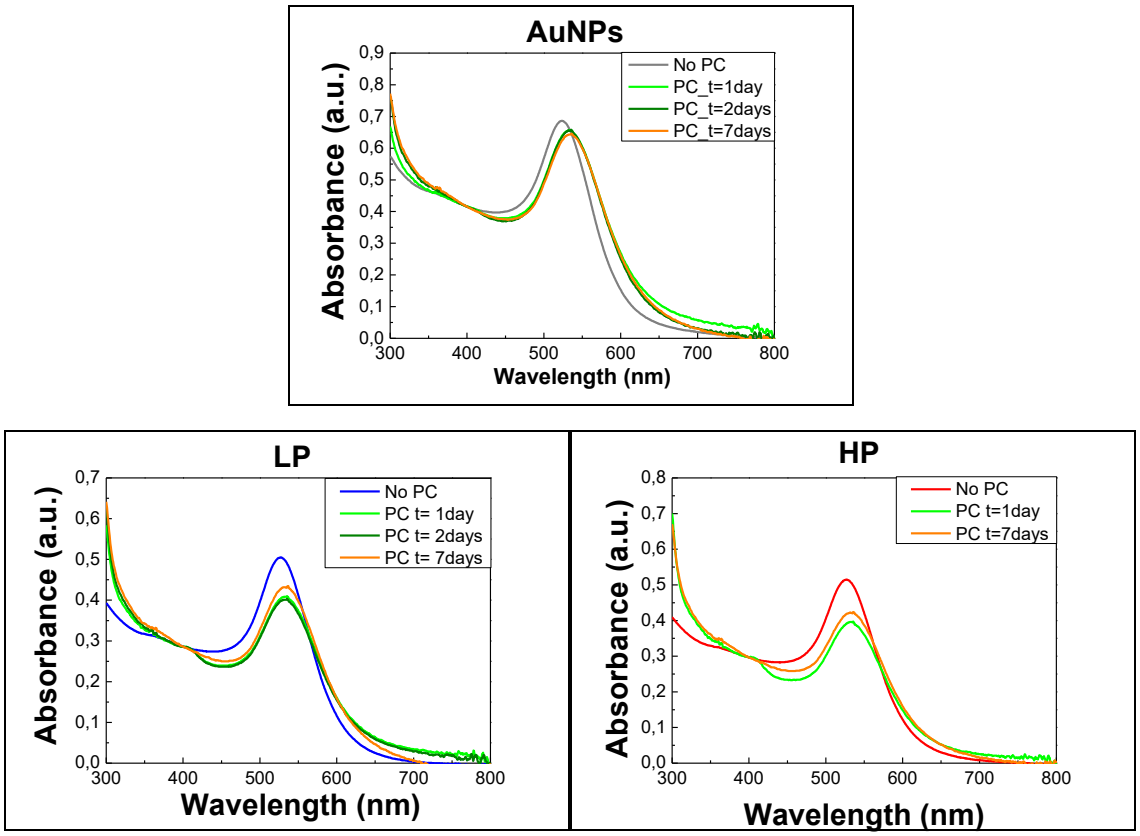

Figure 3.33.: Analysis of Protein Corona formation onto AuNPs and Peptide-conjugated AuNPs (LP and HP types). Absorbance of HP conjugate at 2days of incubation in c-CCM was not possible to measure.

The Protein Corona formation was characterized by UV-Vis spectroscopy (Figure 3.33.). A red-shift in the SPR band was observed after incubation of samples in c-CCM for 1, 2 and 7 days. A decrease in the absorbance of the SPR band can be related to the mild increase of absorbance beyond 600nm indicative of a little bit of possible aggregation.

As it can be observed in Figure 3.34., the increment of peak position in the SPR spectra after Protein Corona formation at 7 days of sample incubation in c-CCM was higher in gold nanoparticles (with a red-shift of 12nm) than in conjugates. Depending on the conjugate type, LP or HP, the red-shift experienced was of 9.5nm or 4.5nm, respectively.

This behavior could be correlated with the fact that HP conjugates presented higher value of size as well as less negative surface charge than LP conjugate, which could correspond to higher peptide coverage onto their surfaces and, therefore, higher distance from the gold nanoparticle surfaces to the final terminal peptide groups. At longer distances, smaller increment of SPR band would be recognized due to the absorption of proteins onto the conjugates surface.

For this reason, as HP conjugates would be covered with higher density of peptides, the protein absorption generating the Protein Corona formation would give less red-shift of the SPR band by UV-Vis spectroscopy since the interaction with proteins would take place as longer distances from the gold nanoparticle core of conjugates than in the case of LP conjugates, where proteins will be closer to the nanoparticle surface.

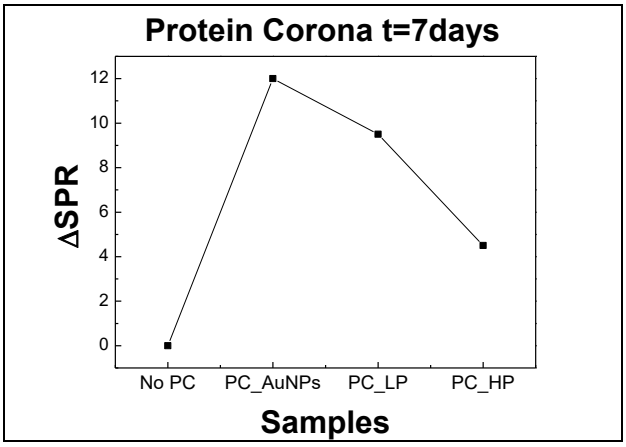

Figure 3.34.: Increment of the SPR band of AuNPs, LP and HP conjugates after Protein Corona formation (at 7 days of incubation in complete cell culture medium). The difference in shift between naked and conjugated NPs is the distance at which the proteins interact with the nanoparticle surface.

3.6.2. Controlling peptide coverage

In order to better study the peptide conjugation procedure, different concentrations of peptide were proved to generate conjugates of gold nanoparticles using the LP method of conjugation, which enables a progressive saturation of the gold nanoparticles surfaces by peptide conjugation. Therefore the control of the peptide gold nanoparticles conjugates using this LP method is of relevant interest. The HP method can not be used to study the kinetics of conjugation since one obtain saturated NPs all the time.

EXPERIMENTAL SECTION

Conjugation

Gold nanoparticles solution was functionalized with CLPFFD-NH_2 peptide through the addition of 2 mL of an aqueous solution of CLPFFD-NH_2 peptide (70µM) dropwise to 5 mL of gold nanoparticle solution (~$3 \cdot 10^{12}$ NPs/mL), following the LP conjugation method procedure. Different final concentrations of peptide gold nanoparticle solution were tested including: 0.2µM, 2µM, 5µM, 10µM, 20µM. The conjugation was carried out by stirring the solution for 15 minutes at room temperature.

Chemical Characterization

Conjugates samples were also analyzed by their resistance to Sodium Cyanide (NaCN)-induced digestion. The more dense coating should work as a better barrier. For this purpose, 1mL of Peptide-conjugated Au NPs of each type of conjugates (LP and HP types) was exposed against NaCN (with a final concentration of 45mM in solution).

Biological Characterization

In order to explore the behavior of conjugates in biological conditions and the consequent Protein Corona (PC) formation, samples were exposed to complete cell cuture medium (c-CCM) consisting in 90% of Dulbecco's Modified Eagle Medium (DMEM) and 10% of Fetal Bovine Serum (FBS). For this purpose, 1mL of each sample

was added to 9mL of c-CCM, followed by incubation at 37°C for 1 and 2 days. Afterwards, samples were purified by centrifugation at 13rpm for 5 minutes and resuspension in sodium citrate (2,2mM) for further characterization by UV-Visible spectrophotometer, DLS and ζ-Potential.

The FBS was previously incubated at 56°C during 30 minutes to deactivate the proteins of the complement system in serum.

RESULTS AND DISCUSSION

Conjugation

The conjugation of the gold nanoparticles solution with CLPFFD-NH_2 peptide was characterized by UV-Vis spectroscopy. The shift of the SPR band observed can be correlated with the concentration of peptide added to generate the peptide conjugated gold nanoparticles.

As it is shown in the following Figure 3.35., which includes three different replicas assays of peptide conjugation, the peak position of the SPR band (originally at 523.5nm before conjugation) increases around 4.5nm as the peptide concentration increases (from 0.2µM to 5µM AuNPs-CLPFFD) until it reaches a value of peptide saturation in which the concentration of peptide does not generate a bigger shift of the SPR band (that maintains at 527nm).

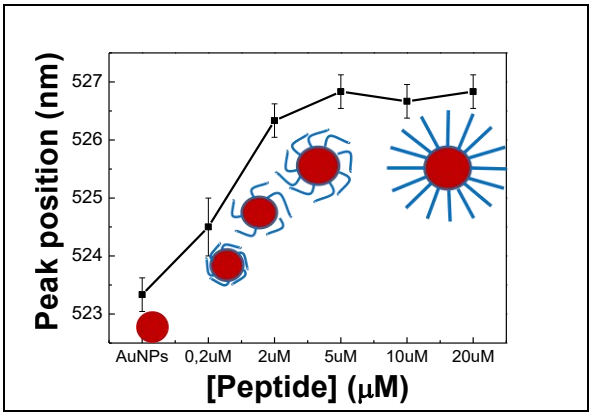

Figure 3.35.: Peak position determination through UV-Vis characterization of gold nanoparticles functionalization at different concentrations of peptide (0.2µM, 2µM, 5µM, 10µM and 20µM). Analysis

is the result of three different replicas assays. Schematic representation of the expected nature of conjugates as the peptide concentration increases.

The shift of the SPR band experienced by the peptide conjugated gold nanoparticles is due to different concentrations of peptide and can be associated to different degrees of conjugation, as it is represented in the above graphic. Higher peptide concentrations that generate bigger shift of the SPR band, corresponds to peptide conjugated gold nanoparticles that are well coated with peptide. These conjugates are considered to present a brush structure of peptides onto the gold nanoparticles surfaces, whereas the conjugates that correspond to lower concentrations of peptide are thought to present a folded structure of peptides onto the gold nanoparticles surfaces generating a smaller shift of the SPR band after the functionalization procedure.

Peptide conjugated gold nanoparticles can be also studied by the analysis of size and surface charge of conjugates by DLS and ζ-Potential measurements. It was expected that conjugate size increased as peptide concentration increases, as well as ζ-Potential changed to less negative surface charge as peptide concentration increases. However, as it can be observed in Figure 3.36., -although three replicas of assays have been done- high variability of results were obtained being difficult to conclude with a size and surface charge evolution in the conjugation procedure. Nevertheless, it seems that there is a change of regime in conjugates at around 5µM of peptide.

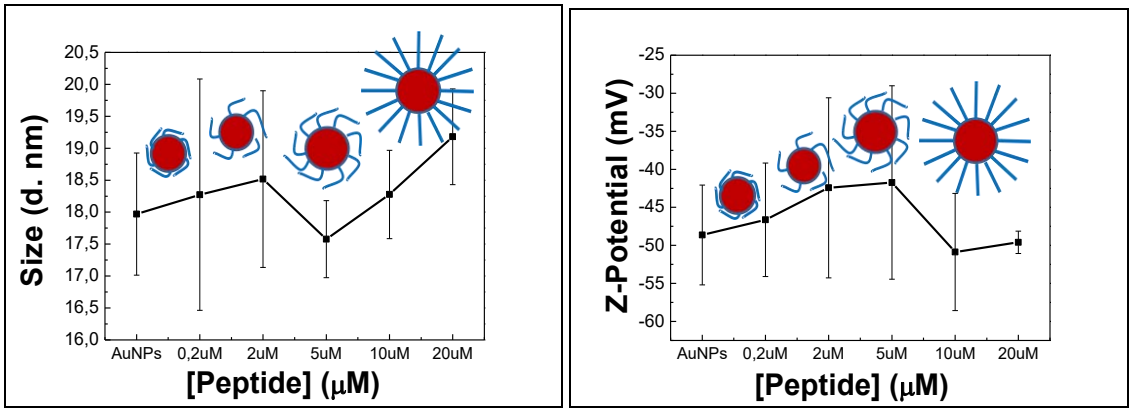

Figure 3.36.: DLS and ζ-Potential characterization of peptide conjugated gold nanoparticles at different concentrations of peptide (0.2µM, 2µM, 5µM, 10µM and 20µM). Analysis is the result of three different replicas assays. Schematic representation of the expected nature of conjugates as the peptide concentration increases.

Chemical characterization

Gold nanoparticles functionalized with CLPFFD-NH_2 peptide were exposed against NaCN-induced digestion in order to study the coverage of peptides onto the gold nanoparticles.

The time of digestion could be quantified by measuring the time-dependent decrease of the SPR absorbance band and fitting it to a first-order exponential decay function where t_D is the decay time and y_0 is the absorbance value at t=0.

$$y = y_0 \times \exp\left(-\frac{t}{t_D}\right)$$

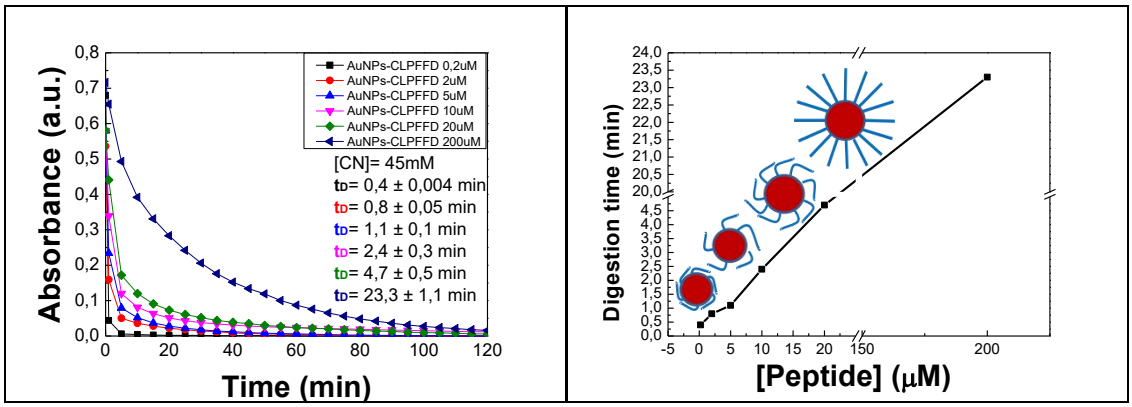

Figure 3.37.: NaCN digestion of peptide conjugated gold nanoparticles at different concentrations of peptide (0.2μM, 2μM, 5μM, 10μM, 20μM and 200μM). Schematic representation of the expected nature of conjugates as the peptide concentration increases.

Figure 3.37. represents the evolution of the maximum absorbance peak of the SPR band. A decrease in the absorbance value can be detected as the digestion time increases. This evolution corresponds to the disappearance of gold nanoparticles as they are digested by the NaCN added.

The rate of digestion, quantified by the time-dependent measurements, shows a clear dependence with the concentration of peptide used for the conjugation with gold nanoparticles. The digestion time (t_D) increases as the peptide concentration does. This can be correlated with the coverage of peptide over the gold nanoparticles surfaces: as the peptide concentration increases, higher is the coverage of gold nanoparticles

surfaces by peptide. Consequently, higher is the protection that gold nanoparticles present against NaCN digestion.

Each conjugate (AuNPs-CLPFFD) can present different rates of surface coverage as they are conjugated with different peptide concentrations that determines the final configuration of conjugates. Therefore, the conjugation is determined by the peptide concentration that results critical for the nature of final conjugates.

The digestion time is expected to reach stability in conditions of peptide saturation, where the Au NP surface will be fully coverage. Under these conditions, any increment in peptide concentration will not generate higher surface coverage that could increase the protection of gold nanoparticles. These states of fully peptide coverage over gold nanoparticles can be determined analyzing the digestion time: no increase in digestion time will appear when the surface is saturated of peptides.

Although at the concentration of 20µM of peptide, the saturation of conjugates was achieved by UV-Vis spectra analysis, a ten times higher concentration of peptide (200µM) was tested in order to explore the potential of peptides to cover and protect the gold nanoparticles surface to be digested. At the mention concentration of peptides, the digestion of the conjugates was almost 5 times slower. As conjugates were not purified from the excess of non conjugated peptide present, the increase of peptide far from the surface saturation shows an increased stability that could be due to multilayered covering of the nanoparticle surface.

Biological Characterization

The absorption of proteins generating the Protein Corona onto gold nanoparticles peptide conjugated gold nanoparticles at concentrations of 0.2µM, 2µM, 5µM, 10µM and 20µM was explored by UV-Vis spectroscopy, as it is shown in Figure 3.38. As expected, the red-shift of the SPR band experienced after Protein Corona formation is higher in gold nanoparticles than conjugates.

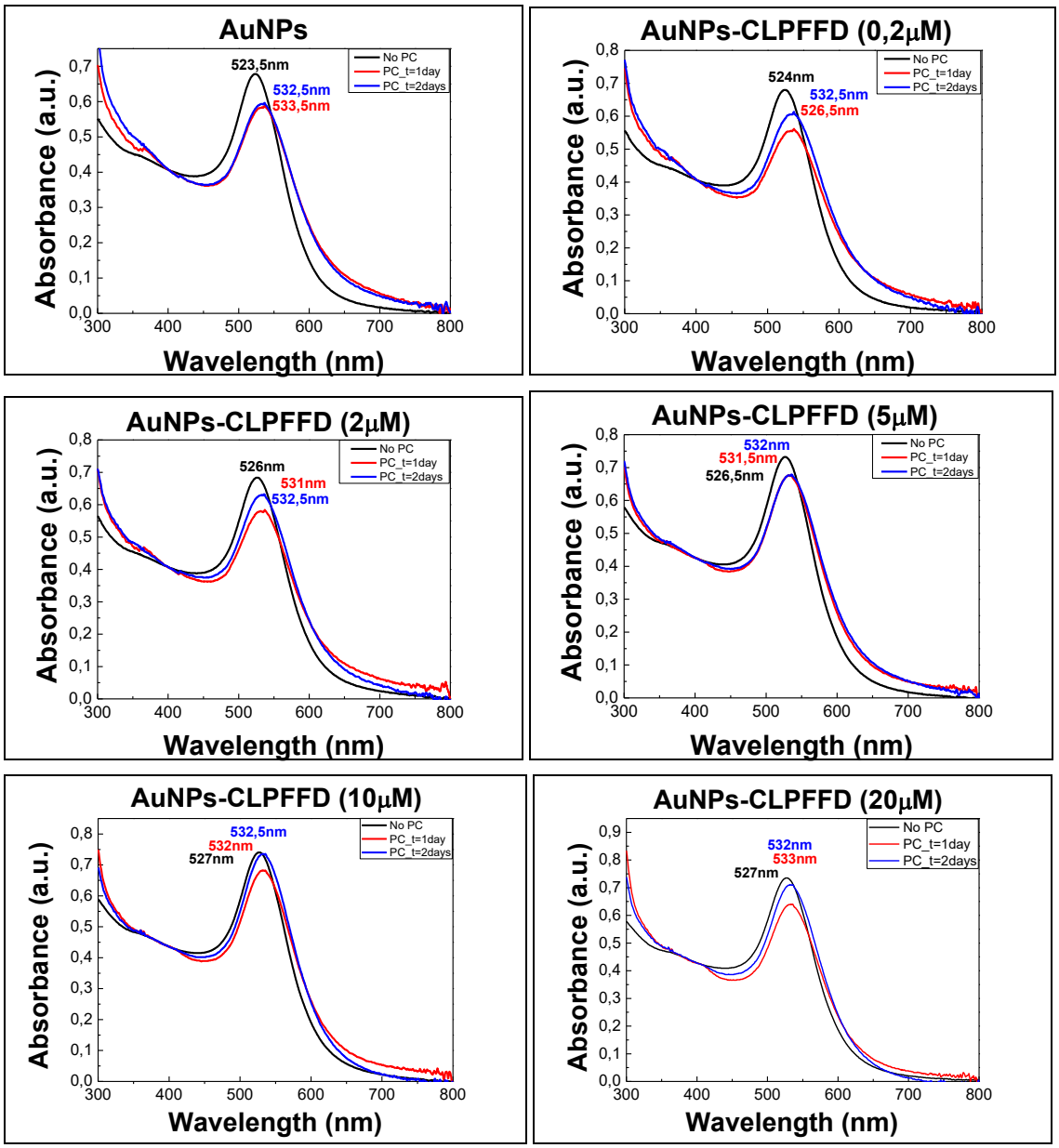

Figure 3.38.: UV-Vis spectra characterization of Protein Corona formation onto gold nanoparticles and peptide conjugated gold nanoparticles at concentrations of 0.2μM, 2μM, 5μM, 10μM and 20μM and incubation times in complete cell culture medium of 1 days and 2 days.

The protein corona formation over peptide conjugated gold nanoparticles can be studied by the shift of the SPR band (ΔSPR) experienced in the UV-Vis spectroscopy (Figure 3.39.).

As the peptide concentration of conjugates increases, the ΔSPR decreases. This can be related to different natures of peptide conjugated gold nanoparticles:

Higher concentrations of peptide generate better coverage onto the gold nanoparticle surface and produce a brush structure of peptides onto gold nanoparticles increasing the distance of terminal groups of peptides respected to the gold nanoparticle surface.

On the other hand, lower concentrations of peptides generate folded structures of conjugates where peptides maintain creased in the vicinity of the gold nanoparticle surface. Consequently, bigger changes of ΔSPR will correspond to shorter distance from the gold nanoparticle surface to the global structure of conjugates.

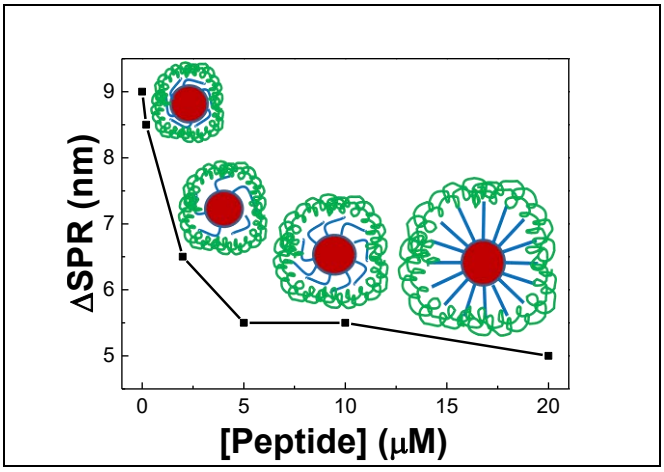

Figure 3.39.: Protein Corona formation onto peptide conjugated gold nanoparticles at different concentrations of peptide (0.2μM, 2μM, 5μM, 10μM and 20μM) based on the ΔSPR band at 2 days of incubation in complete cell culture medium. Schematic representation of the expected nature of conjugates as the peptide concentration increases.

Additionally, the size and surface charge of gold nanoparticles and conjugates after Protein Corona generation can be measured by DLS and ζ-Potential (Figure 3.40.).

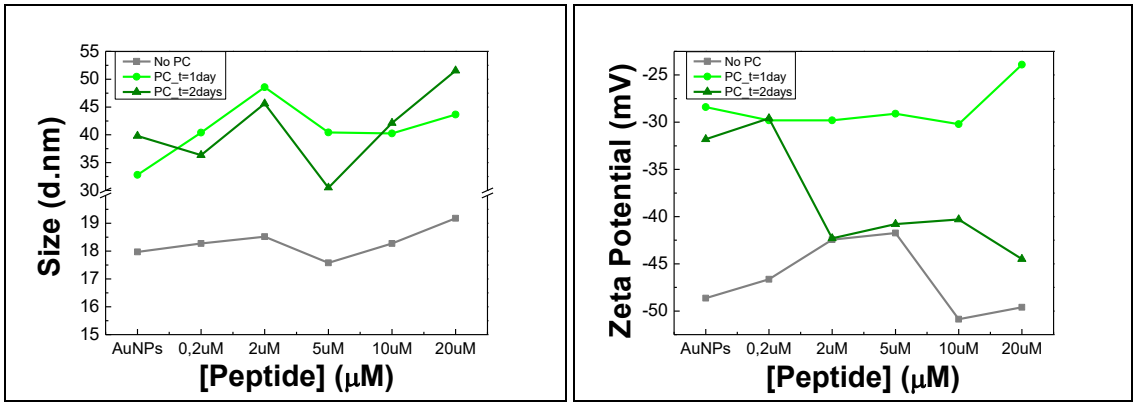

Figure 3.40.: DLS and ζ-Potential characterization before and after Protein Corona formation onto bared gold nanoparticles and peptide conjugated gold nanoparticles at different concentrations of peptide (0.2μM, 2μM, 5μM, 10μM and 20μM) and incubation times (1 day and 2 days) in complete cell culture medium.

Regarding the DLS of peptide conjugates, size after Protein Corona formation follows a similar evolution of sizes of conjugates (as concentration of peptide increases) before exposure to complete cell culture medium. At the highest concentration of peptide in conjugates tested (20µM) as well as in the case of bared gold nanoparticles, the Protein Coronas generated at 2 days of incubation in complete cell culture medium present higher size than the one obtained at 1 day.

After Protein Corona formation, the surface charge of bared gold nanoparticles present less negative values of ζ-Potential due to the protein coverage onto nanoparticles. In the case of conjugates, since the peptide will confers a more neutral charge, the surface charge increase in negativity once Protein Corona is formed onto conjugates.

It is expected that the Protein Corona will be less stable (less 'Hard') in these conditions of peptide conjugation than when compared to MUA-conjugated gold nanoparticles. Since the MUA layer is more ordered and more dense and the peptide one is more disordered and less dense, so the hardening of the protein corona is not as favored.

3.7. Conclusions

The reactive characterization has lead to a better approach of conjugates states through the study of stability against salt and their resistance to NaCN-induced digestion.

On the one hand, conjugates at time zero present a higher stability against salt and corrosion at LP type configuration. At this LP state, conjugates present higher surface charge than HP type (as it was shown in the static characterization section). Therefore, it can be concluded that the increase of surface charge is related to protection of conjugates. It is consistent since surface charge can be attributed to coverage of MUA molecules onto the gold nanoparticles conjugates. As higher is the surface charge, higher is the number of MUA molecules that are expected to be contributing to the coverage of conjugates.

On the other hand, both LP and HP conjugates types after 7 days from the conjugation, evolve towards similar states that present higher stability against the highest concentration of salt analyzed. This is consistent to the similar values of surface charges that conjugates presented through ζ-Potential values after time evolution. Again, surface charge can be correlated to the arrangement and subsequently protection of MUA molecules onto the gold nanoparticles surface.

Regarding resistance against NaCN-induced digestion, HP conjugates evolve to a more stable state than the one presented at time zero. However, LP conjugates type evolve to a less stable state after 7 days of evolution from the conjugation process compared to the resistance that this LP conjugates type experienced at time zero.

Nevertheless, LP conjugates at 7 days after conjugation evolve towards a state that generated a similar resistance against NaCN digestion to the one that HP conjugates presented at 7 days of time evolution.

Consequently, it can be concluded that both types (LP and HP) of conjugates evolve, in an environment of excess of MUA molecules, towards a similar state of MUA-conjugated gold nanoparticles that generate similar responses of stability against salt and resistance to cyanide corrosion.

During mixing, concentration varies in such a way that until homogenization is reached, the initial drops of gold nanoparticles solution find a high MUA concentration. Additionally, the initial gold nanoparticles have more MUA molecules available while the reaction mixture dilutes. Thus it may not be the same that a gold nanoparticles status in an endless MUA solution than a MUA molecule falls down onto an ocean populated with gold nanoparticles.

This hypothesis about the influence of the conjugation method was also analyzed with CLPFFD-NH_2 peptide, which would be of biomedical interest having implications in Alzheimer disease. The nature of the peptide conjugates seemed to be related to the way of addition of elements in the functionalization procedure.

The progressive evolution towards saturation of peptide in conjugates was also tested. The control of the loading of peptides would generate different nature of conjugates that would react, depending on the coverage of peptides onto the nanoparticle surfaces, giving a different protection response against cyanide decomposition or protein corona formation in biological medium.

3.8. References

1. E. Casals, V. F. Puntes, Inorganic nanoparticle biomolecular corona: formation, evolution and biological impact. *Nanomedicine* **7**, 1917–1930 (2012).
2. C. Ge *et al.*, Towards understanding of nanoparticle–protein corona. *Arch Toxicol* **89**, 519–539 (2015).
3. D. Docter *et al.*, No king without a crown – impact of the nanomaterial-protein corona on nanobiomedicine *Nanomedicine (Lond.)* **10**, 503–519 (2015).
4. M. A. Dobrovolskaia, S. E. McNeil, *Immunological properties of engineered nanomaterials Nature Nanotechnology* **2**, (2007).
5. N. G. Bastús *et al.*, Homogeneous Conjugation of Peptides onto Gold Nanoparticles Enhances Macrophage Response. *ACS Nano* **3**, 1335–1344 (2009).
6. E. Casals *et al.*, Inorganic nanoparticles and biology. *Contributions to science* **4**, 171-176 (2008).
7. J. Comenge *et al.*, Detoxifying Antitumoral Drugs via Nanoconjugation: The Case of Gold Nanoparticles and Cisplatin. *Plos One* **7**, (2012).
8. D. F. Moyano *et al.*, Nanoparticle hydrophobicity disctates immune response. *Journal of the American Chemical Society* **134**, 3965−3967 (2012).
9. I. Hamad *et al.*, *ACS Nano* **4**, 6629–6638 (2010).
10. J. Comenge, V. F. Puntes, The role of PEG conformation in mixed layers: from protein corona substrate to steric stabilization avoiding protein adsorption. *ScienceOpen Research*, (2015).
11. J. Comenge, V. F. Puntes, Stabilizing Gold Nanoparticle Bioconjugates in Physiological Conditions by PEGylation. *Nanomaterial Interfaces in Biology: Methods and Protocols* **1025**, 281-289 (2013).
12. J. C. Love, L. A. Estroff, J. K. Kriebel, R. G. Nuzzo, G. M. Whitesides, Self-Assembled Monolayers of Thiolates on Metals as a Form of Nanotechnology. *Chemical Reviews* **105**, 1103-1170 (2005).
13. H. Sellers, A. Ulman, Y. Shnidman, J. E. Eilerss, Structure and binding of alkanethiolates on gold and silver surfaces: implications for self-assembled monolayers. *J. Am. Chem. Soc.* **115**, 9389–9401 (**1993**).
14. E. J. W. Verwey, J. T. G. Overbeek, Theory of the stability of lyophobic colloids. *Elsevier*, (1948).
15. B. Derjaguin, L. Landau, Theory of the stability of strongly charged lyophobic sols and of the adhesion of strongly charged particles in solution of electrolytes. *Acta Phys. Chem. URSS* **14**, 633-662 (1941).
16. I.-I. S. Lim *et al.*, Adsorption of Cyanine Dyes on Gold Nanoparticles and Formation of J-Aggregates in the Nanoparticle Assembly. *J. Phys. Chem. B* **110**, 6673-6682 (2006).
17. I. Ojea-Jiménez, V. F. Puntes, Instability of Cationic Gold Nanoparticle Bioconjugates: The Role of Citrate Ions *American Chemical Society* **131**, 13320–13327 (2009).
18. B. C. Mei *et al.*, Effects of Ligand Coordination Number and Surface Curvature on the Stability of Gold Nanoparticles in Aqueous Solutions. *Langmuir* **25** 10604–10611 (2009).
19. M.-C. Daniel, D. Astruc, Gold Nanoparticles: Assembly, Supramolecular Chemistry, Quantum-Size-Related Properties, and Applications toward Biology, Catalysis and Nanotechnology. *Chem. Rev.* **104**, 293−346 (2004).
20. S. S. Agasti, C.-C. You, P. Arumugam, V. M. Rotello, Structural control of the monolayer stability of water-soluble gold nanoparticles. *J. Mater. Chem.* **18**, 70-73 (2008).
21. Cyanide (https://en.wikipedia.org/wiki/Cyanide_poisoning). Wikipedia, July 2016.

22. J. M. Amigo *et al.*, Analysis of time-dependent conjugation of gold nanoparticles with an antiparkinsonian molecule by using curve resolution methods *Analytica Chimica Acta* **683**, 170–177 (2011).
23. I. Ojea-Jiméneza *et al.*, Engineered Inorganic Nanoparticles for Drug Delivery Applications. *Current Drug Metabolism* **14** 518-530 (2013).
24. J. Comenge, V. Puntes, Kinetically Controlled Seeded Growth Synthesis of Citrate-Stabilized Gold Nanoparticles of up to 200 nm: Size Focusing versus Ostwald Ripening. *Langmuir* **27** 11098–11105 (2011).
25. E. Casals *et al.*, Hardening of the Nanoparticle–Protein Corona in Metal (Au, Ag) and Oxide (Fe3O4, CoO and CeO2) Nanoparticles. *Small* **7**, 3479-3486 (2011).
26. M. J. Kogan *et al.*, Nanoparticle-mediated local and remote manipulation of protein aggregation. *Nano Letter* **6**, 110-115 (2006).

CHAPTER 4:

APPROACHING NANOSAFETY OF NANOBIOCONJUGATES

CHAPTER 4: APPROACHING NANOSAFETY OF NANOBIOCONJUGATES

4.1. Introduction

The surface state of conjugates will determine their biodistribution and interaction with the body. For this reason, the control conjugation of molecules onto the nanoparticle surface is critical and still challenging to promote or avoid certain cell responses.

Consequently, the study of the structural conformation of inorganic nanoparticles' surface coated with conjugated molecules is of interest. It is difficult to precisely characterize conjugated nanoparticles (NPs) by the standard characterization techniques such as UV-Vis spectroscopy, DLS and ζ-Potential that will generate the same signal response to different methods of conjugation and surface states.

However, differences between conjugates not apparent by physicochemical characterization techniques can appear while studying their behaviour. As it was previously described in Chapter 3, dissimilarities can be detected by analysing their colloidal stability against aggregation by NaCl and their resistance to corrosion by NaCN-induced digestion, as well as their interaction with proteins generating the Protein Corona (PC) onto conjugates in cell culture medium.

The coating density of molecules onto NPs' surface will generate differences in conjugates that have an enormous impact in biology. Samples that were thought to be equal demonstrate a completely different behaviour that will determine the biodistribution and toxicity[(1)].

Particularly, it is well known that cells from the immune system can distinguish a pathogen as non self by the subcellular location and the structural conformation of its molecules. This is consistent with the detection of repetitive patterns in large

structures such as in a virus capsid. For this reason, immune cells are believed to be able to detect differences in the structural conformation of conjugated nanoparticles that cannot be clearly detected by other methods.

This is fundamental to better understand the nanosafety of conjugated nanoparticles. For this purpose, inorganic gold nanoparticles of around 10 nm of size were conjugated with 11-mercaptoundecanoic acid (MUA) molecules following two different procedures (LP and HP methods, already described in Chapter 3). The aim of the study was to identify differences in the surface charge of conjugates type LP and HP observed directly after preparation and one week later. Differences could influence the protein corona composition and generate a different uptake and immune response by monocytes.

The Protein Corona of conjugates will be characterized by Differential Centrifugal Sedimentation (DCS) as well as by proteome analysis Liquid Chromatography-Mass Spectroscopy (LC-MS). In addition, LPS detection on samples will be done to avoid a false positive result in cell studies and the cytokines production by immune cells against conjugates will be analysed as a correlation to their surface molecular conformation.

4.2. Generation of functionalized gold nanoparticles

EXPERIMENTAL SECTION

Synthesis of gold nanoparticles

A solution of 2.2mM sodium citrate tribasic dihydrate (Sigma-Aldrich, Saint Louis, USA, S4641) in 150ml Milli-Q® water (Millipore Corporation, Molsheim, France, ultrapure water with a resistance of 18.2 MΩ.cm) was heated with a heating mantle in a 250 ml three-necked round-bottomed flask for 15 minutes under vigorous stirring. A condenser was utilized to prevent the evaporation of the solvent.

After boiling had commenced, 1ml of a 25mM $HAuCl_4$ solution was injected (Sigma-Aldrich, 520918). The color of the solution changed from yellow to dark gray which indicates that nucleation of gold nanoparticles (NPs) is taking place, and then to red in 10 minutes. The resulting particles (~12 nm, ~$3 \cdot 10^{12}$ NPs/mL) are coated with negatively charged citrate ions and, hence, are well suspended in milli-Q water.

Conjugation with 11-Mercaptoundecanoic acid

Once gold NPs are synthesized, a process of conjugation between gold NPs dispersion (~$3 \cdot 10^{12}$ NPs/mL) and an aqueous solution of 98% 11-Mercaptoundecanoic acid (MUA, Sigma-Aldrich, 674427) molecules was carried out. Some drops of 2M sodium hydroxide (NaOH) (Sigma-Aldrich, 221465) were added to MUA solution to promote the dissolution process of MUA molecules. Final concentration of NaOH in MUA solution was approximately 15mM and pH=8.

Two different methods of conjugation have been explored. In the first method, called low pressure (LP), 2mL of an aqueous solution of 0.35mM MUA was added to 5mL of gold nanoparticle dispersion (~$3 \cdot 10^{12}$ NPs/mL). In the second method, called high pressure (HP), the order of admixture in the conjugation procedure was inverted. Here, the conjugation process comprised the addition of 5 mL of gold NPs dispersion (~$3 \cdot 10^{12}$ NPs/mL) to 2 mL of the aqueous solution of 0.35 mM MUA. The gold NPs were added to this solution drop by drop over three to five minutes. The final concentration of MUA in each gold nanoparticle dispersion was 0.1 mM. Both methods of

conjugation were stirred for one hour at room temperature generating fresh conjugates. Exposure of the conjugates within the excess of MUA in solution was carried out for 7 days at room temperature to generate aged MUA-conjugated gold nanoparticles.

Purification and concentration of gold nanoparticles

Naked (unconjugated) and MUA-conjugated gold nanoparticles were purified and concentrated up to 1g/L final concentration (corresponding the initial concentration of ~$3 \cdot 10^{12}$ NPs/mL to 0.0328g/L) by Amicon Ultra Centrifugal filter Units of 10 KDa (Merck Millipore, Darmstadt, Germany) for 10 minutes at 4500×G.

RESULTS AND DISCUSSION

Monodisperse citrate-stabilized gold nanoparticles (Au NPs) with an uniform quasi-spherical shape of ~12 nm and a narrow size distribution were synthesized following a kinetically controlled seeded growth strategy via the reduction of $HAuCl_4$ by sodium citrate[(2)].

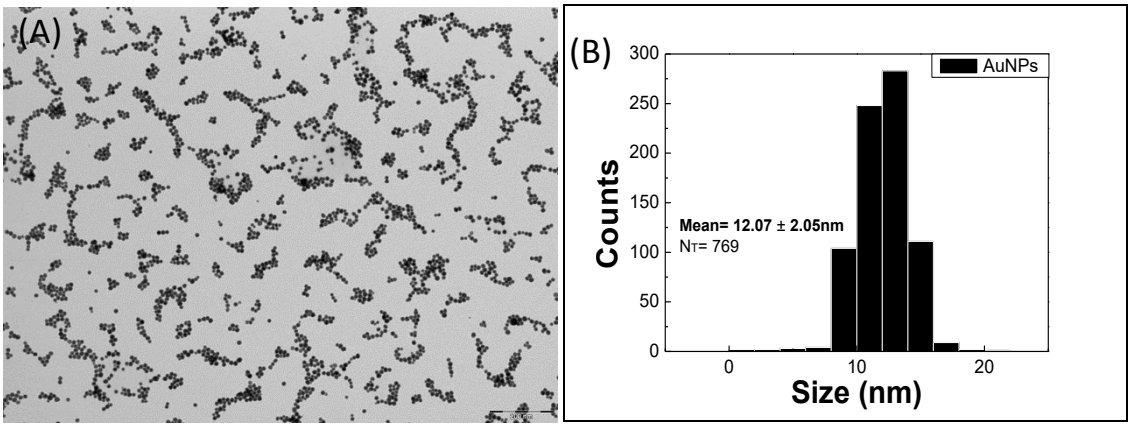

Figure 4.1.: Transmission electron microscopy (TEM) images (A) and Size distribution (B) of monodispersed citrate-stabilized ~12 nm gold nanoparticles prepared by the sodium citrate reduction of hydrogen tetrachloroaurate. The colloid (~$3 \cdot 10^{12}$ NP/mL) was dropcasted onto a Formvar carbon-coated copper grid for microscopy observation. The bar in TEM image indicates 200nm.

As-synthesized gold nanoparticles were further conjugated with MUA molecules trough two different conjugation methods (LP and HP). As it can be observed in Figure 4.2., SPR spectra present a red-shift of around 6nm after conjugation, while absorbance decreases due to dilution of samples after the mixture between gold nanoparticles and MUA solution. No clear differences were observed between conjugates by UV-Vis spectroscopy characterization.

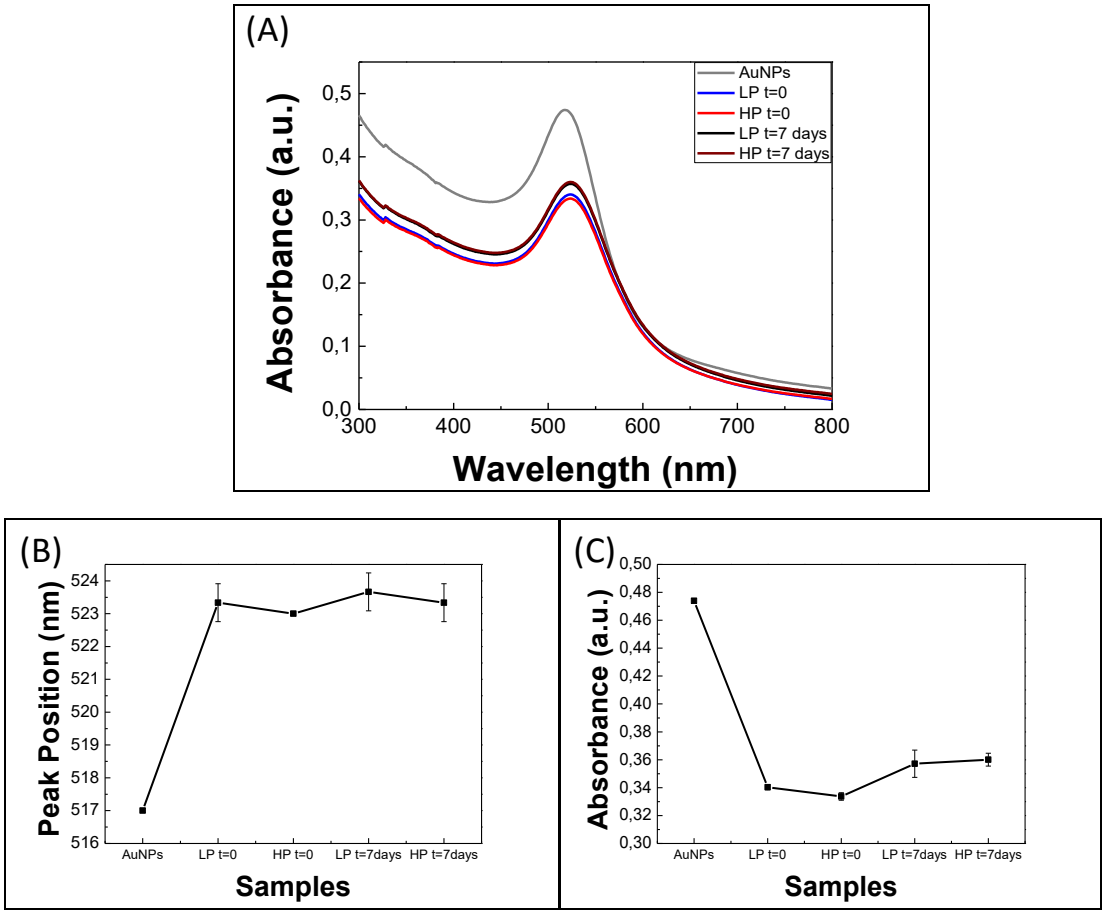

Figure 4.2.: (A) UV-Vis spectra of gold nanoparticles and MUA-conjugated gold nanoparticles (LP and HP types) at time zero and after 7 days of evolution. **(B) Peak positon and (C) Absorbance** characterization.

Samples were characterized by DLS and ζ-Potential (Figure 4.3.), where differences between conjugates could not be determined. The increase of the hydrodynamic radius after conjugation was around 2.5nm for both conjugates types. The surface charge values had high variability with a decrease of the negative charge after conjugation. This behavior could be related with an increase in the conductivity of the media.

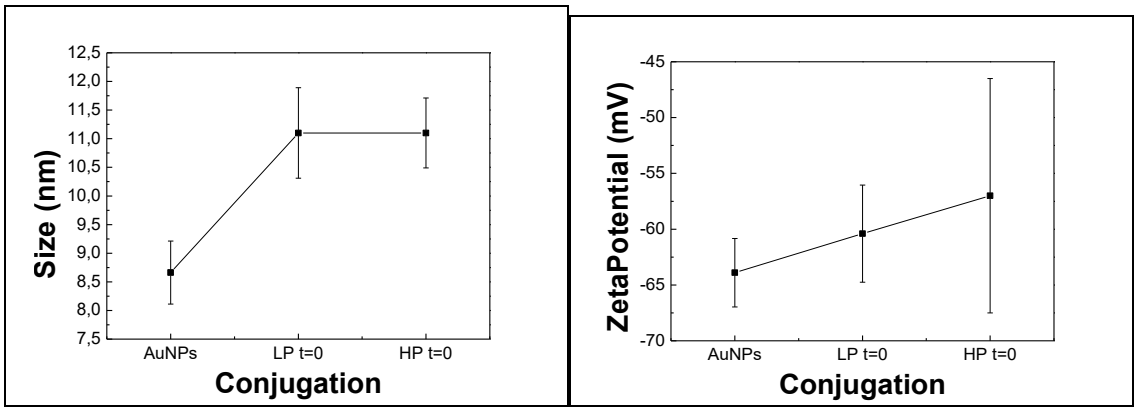

Figure 4.3.: (A) DLS and (B) ζ-Potential characterization of MUA-conjugated Au NPs. An increase in the hydrodynamic radius of around 2,5nm is experienced after conjugation of gold nanoparticles with MUA molecules. A decrease in the charge intensity is experienced after conjugation.

In order to explore dissimilarities in sizes, samples were also analyzed by Differential Centrifugal Sedimentation (DCS). This technique provides higher resolution than Dynamic Light Scattering (DLS) and can detect and resolve peaks down to 2nm.

However, no differences in size could be observed between conjugates as Figure 4.4. presents. The widest peak corresponds to gold nanoparticles and the others, which give the same peak signal, to conjugates generated through LP and HP conjugation methods. Fresh and aged conjugates states are measured. All explored samples obtained the same size value of 9.5nm after DCS characterization.

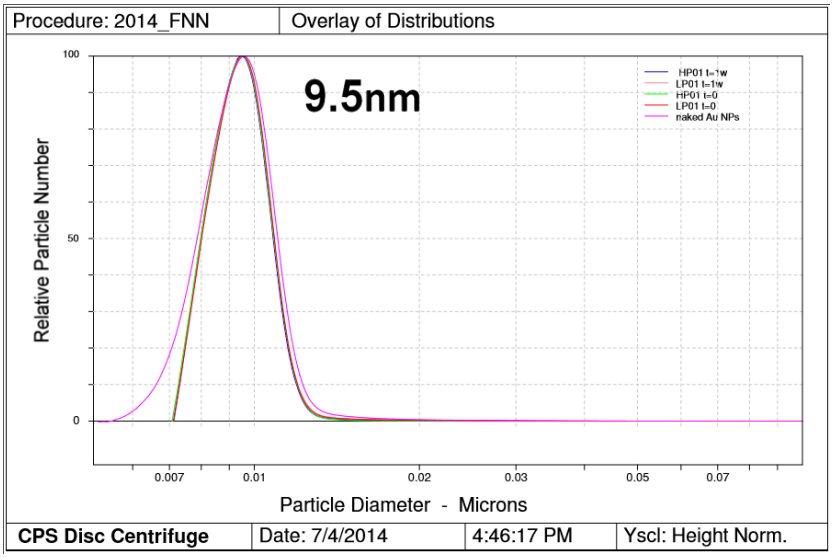

Figure 4.4.: DCS characterization of gold nanoparticles and MUA-conjugated gold nanoparticles (LP and HP types) at time zero and after 7 days of time evolution.

4.3. Cytotoxicity assessment

EXPERIMENTAL SECTION

Cell culture

The human monocytic THP-1 cell line was obtained from American Type Culture Collection (ATCC number: TIB-202, LGC Promochem, Teddington, UK). Cells were grown in complete cell culture medium (c-CCM) containing 89% RPMI Medium 1640 with GlutaMAX™-I and 25 mM HEPES (Gibco, Paisley, UK), 10% Fetal Bovine Serum (PAA Laboratories GmbH, Cölbe, Germany), 1% penicillin (5000 U/ml)-streptomycin (5000 µg/ml) (Gibco) and 0.05 mM β-mercaptoethanol (Sigma-Aldrich). Cells were maintained in a humidified atmosphere at 37 °C and 5% CO_2 and subcultured every 3-4 days.

Cytotoxicity assessment

One day before exposure, 5×10^4 cells were seeded in each well of 96-well conical bottom (V) microtiter plates (Greiner Bio-One, Alphen aan de Rijn, The Netherlands). Thereafter, cells were exposed to different doses (0, 1, 10, 25, 50 and 100µg/mL) of fresh and aged gold nanoparticle conjugates (LP and HP types), naked gold nanoparticles, MUA, sodium citrate and lipopolysaccharide (LPS, Sigma-Aldrich). As a positive control for cytotoxicity, cells were exposed to 50-nm sized amino-modified polystyrene nanoparticles (PS-NH_2, Polysciences, Warrington, USA) which have been reported to cause mitochondrial damage and induce cell death by apoptosis[(3)]. After 24 hours of exposure, cytotoxicity assessment was performed by means of MTS, alamarBlue® and neutral red assays.

The MTS assay (CellTiter 96® Aqueous One Solution Cell Proliferation Assay Kit, Promega, Madison, USA) was performed according to the manufacturers' guidelines. Cells were pelleted at the V-bottom of the microtiter plate by centrifugation for 5 minutes at 150×G. Thereafter, the culture medium containing the exposure items were discarded and cells were washed with phosphate buffer saline containing no Ca^{2+} or Mg^{2+} (PBS^-, Gibco). Next, cells were resuspended in MTS reagent which was obtained by mixing 1.65 parts of Aqueous One Solution Reagent with 8.35 parts of c-CCM. Cells

were subsequently incubated at 37°C for one hour in a humified CO_2 atmosphere. After that, cells were pelleted by centrifugation at 150G for 5 minutes. The supernatant was transferred to new 96-well flat bottom (F) microtiter plate and the absorbance was measured at 492 nm using a microtiter plate reader (Multiskan Ascent, Thermo Fisher, Waltham, USA).

The alamarBlue® (Invitrogen, Carlsbad, USA) and neutral red assay (Sigma-Aldrich) were conducted consecutively on the same set of microtiter plates and according to the manufacturers' guidelines. After exposure, cells were pelleted by centrifugation at 150G for 5 minutes. Thereafter, the culture medium containing the exposure items were discarded and cells were rinsed with PBS^-. Next, cells were resuspended in fresh complete cell culture media supplemented with 5% alamarBlue® solution and 1.25% neutral red medium and incubated at 37°C for two hours in a humified CO_2 atmosphere. Thereafter, cells were pelleted by centrifugation at 150G for 5 minutes. The supernatant was transferred to new 96-well flat bottom (F) microtiter plate and the fluorescence of alamarBlue® was measured at the respective excitation and emission wavelength of 530 nm and 595 nm using a microtiter plate reader (FluoroSkan Ascent, Thermo Fisher). The cell pellet was resuspended and rinsed with PBS^-. Thereafter, cells were again pelleted and resuspended in colour removal solution which is composed of 10% glacial acetic acid (Merck Millipore) and 90% ethanol (Merck Millipore). Cells were incubated for 10 minutes at room temperature on a shaking platform. Thereafter, cells were pelleted by centrifugation at 150G for 5 minutes. The supernatant was transferred to new 96-well flat bottom (F) microtiter plate and the neutral red fluorescence was subsequently measured using the same instrument, at the respective excitation and emission wavelength of 530 nm and 620 nm.

Endotoxin detection

The presence of Gram-negative bacterial endotoxin in the gold nanoparticles solution, MUA and sodium citrate was investigated using the endpoint chromogenic Limulus Amebocyte Lysate (LAL) Test (Lonza, Walkersville, USA) according to the

manufacturers' guidelines. The absorbance was measured at 405 nm using a microtiter plate reader (Multiskan Ascent).

RESULTS AND DISCUSSION

After MTS cytotoxic assay, no cytotoxic effect was determined in monocytes when exposing cells to gold nanoparticles or MUA-conjugated gold nanoparticles. Both LP and HP conjugate types were explored, at time zero of conjugation and at 7 days of time evolution.

As it can be observed in Figure 4.5., cell viability is not compromised against MUA or Sodium Citrate control solutions. However, cell viability drastically decreases while exposing cells to positive control of amino-modified polystyrene nanoparticles (PS-NH_2 NPs), indicating that the MTS analysis was being carried out correctly.

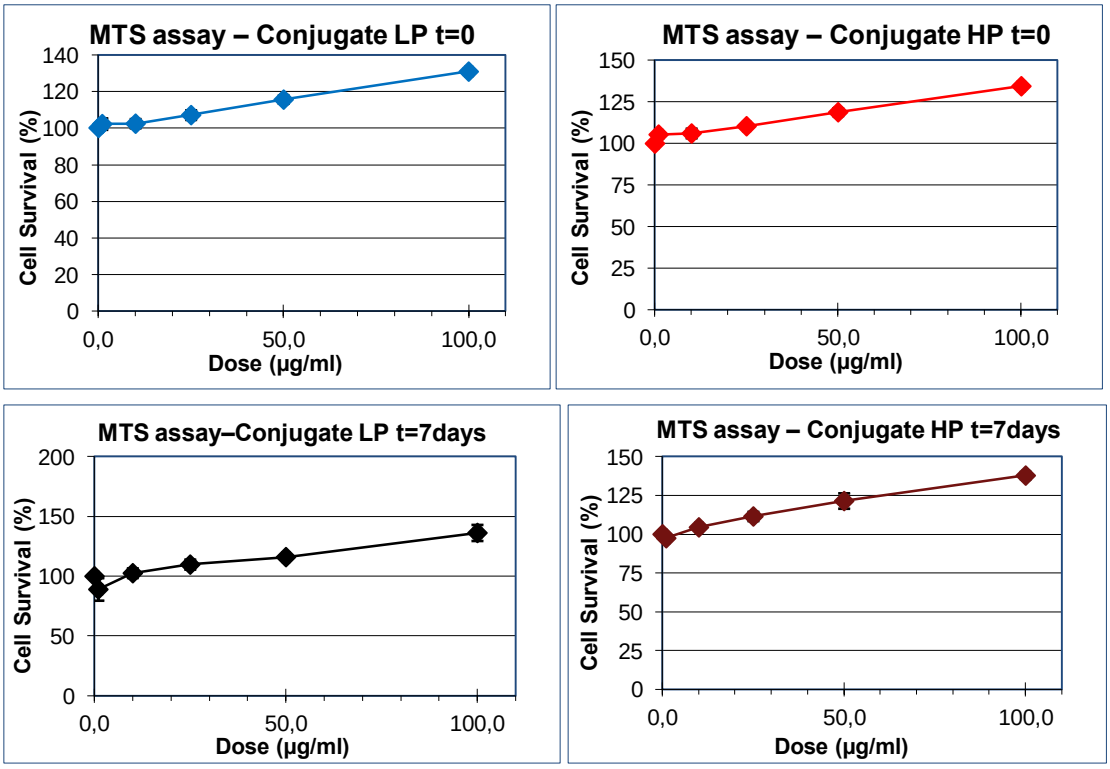

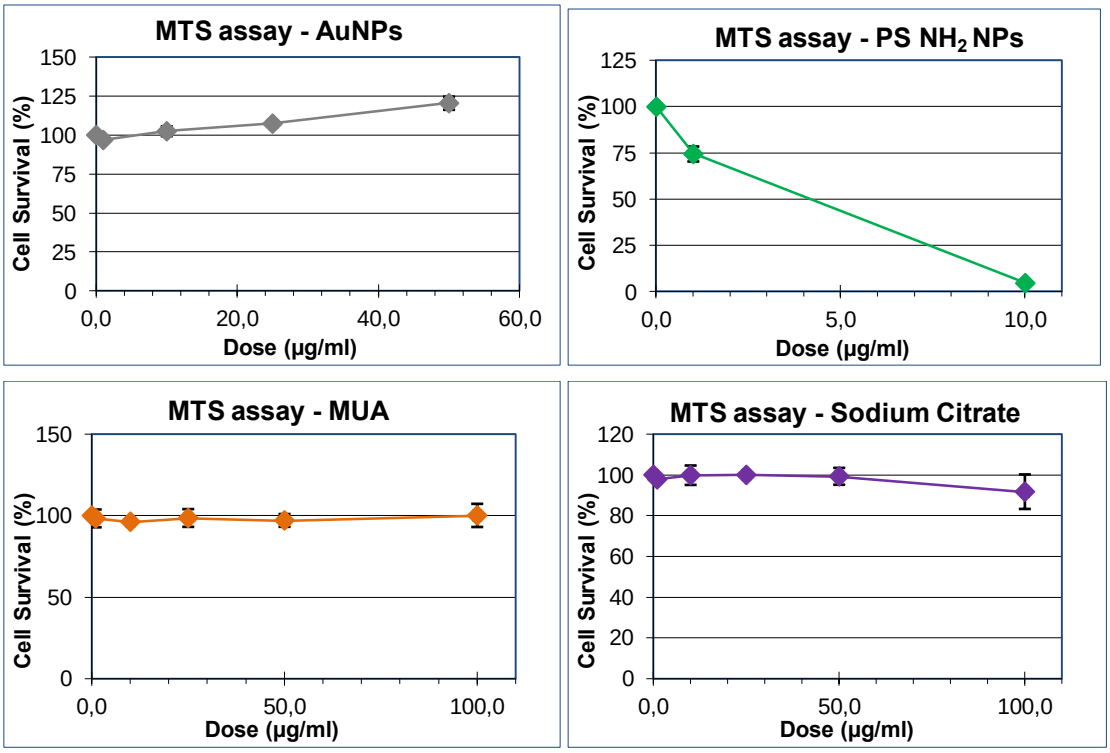

Figure 4.5.: MTS cytotoxic assay of gold nanoparticles and MUA-conjugated gold nanoparticles (LP and HP types) at time zero and after 7 days of time evolution of conjugates. MUA and Sodium Citrate solutions were also tested as well as a positive control of PS-NH_2 NPs.

Cytotoxicity was further analyzed by fluorescence methods such as Alamar Blue and Neutral Red tests (Figure 4.6.). Similar to MTS assay, no cytotoxic effects were determined in monocytes while exposing cells to gold nanoparticles or MUA-conjugated gold nanoparticles. As well as in the case of MUA and Sodium Citrate solution were cell viability was not compromised. The positive control of PS-NH_2 NPs was also used to assess the suitability of the assay.

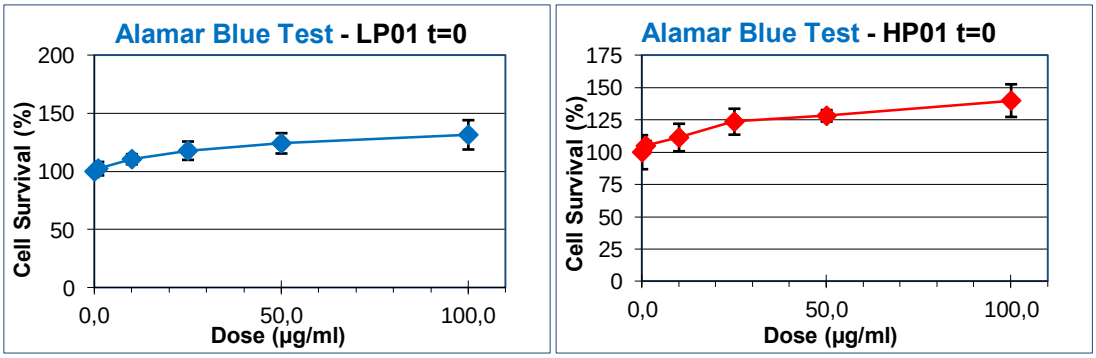

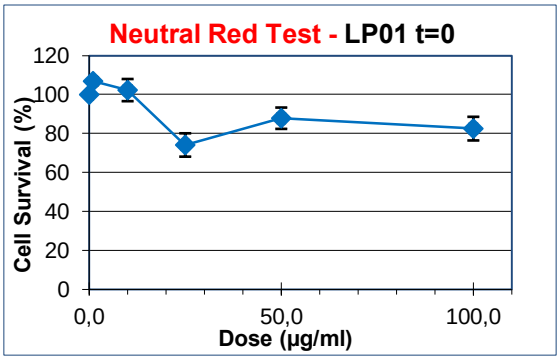
Neutral Red Test - LP01 t=0
Cell Survival (%)
120
100
80
60
40
20
0
0,0
50,0
100,0
Dose (µg/ml)

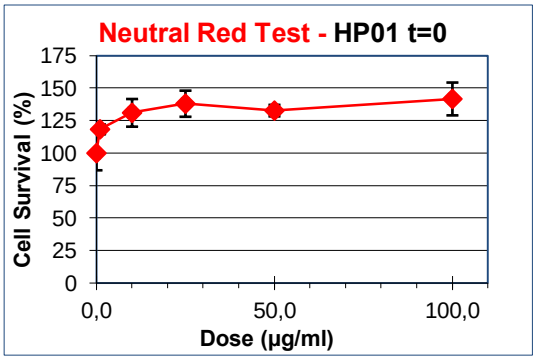
Neutral Red Test - HP01 t=0
Cell Survival (%)
175
150
125
100
75
50
25
0
0,0
50,0
100,0
Dose (µg/ml)

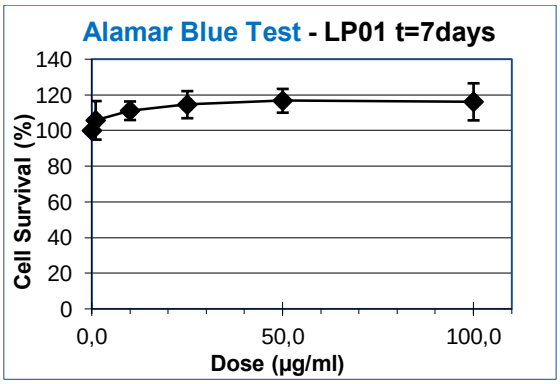
Alamar Blue Test - LP01 t=7days
Cell Survival (%)
140
120
100
80
60
40
20
0
0,0
50,0
100,0
Dose (µg/ml)

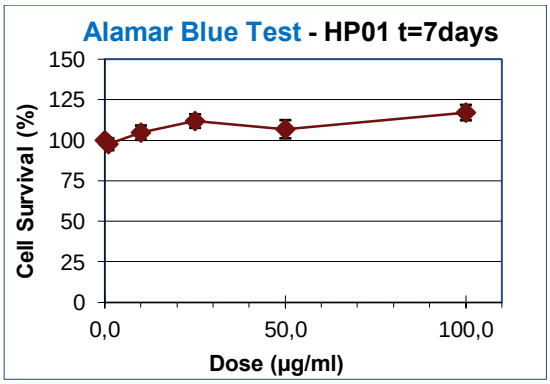
Alamar Blue Test - HP01 t=7days
Cell Survival (%)
150
125
100
75
50
25
0
0,0
50,0
100,0
Dose (µg/ml)

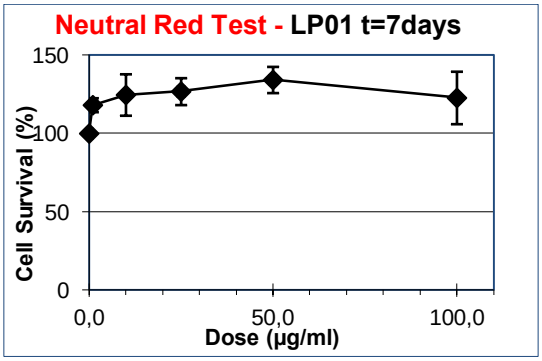
Neutral Red Test - LP01 t=7days
Cell Survival (%)
150
100
50
0
0,0
50,0
100,0
Dose (µg/ml)

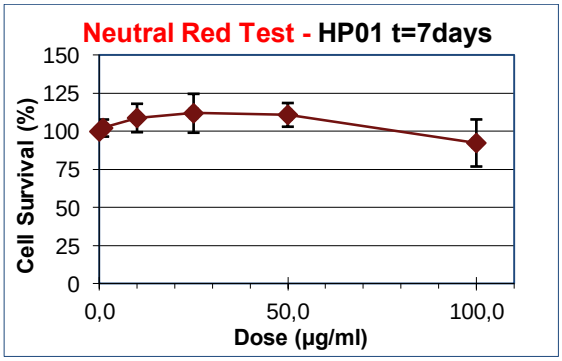
Neutral Red Test - HP01 t=7days
Cell Survival (%)
150
125
100
75
50
25
0
0,0
50,0
100,0
Dose (µg/ml)

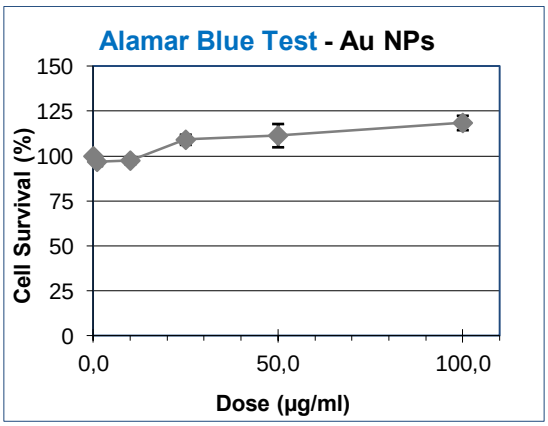
Alamar Blue Test - Au NPs
Cell Survival (%)
150
125
100
75
50
25
0
0,0
50,0
100,0
Dose (µg/ml)

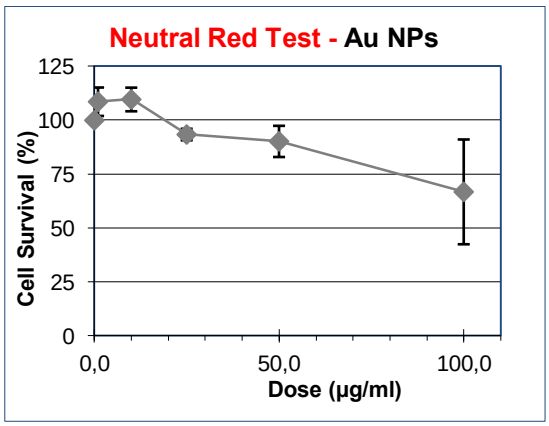
Neutral Red Test - Au NPs
Cell Survival (%)
125
100
75
50
25
0
0,0
50,0
100,0
Dose (µg/ml)

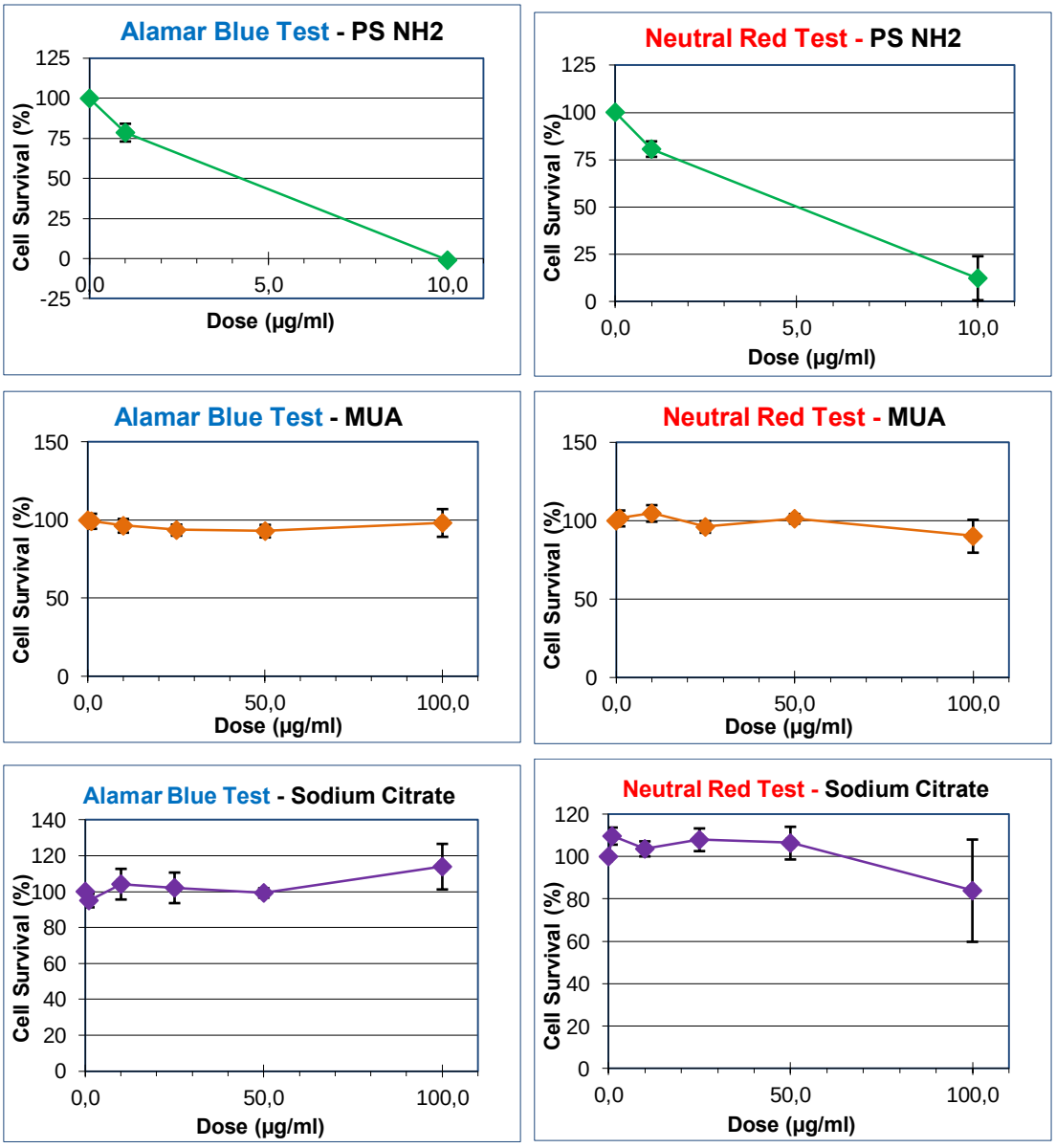

Figure 4.6.: Fluorescence Alamar Blue and Neutral Red assays of gold nanoparticles and MUA-conjugated gold nanoparticles (LP and HP types) at time zero and after 7 days of time evolution of conjugates. MUA and Sodium Citrate solutions were also tested as well as a positive control of PS-NH_2 NPs.

The presence of Lipopolysaccharides (LPS) was analyzed in order to determine a possible pro-inflammatory effect such as cytokine secreation due to the presence of endotoxin from bacteria contamination of samples (Figure 4.7.). However, no endotoxin was detected in any nanobioconjugate sample.

In the case of the study of LPS presence in gold nanoparticles, MUA and sodium citrate solutions; the absorbance values from endotoxins presence corresponded to less than 2.5 a.u. of LPS, being near zero in the case of gold nanoparticles. Absorbance values

obtained are: 0.245a.u. in gold nanoparticles, 1.537 a.u. in MUA solution and 2.176 a.u. in sodium citrate solution. These values correspond with the following doses of LPS present in samples: 0.009 ng/mL in gold nanoparticles, 0.062 ng/mL in MUA solution and 0.088 ng/mL in sodium citrate solution.

The equivalent doses for all samples explored are in a very low range that will not compromise cell viability. This could be analyzed while exploring the cell viability of THP-1 monocytes exposed to LPS by fluorescence methods such as Alamar Blue or Neutral Red Tests. Results indicated that there was not significant cytotoxic effect in the concentration range explored (up to 10µg/mL).

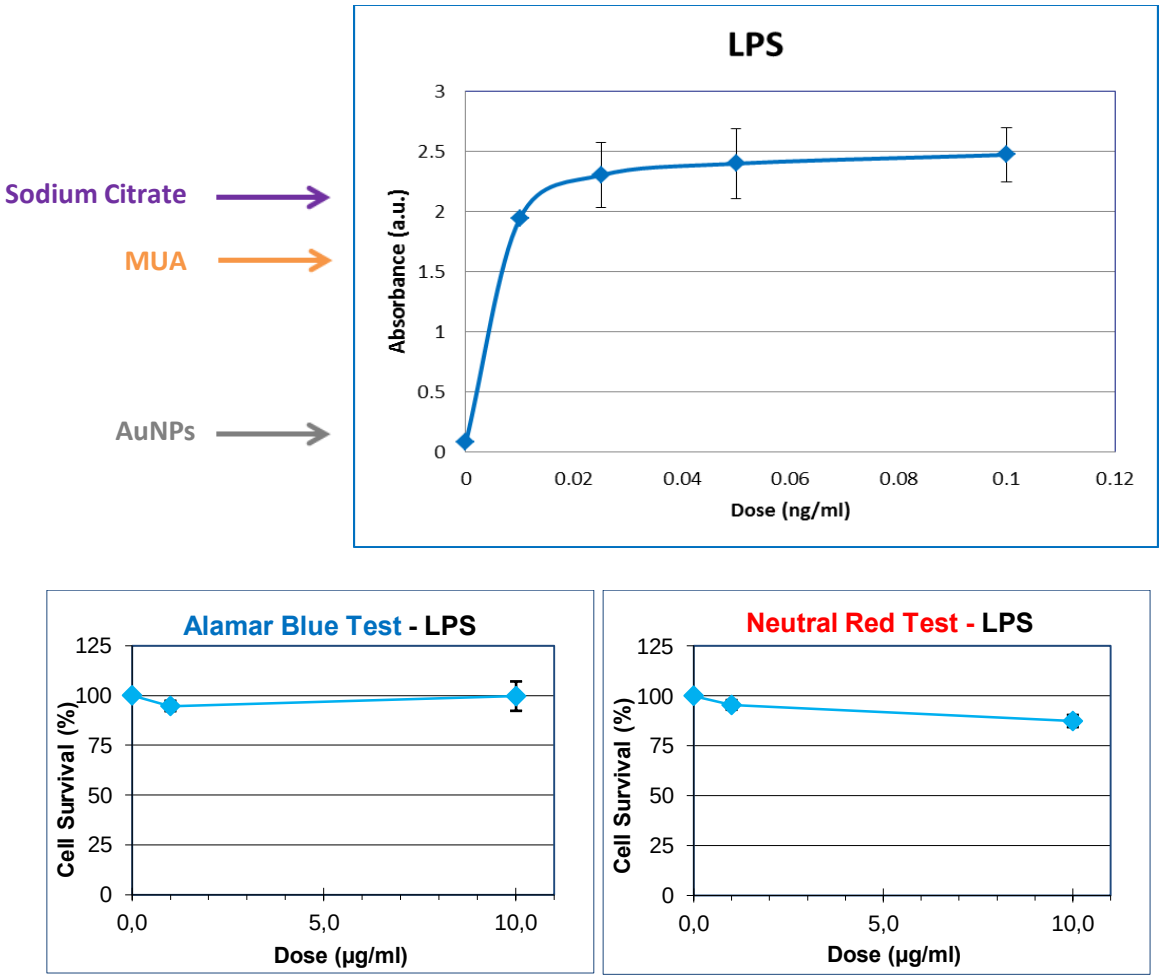

Figure 4.7.: Endotoxin analysis of samples and cell viability assessment in the presence of LPS by fluorescence methods (Alamar Blue and Neutral Red tests).

4.4. Cellular uptake and cytokine release

EXPERIMENTAL SECTION

Cellular uptake by transmission electron microscopy

The cellular uptake of the gold nanoparticles was assessed by Transmission Electron Microscopy (Jeol 1010 TEM). For this purpose, THP-1 cells were seeded in 12-well plates at a density of 5×10^5 cells/well one day before the exposure. After 24 hours of exposure, cells were collected by centrifugation for 5 minutes at 200G in microcentrifuge tubes (Eppendorf AG, Hamburg, Germany). Supernatant was discarded and pellet was resuspended in 2.5% glutaraldehyde (Sigma-Aldrich) in 0.1M Phosphate Buffer (PB, pH 7.4) which was freshly prepared from Sodium phospate monobasic dihydrate (Sigma-Aldrich - Ref: 71505) and Sodium phospate dibasic (Sigma-Aldrich – Ref: S5136).

Cells were fixed with glutaraldehyde in two steps for 1h and 30 min at 4°C and rinsed with PB (0.1M) for tree times. Cell material from culture plates was scraped and purified by tree cycles of centrifugation for 10 minutes at 200G rinsed with PB (0.1M). Then, samples were washed with milli-Q water four times for 10 minutes. And they were left in water overnight.

Then, dehydration of samples by the replacement of water with organic solvent (acetone) was done at room temperature under agitation following these steps: 50% acetone for 10 minutes, 70% of acetone for 10 minutes (2 times), 90% of acetone for 10 minutes (2 times), 96% of acetone for 10 minutes (3 times), 100% of acetone for 30 minutes and 15 minutes (2 times).

Afterwards, infiltration with embedding resin was carried out. EPON resin was prepared by mixing 23.5g of Eponate 12 (Glycerol polyglycidyl Ether), 12.5g of DDSA (Dodecenyl Succinic Anhydride, double distilled) and 14g of NMA (Nanic Methyl Anhydride) for few minutes following by addition of 0.37mL of DMP-30 (2,4,6-Tris (dimethylaminomethyl) phenol) and agitation for 1 hour. If generation of bubbles appears, resin should rest for 5 minutes at 60°C or outside heater until bubbles disappear. Infiltration of resin was done at RT under agitation following these steps:

1V/3V (resin/acetone) for 2 hours, 2V/2V for 1 hour, 3V/1V for 1 hour, EPON (without DMP-30) overnight (2 times) and EPON + DMP-30 for 2 hours 30 minutes. Generation of blocks of Epon 12 resin was done in BEEM capsules and polymerization at 60°C for 48 hours. Ultrafine cuts (~50nm) were carried out in order to prepare the samples for TEM. Samples were stained by uranyl acetate 2% for 20 minutes.

Cytokine release

The cytokine release was measured on the supernatant of the cells exposed to the different test solutions. Cell preparations and cell exposure were performed as previously described for the cytotoxicity assessment. After incubation of 24 hours, cells were pelleted and the supernatant was transferred to Eppendorf® LoBind tubes (Eppendorf AG) and stored at -20°C upon processing. The expression of TNF-α and IL-1β were measured using the Meso Scale Discovery multiplex Proinflammatory Panel 1 assay kit (Meso Scale Diagnostics, Rockville, USA) according to the manufacturers' guidelines and analyzed using a Meso Quick Plex SQ120 Instrument and Discovery Workbench® software (Meso Scale Diagnostics).

RESULTS AND DISCUSSION

Cytokines release was higher in nanobioconjugates than in the case of naked gold nanoparticles, which presents a similar signal to the non-treated THP-1 monocytes control (Figure 4.8.).

After time evolution, conjugates present higher cytokines release being much more evident in the case of LP type than in the case of conjugates HP type, which maintain almost similar before and after time evolution in the case of IL-1β secretion.

While analyzing TNF-α release at time zero, it can be observed that conjugates LP type generate less cytokine secretion than conjugates HP type. However, after 7 days of time evolution, conjugates LP type generate a higher cytokine TNF-α release than conjugates HP type (which present a similar cytokine release than at time zero).

In the other hand, while exploring IL-1β secretion, no significant differences between conjugates (LP and HP types) can be observed at time zero. However, as it happened in the case of TNF-α, after 7 days of time evolution conjugates LP type generate a higher

cytokine IL-1β release than conjugates HP type (which present again a similar cytokine release than at time zero).

Because of the analysis of cytokine release of THP-1 monocytes in the presence of MUA-conjugated gold nanoparticles, the evolution of conjugates through time can be explored. It can be concluded that LP conjugates evolve more than HP conjugates towards a different surface state that can produce a different cell response.

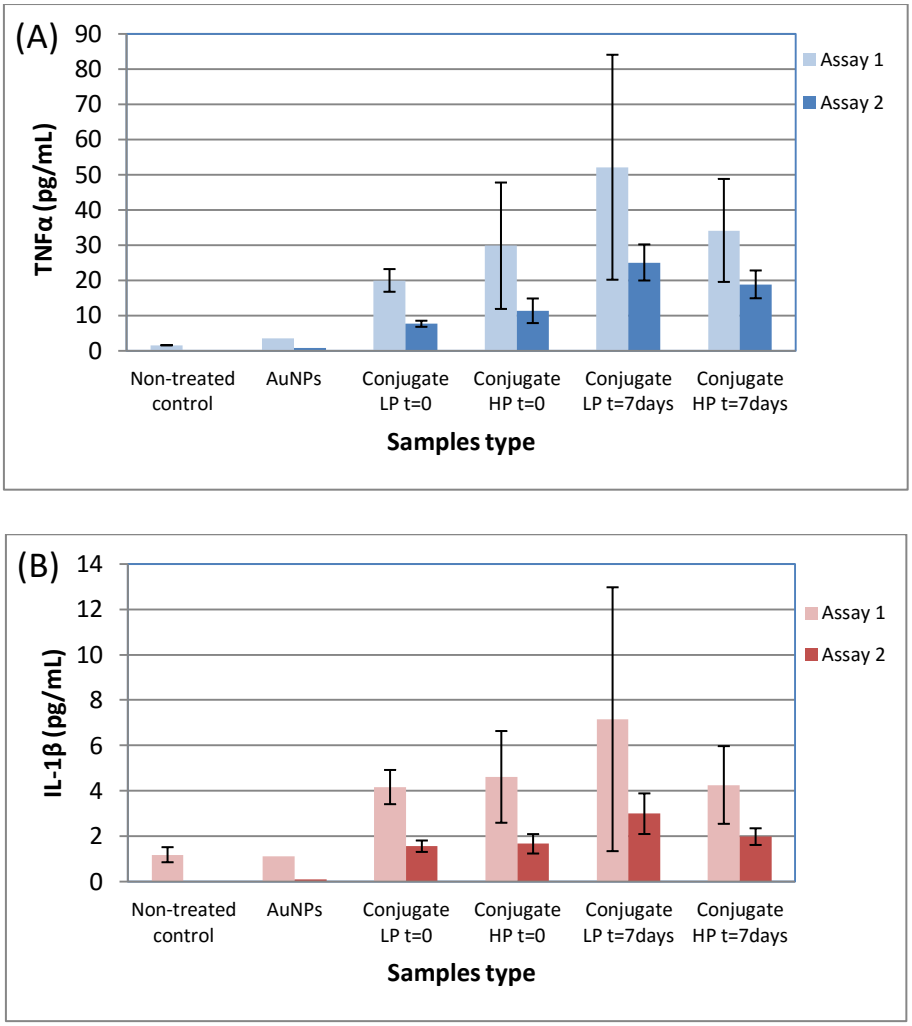

Figure 4.8.: Cytokines release assay. Levels of TNF-α **(A)** and IL-1β **(B)** secreted by THP-1 monocytes after 24 hours exposure to naked gold NPs (100µg/mL) and conjugates type LP and HP (100µg/mL) directly after preparation or after 7 days of ageing.

TEM analyses (Figure 4.9.) indicate that endocytosis of naked gold nanoparticles in monocytes was higher than in the case of nanobioconjugates. The uptake of MUA-conjugated gold nanoparticles is carried out by vesicles where nanoparticles seem to be less aggregates than in the case of bare gold nanoparticles.

It is not possible to elucidate significant differences between the internalization of conjugates in THP-1 monocytes by TEM images, neither depending on the conjugate type (LP or HP) nor due to the fresh or aged state, after 7 days of time evolution.

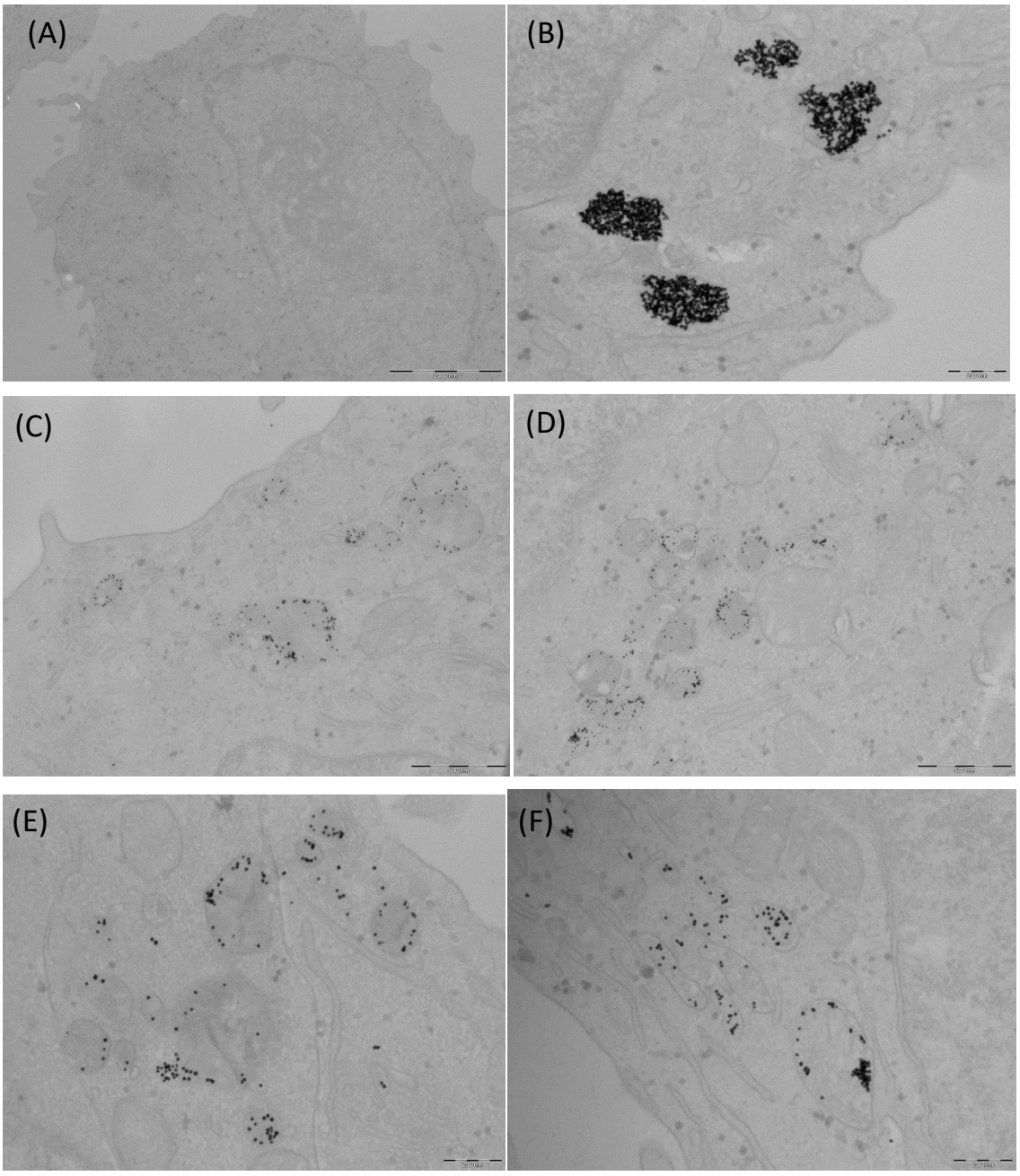

Figure 4.9.: Representative TEM images showing **(A)** untreated THP-1 monocytes, as well as cells after endocytosis of **(B)** naked gold NPs or MUA-conjugated gold NPs: **(C)** LP type and **(D)** HP type at time zero; **(E)** LP type and **(F)** HP type after 7 days of time evolution. Scale bars: (A) 2000nm; (B), (D) and (E) 200nm; (C) and (D) 500nm.

4.5. Proteomic analysis

EXPERIMENTAL SECTION

Protein corona formation

Naked and MUA-conjugated gold nanoparticles (LP and HP types at fresh and aged states) at 1g/L, were exposed to c-CCM for the Protein Corona (PC) formation. Ratios of exposure were 1:2 and 1:10 (NPs: c-CCM). Samples were incubated for 48 hours and purified by centrifugation for 20 minutes at 16100×G. Resuspension was done in phosphate buffer saline containing no Ca^{2+} or Mg^{2+} (PBS^-, Gibco).

Characterization

UV-Visible spectra were acquired with a Shimadzu UV-2400 spectrophotometer recording UV-Visible absorption spectra in the wavelength range of 300-800 nm. Dynamic light scattering (DLS) measures were made with a Malvern ZetaSizer Nano ZS instrument operating at a light source wavelength of 532 nm and a fixed scattering angle of 173°. ζ-Potential was determined using a Malvern ZetaSizer analyzer.

Differential centrifugal sedimentation (DCS) under a sucrose gradient with a serie of sucrose mixtures of sucrose 26% and 18% was done as well as Liquid Chromatography-Mass Spectrometry (LC-MS).

RESULTS AND DISCUSSION

A new batch of conjugated gold nanoparticles was generated for Protein Corona formation after incubation in complete cell culture medium for 2 days. Figure 4.10. represents the Protein corona of conjugates at time zero after conjugation. A higher red-shift is experienced after Protein Corona formation (ratio 1:2) onto LP conjugates than HP conjugates.

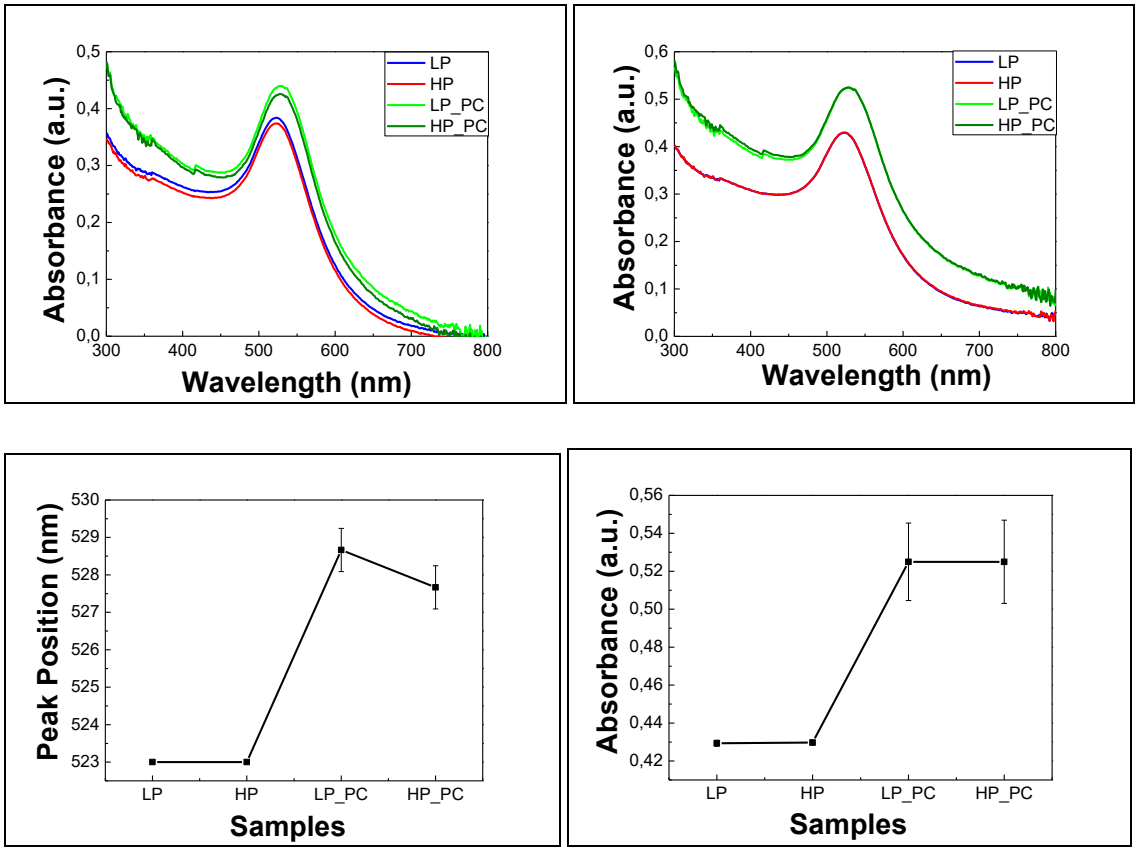

Figure 4.10.: UV-Vis spectra of the Protein Corona formation onto MUA-conjugated gold nanoparticles (LP and HP types) at time zero. Measurements are results of three replicas.

The Protein Corona formation was also analyzed by DLS and ζ-Potential (Figure 4.11). The increment in size after Protein Corona formation is 7nm higher in the case of HP conjugates than in the case of LP conjugates, presenting final sizes of 28nm and 21.24nm respectively.

Regarding surface charge, the LP conjugates evolve towards a less negative surface charge (-61mV) than HP conjugates (-56.7mV) after Protein Corona formation.

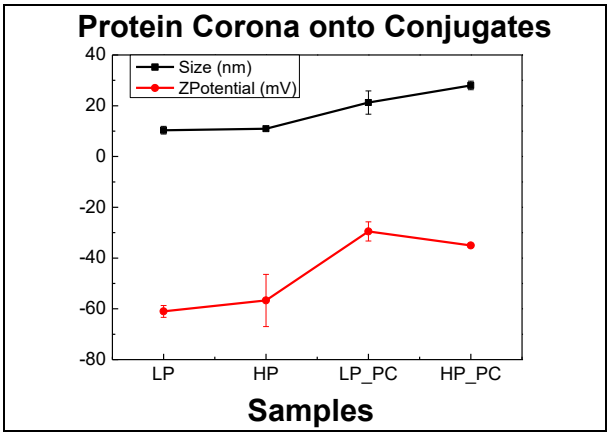

Figure 4.11.: DLS and ζ-Potential characterization of the Protein Corona formation onto MUA-conjugated gold nanoparticles (LP and HP types) at time zero. Measurements are results of three replicas.

The Protein Corona onto gold nanoparticles and conjugates could be detected through DCS characterization (Figure 4.12.). Gold nanoparticles increase 0.5nm after Protein Corona formation (10nm size by DCS) while conjugates at time zero present the same size (12nm). However, after 7 days of time evolution, a difference in size between LP and HP types can be observed. Protein Corona onto aged HP conjugates is 1nm higher than onto LP conjugates. More replicas are needed in order to determine if these differences in sizes after PC formation onto conjugates could be related with the conjugate type.

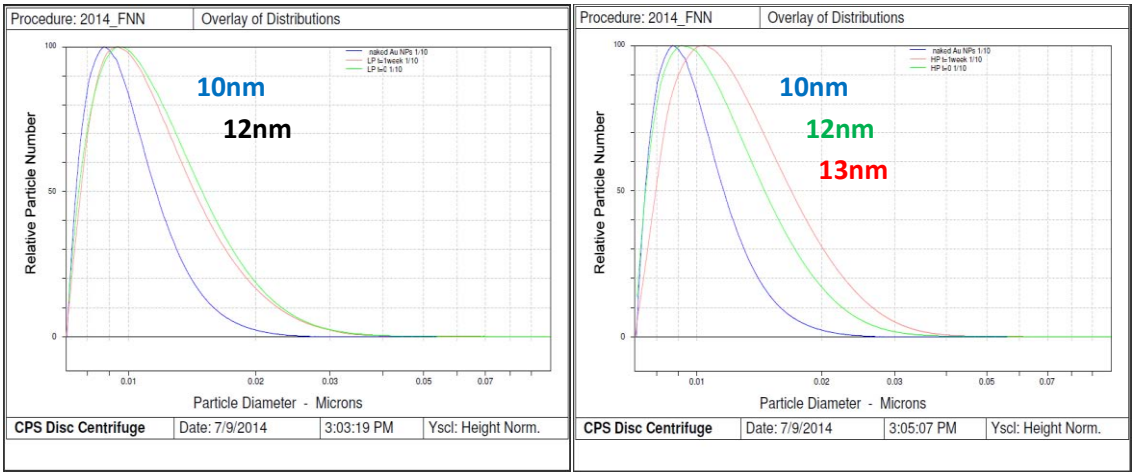

Figure 4.12.: DCS characterization of the Protein Corona formation (ratio 1:10) onto gold nanoparticles and MUA-conjugated gold nanoparticles (LP and HP types) at time zero and after 7 days of time evolution.

Samples were analyzed by Liquid Cromatography-Mass Spectroscopy (LC-MS) in order to determine the presence of peptides that could correspond to specific proteins. The analysis did not enable a quantitative determination of proteins, but a qualitative approach can be considered under a criterion of selection. It was established in determining the presence of proteins with score values >8 and number of peptides>1.

Under these considerations, the number of proteins that could be present in the corona of conjugates was higher (~60 proteins) than in the gold nanoparticles (48 proteins). As it can be observed in Figure 4.13., in the case of HP conjugates the number of proteins does not vary after aging of the sample. However, LP conjugates present an evolution in the number of proteins changing from 61 proteins, in the case of LP conjugates at time zero, to 59 proteins in the case of LP conjugates after time evolution. This could be in accordance with the higher evolution of LP conjugates through time, as it was previously described in Chapter 3.

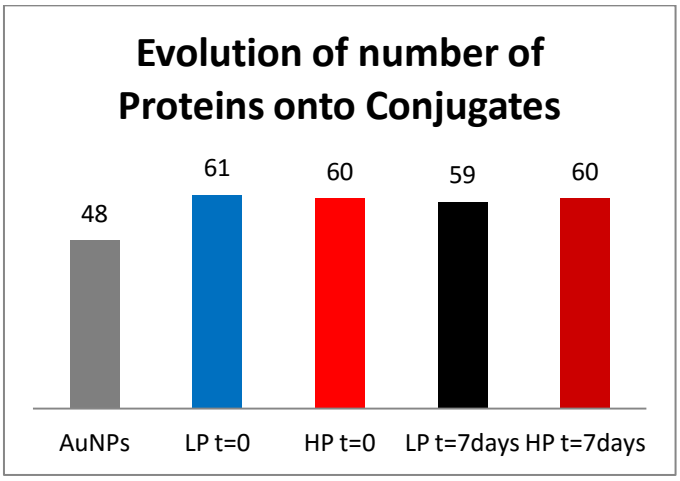

Figure 4.13.: Number of proteins determination by LC-MS analysis and evolution of proteins onto conjugates.

Moreover, it could be determined that the presence of some proteins like Thrombospondin-1 was higher in gold nanoparticles than in conjugates. The opposite occured in the case of Serum Albumin.

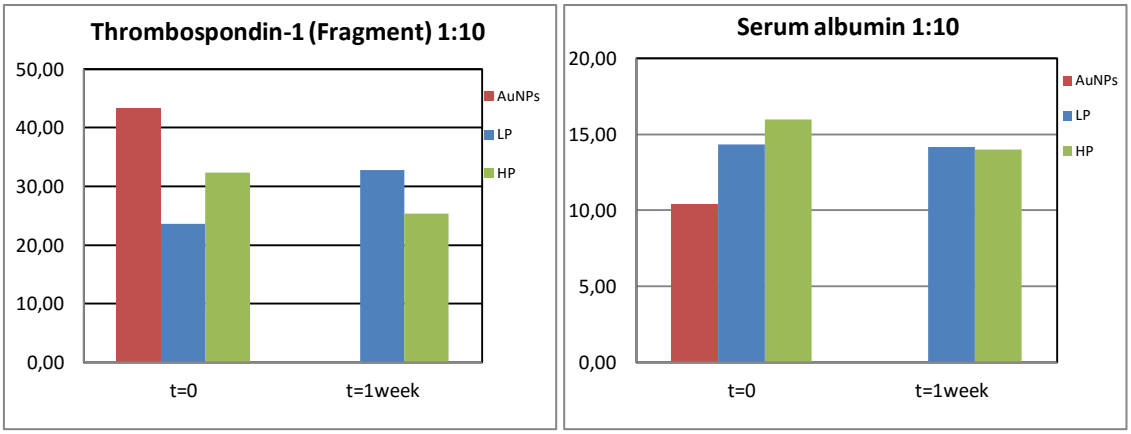

Figure 4.14.: Abundance of Thrombospondin-1 onto gold nanoparticles and conjugates at ratio 1:10 of Protein Corona formation.

Fingerprints analysis of proteins in relation to nanoparticles and conjugates as well as green-red maps that would indicate the presence or absence of proteins in the different samples, were analyzed but no congruent results were obtained. In order to better resolve the study, a deeper analysis is being carried out by the Proteomic Department of the Antwerp University in collaboration with the Flemish Institute for Technological Research (VITO).

4.6. Conclusions

Regarding the cellular uptake, the endocytosis of gold nanoparticles in monocytes was higher than in the case of conjugates.

No endotoxin was detected in any nanoparticle or conjugate sample. No cytotoxic effect was determined in monocytes.

Cytokines release was higher in nanobioconjugates than in the case of gold nanoparticles, and increased after time evolution of conjugates LP type, but not conjugates HP type.

After DCS characterization, it seems that Protein corona onto aged HP conjugates is higher than onto LP conjugates.

The presence of proteins, by LC-MS analysis, is higher in conjugates samples than in gold nanoparticles. LP conjugates evolve in the presence of proteins after aging, whereas HP conjugates no present variability.

Further detailed proteomic analysis is required in order to elucidate clear differences in Protein Corona between gold nanoparticles and conjugates, as well as between both conjugates (LP and HP) types.

4.7. References

1. M. A. Dobrovolskaia, S. E. McNeil, *Immunological properties of engineered nanomaterials Nature Nanotechnology* **2**, (2007).
2. J. Comenge, V. Puntes, Kinetically Controlled Seeded Growth Synthesis of Citrate-Stabilized Gold Nanoparticles of up to 200 nm: Size Focusing versus Ostwald Ripening. *Langmuir* **27** 11098–11105 (2011).
3. F. Wang *et al.*, Time resolved study of cell death mechanisms induced by amine-modified polystyrene nanoparticles. *Nanoscale* **5**, 10868-10876 (2013).

CHAPTER 5: ALTERED PROTEIN METABOLIZATION

CHAPTER 5: ALTERED PROTEIN METABOLIZATION

5.1. Introduction

Proteins are inherently flexible by virtue of the fact that the forces that hold together the tertiary structure are weak noncovalent forces. At physiological conditions, there is enough thermal energy available to cause weak interactions to break and reform these weak bonds. The motions that are the consequence of such rearrangements are essential for function such as ligand binding and catalysis[(1)].

The dynamics of proteins is of prime importance because the mobility of the protein is directly related with its functionality and accessibility of different ligands[(2)]. The functionality of biomolecules requires flexibility because all interactions usually involve rearrangements of atoms of molecular units.

A globular protein is a dynamic system capable of fluctuations around its average native state at level of both side chains and polypeptide backbone. The structure or mobility of proteins could be modified by being attached onto the nanoparticles. In this respect, limited proteolysis can provide important information about the dynamics of bound proteins.

In addition, protein activity is strongly dependent on the interaction with the environment. In fact, the function of proteins cannot be interpreted only on the basis of their static 3D structures[(3)] since the folded state of proteins has some characteristics of a crystal and some of an amorphous solid[(4)].

Proteins bound onto gold nanoparticles suffer dynamical restrictions that may implicate in its reactivity and function. Conformational distribution of proteins is known to be a key determinant of protein activity[(5)].

In this case, limited proteolysis provides a tool to quantify the grade of flexibility and the changes between free protein and bound protein. This technique uses different types of proteases to break specific peptide bonds depending on the amino acid

sequence of the protein. At short reactions times, only the most exposed sites will be cut by the protease but changes in the protein structure or changes in protein dynamics upon binding of nanoparticles can expose other sites and a different pattern may be obtained[6-7] .

Exposure is required characteristic of the cleavage site, but not sufficient to explain the specific proteolysis. Indeed, flexibility of the chain segment suffering proteolytic attack is the key parameter dictating limited proteolysis. In several studies it has been shown that there is a correlation between sites or regions of enhanced segmental mobility and sites of limited proteolysis[8-12].

In this study, trypsin was employed to partially digest BSA both in solution and adsorbed onto gold nanoparticles. Trypsin is a serine protease that cleaves on the C-terminal side of positively charged residues lysine and arginine, it is one of the most widely studied proteases and behaves as an endopeptidase because hydrolises peptide bonds of nonterminal aminoacids.

In order to visualize the fragments obtained from digestion, Sodium Dodecyl Sulfate-PolyAcrylamide Gel Electrophoresis (SDS-PAGE) was carried out. This technique determines relative molecular weights by electrophoresis. Polyacrylamide gels were employed for separation and it is used sodium dodecyl sulfate (SDS) for binding to the polypeptide chain in proportion to its relative molecular mass. SDS provides an overall negative charge resulting in a fragmentation according to size.

5.2. Bioconjugates generation

EXPERIMENTAL SECTION

Synthesis of gold nanoparticles

Monodisperse citrate-stabilized gold nanoparticles (Au NPs) with an uniform quasi-spherical shape of ~20 nm and a narrow size distribution were synthesized following a kinetically controlled seeded growth strategy via the reduction of $HAuCl_4$ by sodium citrate[(13)].

A solution of 2.2mM sodium citrate in milli-Q water (150 mL) was heated with a heating mantle in a 250mL three-necked round-bottomed flask for 15 min under vigorous stirring. A condenser was utilized to prevent the evaporation of the solvent. After boiling had commenced, 1 mL of $HAuCl_4$ (25 mM) was injected. The color of the solution changed from yellow to dark gray and then to red in 10 min. The resulting particles (~12 nm, ~$3 \cdot 10^{12}$ NPs/mL) are coated with negatively charged citrate ions and hence are well suspended in H_2O.

After generation of the Au seeds, nanoparticles are grown in the same vessel. For this purpose, the reaction was cooled until the temperature of the solution reached 90°C. Then, 1 mL of sodium citrate (60 mM) and 1 mL of a $HAuCl_4$ solution (25 mM) were sequentially injected. The nanoparticles size was controlled by the number of times these additions were performed. For the experiments, two additions were carried out in order to obtain ~20 nm gold nanoparticles (concentration 10^{12} NP/ml).

Protein Corona formation onto gold nanoparticles

Nanoparticles were conjugated to Bovine Serum Albumin (BSA) in order to generate a Protein Corona (PC) formation onto the nanoparticle surface via protein absorption. For the bioconjugation procedure, the number of albumins per nanoparticle were calculated using the following equation(*14*):

$$Nmax = 0.65\left[\frac{Rcomplex^3 - RAu^3}{Ralb^3}\right]$$

Where $R_{complex}$ is the radius of the bioconjugate; R_{Au} is the radius of the AuNP; R_{alb} is the radius of the BSA and 0.65 is the factor of hard spheres.

It was obtained 74 albumins/NP for a sphere of ~20 nm considering Ralb = 3 nm.

For the bioconjugates generation, an excess of 100x albumin was added to ensure a complete surface coverage and kept under stirring for 2 days. After that, bioconjugates were centrifuged twice (12000 rpm for 10 min) in order to remove unbound proteins and the Hard-Protein Corona nanoparticles were isolated.

RESULTS AND DISCUSSION

Highly monodisperse citrate-stabilized gold nanoparticles (Au NPs) with an uniform quasi-spherical shape of ~20 nm and a narrow size distribution were synthesized.

The gold nanoparticle generation was characterized by Transmission Electron Microscopy (TEM) and UV-Vis spectroscopy, as it can be seen in Figure 5.1.

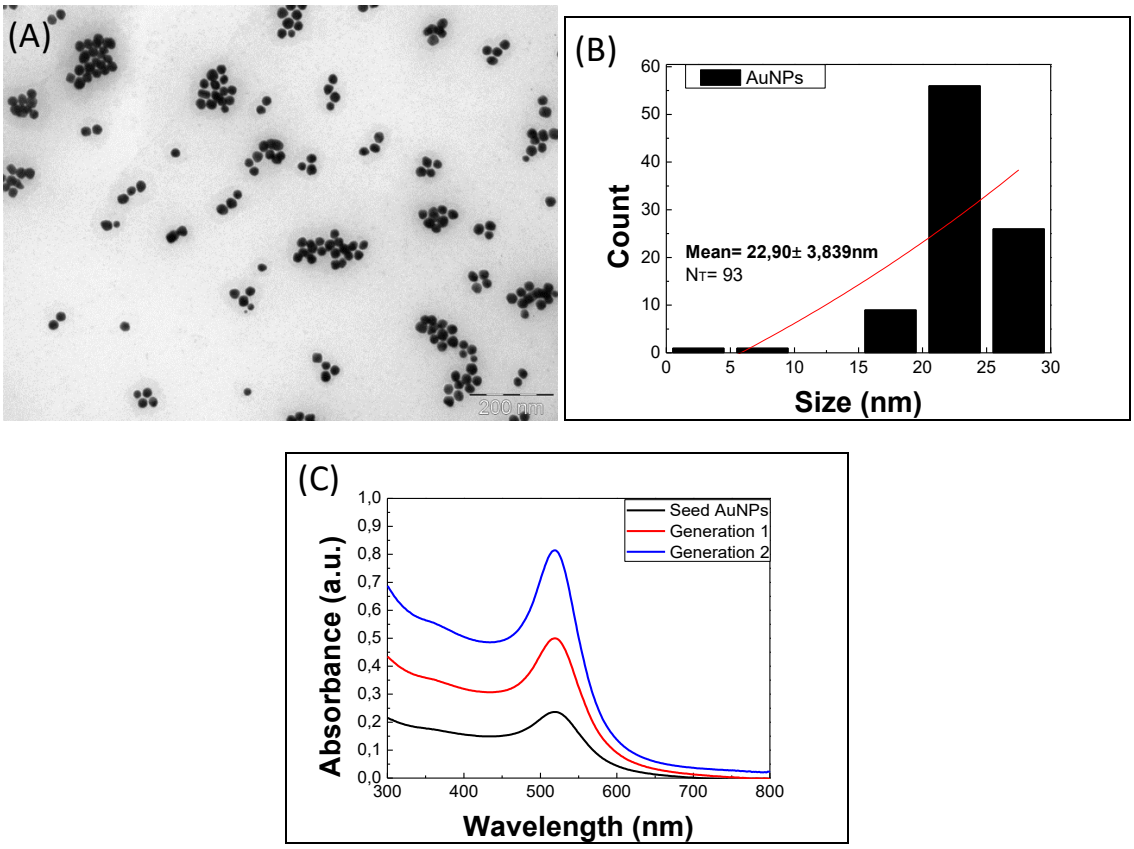

Figure 5.1.: **(A) TEM Characterization** of the formation of gold nanoparticles. **(B) Size distribution** of the gold nanoparticle synthesis and **(C) UV-Vis spectroscopy** characterization.

Nanoparticles were incubated with BSA for 2 days generating the Protein Corona via the absorption of proteins onto the gold nanoparticle surface. The bioconjugates (BSA-gold NPs) formation was characterized by UV-Vis spectroscopy and Zeta Potential (Figure 5.2.).

After Protein Corona formation, a red-shift of ~5nm was experienced in the UV-Vis spectra of bioconjugates and a decrease of negative charge in the ZetaPotential values from -48.5mV to -29.2mV. Both events, are indicatives the absorption of proteins onto gold nanoparticles surface.

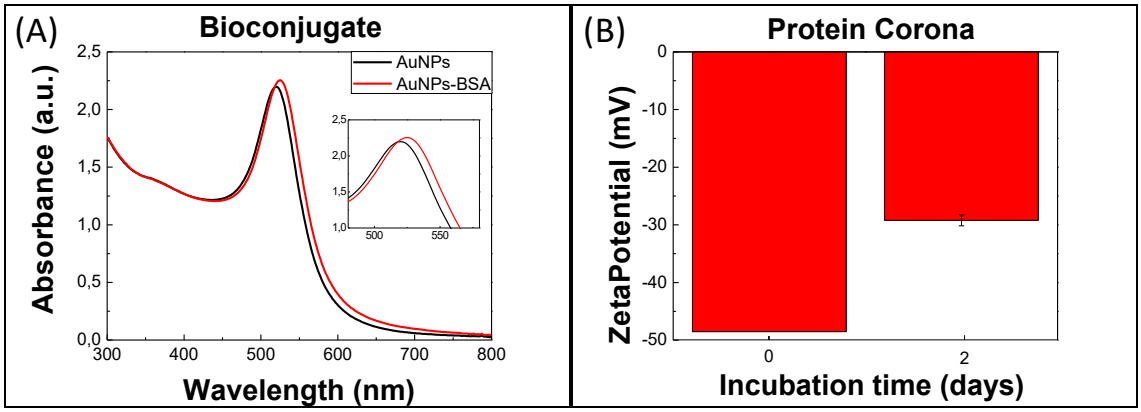

Figure 5.2.: **(A) UV-Vis spectroscopy** characterization and **(B) ZetaPotential** determination of the bioconjugate formation.

5.3. Protein metabolization

The metabolization of BSA protein by trypsin enzyme was explored. An analysis of the digestion of free proteins against the digestion of proteins while they are absorbed onto gold nanoparticles surfaces was carried out. Different protein residues after trypsinization are expected depending on the availability of proteins to be digested due to their conformational state.

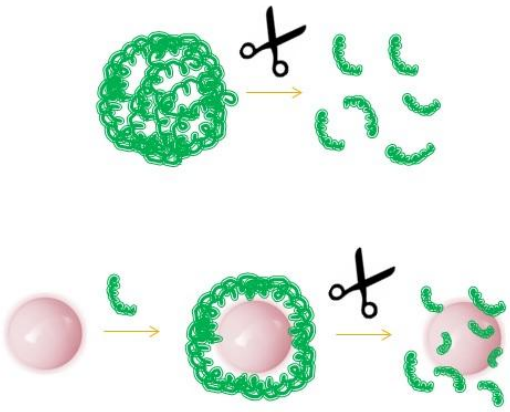

Image 1: Schematic picture of protein metabolization of free BSA protein or bioconjugates where BSA is absorbed onto gold nanoparticles surfaces.

EXPERIMENTAL SECTION

Gel electrophoresis preparation

Gel preparation for SDS-PAGE was done considering a stacking gel (4%) and a running gel (12.5%) containing PAA (Acrylamide / Bisacrylamide) at 40%; Tris buffer (1M, pH=8.8); Sodium Dodecyl Sulfate (SDS) at 10%; milli-Q water; (N, N, N', N'-tetramethylethylenediamine (TEMED) and Ammonium Persulfate (APS) at 10%. Addition of components was done for a final volume of 8mL.

Volumes for preparing the stacking gel (4%) were added in the following order and quantities: 0.8mL of PAA (40%); 1mL of Tris (1M, pH=8,8); 0.08mL of SDS (10%); 6.068mL milli-Q water; 0.012mL TEMED and 0.04mL of APS (10%).

Volumes for preparing the running gel (12,5%) were added in the following order and quantities: 2.5mL of PAA (40%); 3mL of Tris (1M, pH=8,8); 0.08mL of SDS (10%); 2.368mL milli-Q water; 0.012mL TEMED and 0.04mL of APS (10%).

For assembling the gel, isopropanol was added after the running gel into the glass plates in order to obtain a flat surface of the running gel polymerization which takes around 20 minutes. Afterwards, isopropanol is discarded and the stacking gel is added with the final comb to generate the pockets in the gel.

Running the gel

Pockets of the gel are filled with the sample and the loading buffer which is a non-reductive 6X buffer containing: 1.75mL of Tris-HCl (1M, pH=6.8); 0.5g of SDS; 1.5mL of glycerol; 0.6g of Bromophenol Blue and 1.75mL of milli-Q water.

This is a non-reducing buffer, the next step is addition of 20% of mercaptoethanol to break disulfide bonds between proteins. So the non-reducing buffer becomes a reducing buffer (5x).

The running buffer was created by mixing 100mL of TrisGlycine 10X and 10mL of SDS 10%, reaching a final volume of 1L with milli-Q water. Being previously prepared the 10X Tris-Glycine buffer by the combination of: 30.3g of Trizma base; 144.4g of Glycine and milli-Q water to 1L. The final running buffer gets into TrisGlycine 1X and SDS 0.1%.

The running of the gel is done at 20 mA and ~1h and 15minutes. Gel should be checked to detect when bromophenol blue goes out of the gel to stop the running.

Stain the gel

Once the running is done, the gel is taken out of the tank and washed with destilled water in order to remove the SDS. Then, the gel is submersed into 20mL of Instant Blue to be stained around 1hour until bands of the gel are clearly detected and subsequently wash with destilled water.

Digestion of free Bovine Serum Albumin

First of all, conditions for free albumin digestion by trypsin enzyme should be explored. For this purpose, the ratio enzyme:protein was adjusted maintaining the time of reaction constant. Afterwards, the digestion time was also explored by fixing the enzyme:protein ratio estimated to be the most favorable for digestion.

Free albumin (BSA) mass was fixed to 2µg BSA. The ratio enzyme:protein (w:w) varied in the following: 1:1000 (2ng of trypsin 2µg of BSA); 1:500 (4ng of trypsin 2µg of BSA); 1:200 (10ng of trypsin 2µg of BSA); 1:100 (20ng of trypsin 2µg of BSA); 1:50 (40ng of trypsin 2µg of BSA); 1:20 (100ng of trypsin 2µg of BSA).

The conditions used were 1µg/2µg of BSA in each gel pocket depending on the gel, being the limit of the detection in the gel 100ng in mass. An excess of mass should be needed since protein will be fragmented.

A stock of BSA 1mg/ml and another one of trypsin 100µg/ml which was dissolved in HCl (1mM, pH=3) to prevent autolysis (storage buffer). Aliquots were put in the freezer being used a new one for each experiment. The final volume of the sample was 15µl for 1mm spacer gel.

Trypsin has an optimal operating pH≈ 8 and a temperature≈ 37°C. So the operating buffer used in samples was ammonium bicarbonate NH_4HCO_3 (pH≈ 8; 50mM) for the trypsin acts. Ammonium bicarbonate should be freshly prepared for each use.

After preparation, samples were put in a bath (37°C) for 1 hour. In order to stop the digestive reaction, 1µl of HCl (1M) was added. Subsequently, loading buffer was added containing bromophenol blue which is an pH indicator. In case, samples change pH turning yellow colour, 2µl of Tris (1M ph=8.8) can be added. Samples were heated at 95°C for 5 min. Afterwards pockets of the gel were filled and the gel was run.

Digestion of immobilized Bovine Serum Albumin

The concentration of albumin in the bioconjugates while forming the Protein Corona, is only known theoretically. For this reason, an experiment was performed to accurately

determine the quantity of bioconjugates that should be put in each pocket for enabling the trypsinization and the comparison wih free BSA.

Bioconjugates were prepared by centrifugation of 1ml of bioconjugates ($1.9x10^{12}$ NP/ml and 74 alb/NP) two times and resuspension of the pellet in 15µl of Sodium Citrate (2.2 mM). From these 15µl, 5µl that experimentally correspond to 1µg of BSA are taken. This experimental value was obtained by comparing intensities of bands through ImageJ program.

Bioconjugates digestion was compared to the free BSA digestion at the same enzyme:protein ratio. The procedure is the following: BSA (1mg/ml) and trypsin (100µg/ml). Final volume of the sample 15µl.

Sample	Trypsin (µl)	Bioconjugates (µl) (0.2mg/ml)	BSA (µl) (1mg/ml)	Ammonium bicarbonate (µl)
1	1µl (diluted ½)	5µl	x	9µl
2	1µl	5µl	x	9 µl
3	2µl	5µl	x	8 µl
4	x	5µl	x	10 µl
5	x	x	1µl	14 µl
6	1µl (diluted ½)	x	1µl	13 µl
7	1µl	x	1µl	13 µl
8	2µl	x	1µl	12 µl

Table 1: conditions for comparison between digestion of free BSA and digestion of bioconjugates.

In order to study the digestion of bioconjugates and free BSA, the following samples were compared: Sample 1 and 6; 2 and 7; 3 and 8. Samples 4 and 5 are the control with only bioconjugates and only BSA respectively.

Samples 6, 7 and 8 contained 1µg of BSA in with different ratios of trypsin:

Sample 6: Ratio 1:20 →1µg BSA (1µl of stock 1mg/ml) 20 times less of trypsin (1µl of stock trypsin 100µg/ml diluted to the half in 1 mM of HCl pH=3).

Sample 7: Ratio 1:10→1 µg BSA (1µl of stock 1mg/ml). 10 times less of trypsin (1µl of non-diluted stock trypsin 100µg/ml).

Sample 8: Ratio 1:5→1 µg BSA (1µl of stock 1mg/ml). 5 times less of trypsin (2µl of non-diluted stock trypsin 100µg/ml).

RESULTS AND DISCUSSION

Digestion of free Bovine Serum Albumin

Exploring ratio enzyme protein

Trypsinization of BSA in ratio 1:20 was carried out by addition of this combined products: 1µl trypsin (100µg/ml) + 2µl BSA (1mg/ml) + Ammonium bicarbonate (50mM) up to 15 µl.

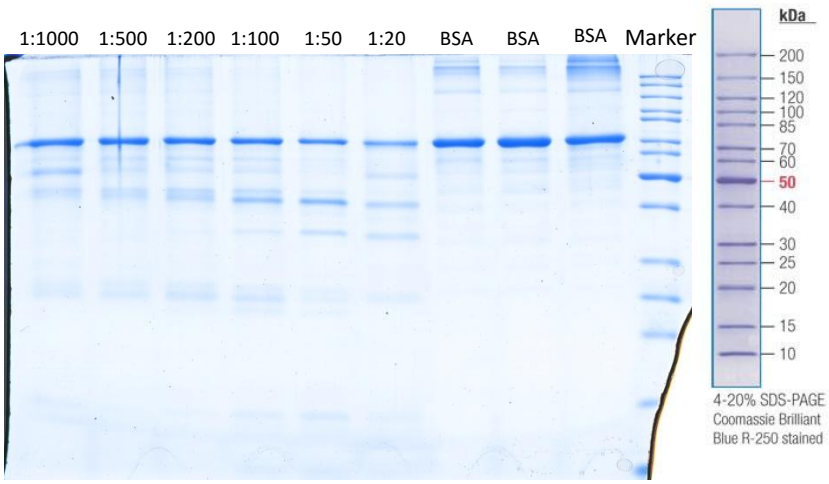

Figure 5.3.: Electrophoresis gel containing the following information in each lane: Lane 1 ratio 1:1000; Lane 2 ratio 1:500; Lane 3 ratio 1:200; Lane 4 ratio 1:100; Lane 5 ratio 1:50; Lane 6 ratio 1:20; Lane 7, 8 and 9 different types of BSA. Lane 10 marker.

As it can be observed in Figure 5.3., the ratio that contributed for the generation of more digestion bands of protein is the ratio 1:20. So it was determined to be the best enzyme:protein ratio to carry out experiments.

Exploring digestion time

Digestion time was explored by fixing the enzyme:protein ratio at 1:20.

Trypsinization conditions were the same as the previous experiment of ratio 1:20, combining: 1µl trypsin (100µg/ml) + 2µl BSA stock (1mg/ml) + Ammonium bicarbonate (50mM) to 15 µl.

The explored digestion times were 1 hour, 2 hours, 4 hours, 6 hours, and 24 hour of incubation in the bath.

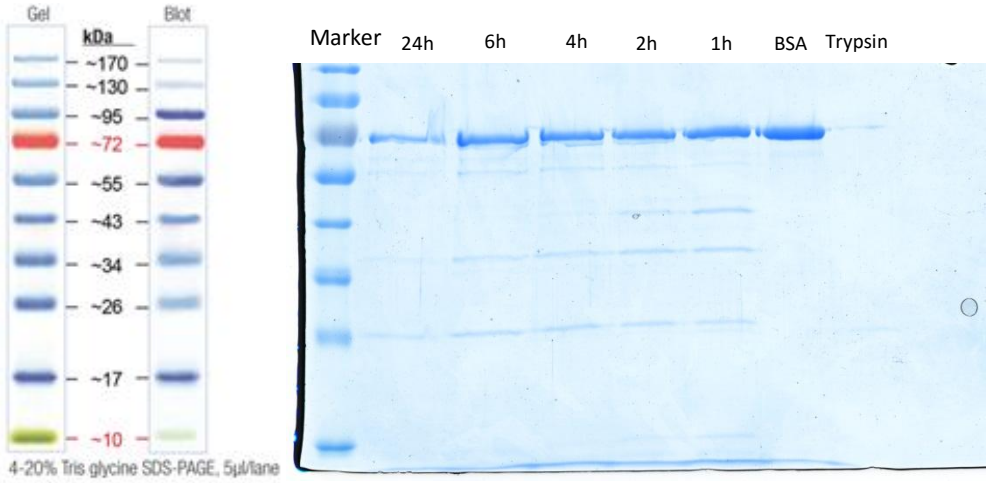

Figure 5.4.: Electrophoresis gel containing the following information in each lane: Lane 1 marker; Lane 2 (24h); Lane 3 (6h); Lane 4 (4h); Lane 5 (2h) Lane 6 (1h); Lane 7 BSA; Lane 8 trypsin.

As it can be observed in Figure 5.4., the best digestion time condition is 1 hour (Lane 6) where more well-defined digestion bands appear.

Digestion of immobilized Bovine Serum Albumin

Bioconjugates digestion was compared to the free BSA digestion at the same enzyme:protein ratio.

For estimation the quantity of BSA, ImageJ program was used. This program “read” the bands in the picture and transforms the intensity of the bands into different peaks. The

area of the peak is proportional to the quantity of protein. For this purpose, a known concentration of protein was put in one lane and arbitrary quantity of bioconjugates in another lane. The areas of the peaks of these two lanes were compared. By division of both areas, the ratio between the known concentration and the unknown can be obtained. By ImageJ analysis, it can be observed that 5µl of bioconjugates are approximately 1µg of BSA.

As it was previously described in the Experimental Section, 8 types of samples were prepared for Electrophoresis gel. Results of digestion by trypsin can be seen in the following Figure 5.5.

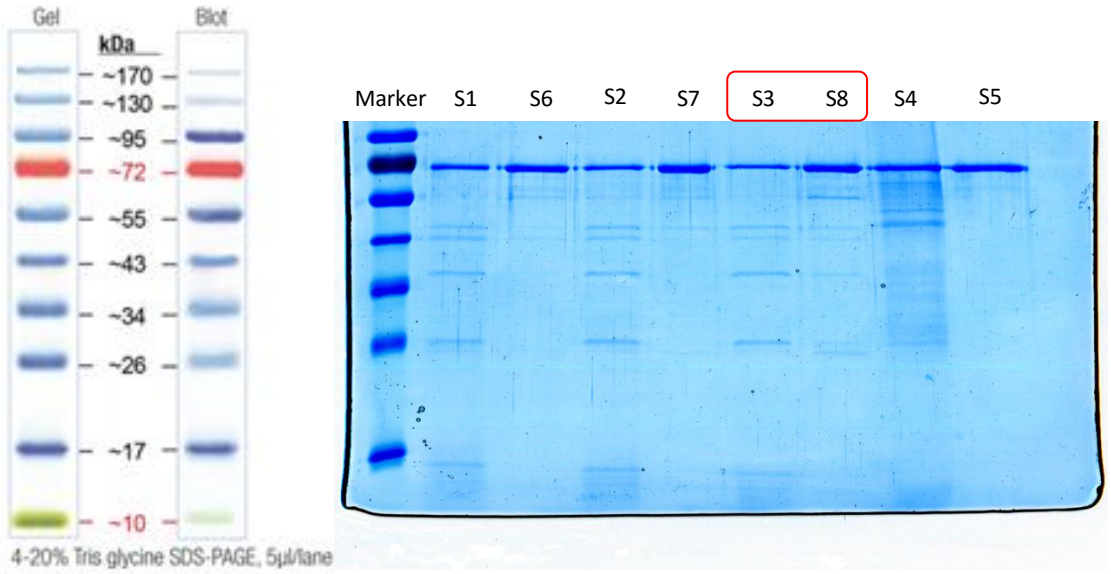

Figure 5.5.: Electrophoresis gel containing the following information in each lane: Lane 1 marker, Lane 2 Sample 1 (Bioconjugates + trypsin 1:20); Lane 3 Sample 6 (Free BSA + trypsin 1:20); Lane 4 Sample 2 (Bioconjugates + trypsin 1:10); Lane 5 Sample 7 (Free BSA + trypsin 1:10); Lane 6 Sample 3 (Bioconjugates + trypsin 1:5); Lane 7 Sample 8 (Free BSA + trypsin 1:5); Lane 8 Sample 4 (Bioconjugates without trypsin); Lane 9 Sample 5 (Free BSA without trypsin).

A different pattern can be clearly observed in Figure 5.5. between Lane 6 and Lane 7, corresponding to Sample 3 (bioconjugates) and Sample 8 (free BSA) respectively at conditions of ratio 1:5.

The main difference can be seen in Lane 7 where it appears two new bands between 55 and 72 KDa and another one under 26 KDa in the case of the free BSA digestion that does not appear in the case of bioconjugates digestion in Lane 6.

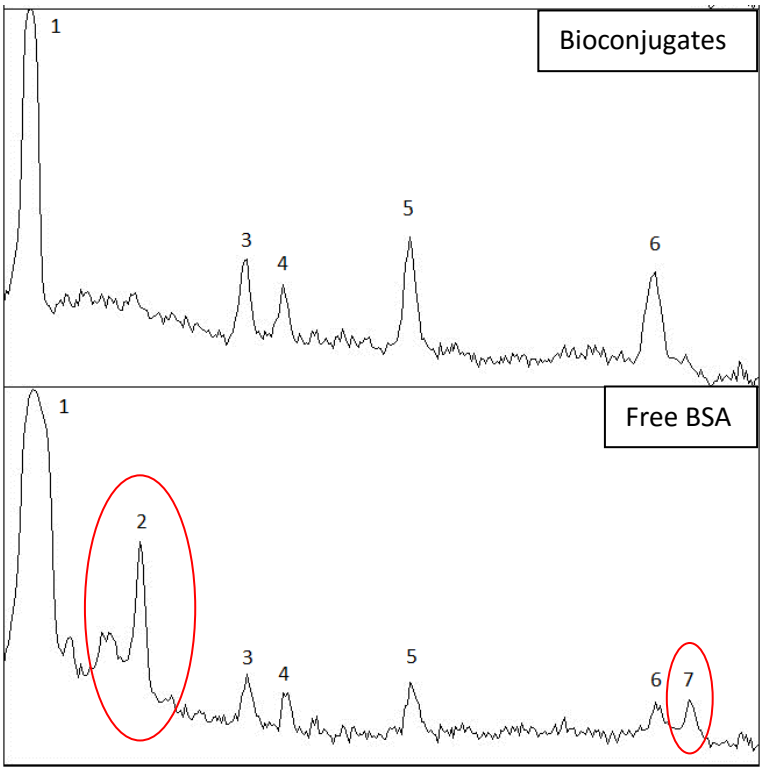

Figure 5.6.: Spectra from Lane 6 (bioconjugates + trypsin 1:5) and Lane 7 (free BSA + trypsin 1:5) of electrophoresis gel shown at Figure 5.5. In the case of free BSA, two new peaks (2 and 7) appeared in the spectra. These peaks corresponded with electrophoresis bands of free BSA trypsinization that do not appear in the case of bioconjugate digestion. Differences in peaks (1, 5 and 6) intensities can be also observed due to different BSA digestion mechanisms of trypsin against free BSA or bioconjugates.

The conformational state of BSA protein, either free or absorbed onto gold nanoparticles surface generating the Protein Corona of bioconjugates, can be determined as critical in the trypsinization procedure.

As it can be observed in Figure 5.6., the protein digestion of BSA at ratio 1:5 (enzyme:protein) generate different patterns depending on the state of BSA (free or bioconjugated to gold nanoparticles). When BSA is free, the protein is more susceptible to be digested by trypsin than when BSA is attached onto gold nanoparticle surfaces in bioconjugates. This can be a consecuence of a decrease of exposed regions to trypsin digestion in the case of bioconjugates, where BSA conformation is modified because of their absorbed state onto gold nanoparticles. Consequently, less fragments are generated after trypsinization in the case of bioconjugates than in the case of free BSA where more digestion events can occur.

5.4. Exploring the secondary protein corona

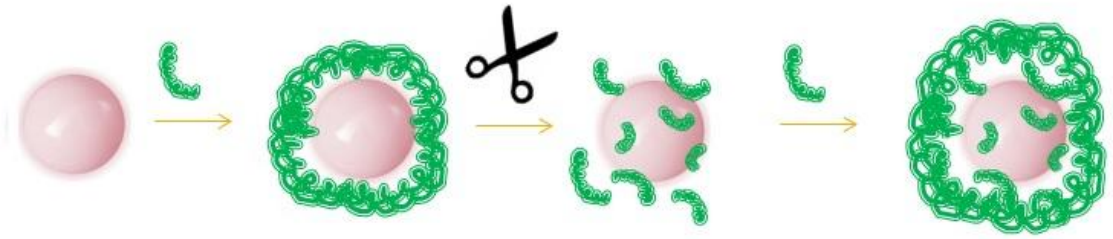

Image 2: Schematic picture of protein metabolization of bioconjugates where BSA is absorbed onto gold nanoparticles surfaces and the subsequently Protein Corona formation onto the BSA-digested bioconjugates.

The conformation of proteins has been seen to be critical for digestion. BSA absorbed onto gold nanoparticles surface forming the Protein Corona, are seen to present less regions susceptible for tryosinization.

Bioconjugates can be further studied after trypsinization, where residues from BSA digestion can remain onto gold nanoparticles surfaces. These conditions can be explored by generating a secondary Protein Corona onto already trypsinized bioconjugates, as Image 2 illustrates.

EXPERIMENTAL SECTION

Highly monodisperse citrate-stabilized gold nanoparticles (Au NPs) of ~20 nm were incubated with BSA for 2days under stirring conditions. Bioconjugates were purified by centrifugation (12000 rpm for 10 min) in order to remove the excess of proteins that were not attached to gold nanoparticles surfaces. Samples were subsequently resuspended in ammonium bicarbonate (50mM) to proceed with the trypsinization.

Afterwards, trypsinization was carried out in ratio 1:5 (enzyme:protein) by addition of 30 µl of trypsin (100µg/ml) to 1mL of bioconjugate (containing 15.18µg BSA/ml). Digestion was done for 1h, 6h and 24h at 37°C in the bath.

After digestion of bioconjugates took place, samples were purified by 2 cycles of centrifugation (12000 rpm for 10 min) and resuspended in Sodium Citrate (2.2mM).

Finally, these already trypsinized bioconjugates were incubated with BSA for 2 days under stirring and subsequently purified by centrifugation (12000 rpm for 10 min), creating a secondary Protein Corona onto the fragmentation from BSA digestion in order to study indirectly the result of trypsinization.

RESULTS AND DISCUSSION

The secondary Protein Corona formation onto bioconjugates previously trypsinizated, can be characterizaed by UV-Vis spectroscopy (Figure 5.7.). After the first Protein Corona formation, a red-shift (5nm) of the peak position in SPR spectra is observed as well as an increase in absorbance. After trypsinization of the first Protein Corona, a blue-shift of 1nm was experienced in the SPR spectra. This indicates that not all the protein attached onto the nanoparticles was removed since the bioconjugates did not recovered the original naked nanoparticle state.

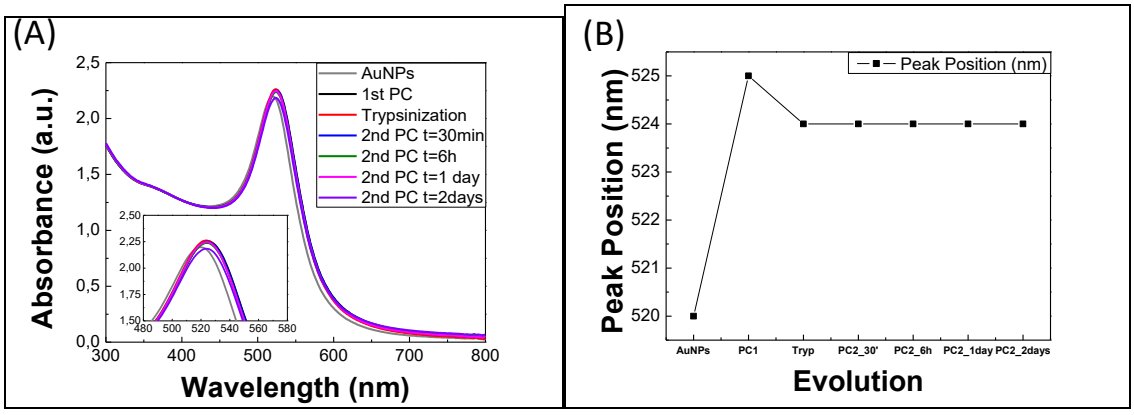

Figure 5.7.: **UV-Vis spectroscopy and Peak Position** characterization of secondary Protein Corona onto trypsinizated bioconjugates.

Additionally, the secondary Protein Corona can be explored by UV-Vis spectroscopy, where no changes in peak position were detected after secondary Protein Corona formation onto trypsinized bioconjugates. SPR spectra maintained a constant peak position at 542nm.

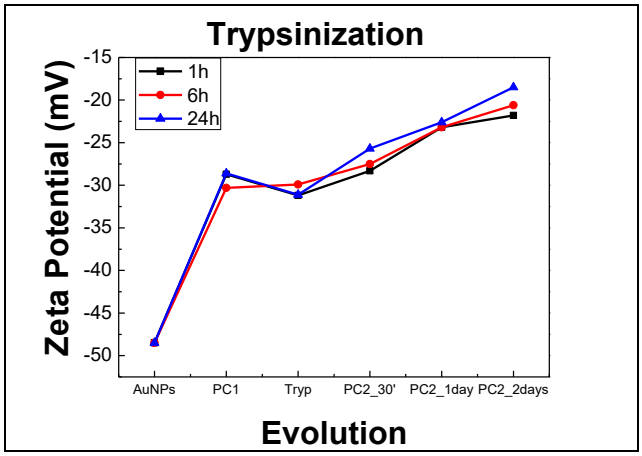

Figure 5.8.: **Zeta-Potential** characterization of secondary Protein Corona onto trypsinizated bioconjugates. Trypsinization was carried out at different time: 1h, 6h and 24h.

Analyzing bioconjugates by Zeta-Potential characterization (Figure 5.8.) it can be observed how the nanoparticles experienced a decrease of ~20mV (from -48.5mV to -28.7mV) in the negative surface charge after the first Protein Corona formation.

Once bioconjugates are trypsinizated, an increase of the negative surface charge of around 2.5mV is experienced reaching a Zeta-Potential value of -31.2mV. However, the original Zeta-Potential value of naked nanoaprticles (-48.5mV) is not reached any more. It can be concluded that the Protein Corona get less dense after trypsinization due to the increase in negative charge, but bioconjugates do not recovered the original naked state.

As a consequence, the secondary Protein Corona should be formed over fragments of BSA of the first Protein Corona that were not possible to digest by trypsinization. Three different trypsinization times were carried out in order to analyze if prolonged digestion times could revert the first Protein Corona. However, contrary as what it was expected, it was not reached at all. As it also happened in the digestion of free BSA, where increasing time not better trypsinization was obtained.

The subsequently secondary Protein Corona was generated onto the not completely trypsinizated surface of bioconjugates. A decrese in the negative charge of bioconjugates was observed from 30 minutes to 2 days of BSA incubation.

Improvements were not identified while increasing the time of trypsinization for the recovering of the first Protein Corona. However, in the case of Secondary Protein Corona, some influence of the trypsinization time was observed. At 2 days of protein incubation for the generation of secondary Protein Corona, surface charges changed reaching Zeta Potential values of -21.8mV, -20.6mV and -18.5mV depending on the trypsinization time (1h, 6h or 24h, respectively). Less negative charge is an indicative of more protein absorbed onto bioconjugates surfaces generating the Protein Corona. Consequently, it can be concluded that the non-observable effects of increasing trypsinization time can be determined through an indirect analysis by the creation of a secondary Protein Corona that would provide information of the surface state in which they are getting absorbed.

5.5. Conclusions

Protein metabolization is extremely determined by the state in which proteins are presented, either free proteins or proteins adsorbed onto nanoparticle surfaces generating the Protein Corona.

In the later case, proteins will provide a more static conformation than non-attached protein states, where some residues of the macromolecule will be adsorbed onto the nanoparticle surfaces and will not be exposed to possible enzyme degradation being protected from digestion.

Additionally, the recover of Protein Corona by trypsinization is challenging since naked nanoparticle was not identified to obtain after digestion where some fragments of proteins maintained attached to the nanoparticles surfaces.

The secondary Protein Corona was observed to be a very sensitive method for studying nanoparticle surface states after trypsinization, being able to detect differences in bioconjugates not detectable by standard characterization techniques.

5.6. References

1. J. R. E. T. Pineda, R. Callender, S. D. Schwartz, Ligand binding and protein dynamics in lactate dehydrogenase. *Biophys J* **93**, 1474-1483 (2007).
2. P. J. Steinbach *et al.*, Ligand-Binding to Heme-Proteins - Connection between Dynamics and Function. *Biochemistry-Us* **30**, 3988-4001 (1991).
3. A. Fontana *et al.*, Probing protein structure by limited proteolysis. *Acta Biochim Pol* **51**, 299-321 (2004).
4. Y. Wang, G. Zocchi, Viscoelastic Transition and Yield Strain of the Folded Protein. *Plos One* **6**, (2011).
5. D. M. Ming, M. E. Wall, Interactions in native binding sites cause a large change in protein dynamics. *J Mol Biol* **358**, 213-223 (2006).
6. R. Cukalevski *et al.*, Structural Changes in Apolipoproteins Bound to Nanoparticles. *Langmuir* **27**, 14360-14369 (2011).
7. M. Lundqvist *et al.*, Proteolytic cleavage reveals interaction patterns between silica nanoparticles and two variants of human carbonic anhydrase. *Langmuir* **21**, 11903-11906 (2005).
8. C. J. Tsai, P. P. de Laureto, A. Fontana, R. Nussinov, Comparison of protein fragments identified by limited proteolysis and by computational cutting of proteins. *Protein Sci* **11**, 1753-1770 (2002).
9. A. Fontana *et al.*, Correlation between Sites of Limited Proteolysis and Segmental Mobility in Thermolysin. *Biochemistry-Us* **25**, 1847-1851 (1986).
10. A. Fontana, P. P. Delaureto, V. Defilippis, Molecular Aspects of Proteolysis of Globular-Proteins. *Stud Org Chem* **47**, 101-110 (1993).
11. A. Fontana, P. P. deLaureto, V. DeFilippis, E. Scaramella, M. Zambonin, Probing the partly folded states of proteins by limited proteolysis. *Fold Des* **2**, R17-R26 (1997).
12. P. P. De Laureto *et al.*, Limited proteolysis of bovine alpha-lactalbumin: Isolation and characterization of protein domains. *Protein Sci* **8**, 2290-2303 (1999).
13. J. Comenge, V. Puntes, Kinetically Controlled Seeded Growth Synthesis of Citrate-Stabilized Gold Nanoparticles of up to 200 nm: Size Focusing versus Ostwald Ripening. *Langmuir* **27** 11098–11105 (2011).
14. L. Calzolai, F. Franchini, D. Gilliland, F. Rossi, Protein-Nanoparticle Interaction: Identification of the Ubiquitin-Gold Nanoparticle Interaction Site. *Nano Lett* **10**, 3101-3105 (2010).

Anex I: Electrophoresis gel anaylisis

Analysis of the eletrophoresis gel, previously shown in Figure 5.5., that includes bands at fixed molecular weights. Comparison between bioconjugates and BSA digestion can be correlated at different ratios of enzyme:protein.

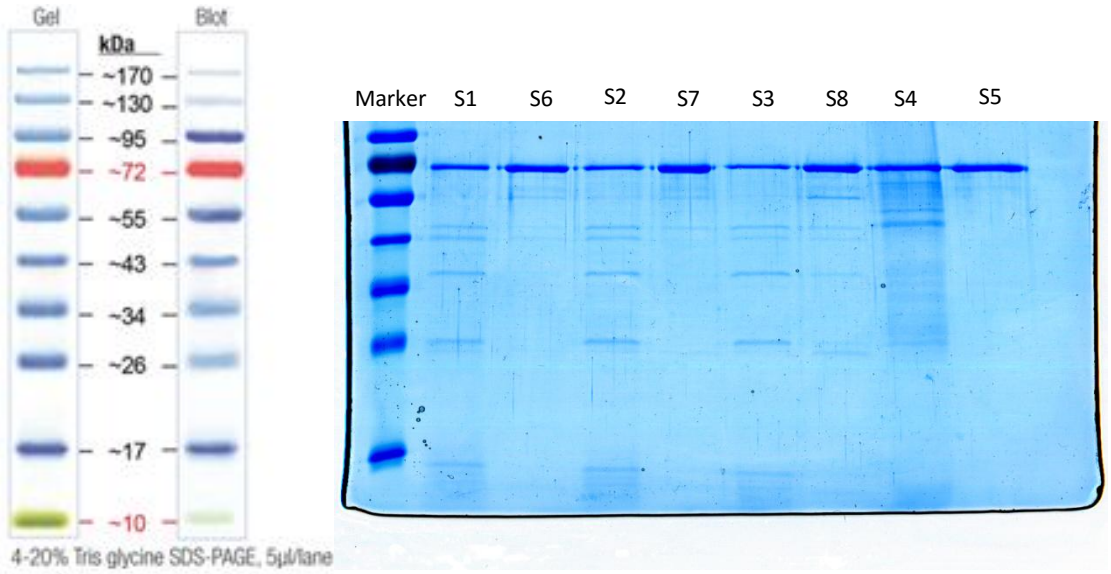

Figure 5.9.: Electrophoresis gel containing the following information in each lane: Lane 1 marker, Lane 2 Sample 1 (Bioconjugates + trypsin 1:20); Lane 3 Sample 6 (Free BSA + trypsin 1:20); Lane 4 Sample 2 (Bioconjugates + trypsin 1:10); Lane 5 Sample 7 (Free BSA + trypsin 1:10); Lane 6 Sample 3 (Bioconjugates + trypsin 1:5); Lane 7 Sample 8 (Free BSA + trypsin 1:5); Lane 8 Sample 4 (Bioconjugates without trypsin); Lane 9 Sample 5 (Free BSA without trypsin).

Spectra analysis of each Lane of the electrophoresis gel is shown in Figure 5.10 and Figure 5.11. where all the ratios of enzyme:protein tested (1:20, 1:10 and 1:5) have been analyzed. Ratio 1:5 was determined to be the best one for BSA digestion (presenting the highest number of peaks) and suitable for comparison with Bioconjugates trypsinization.

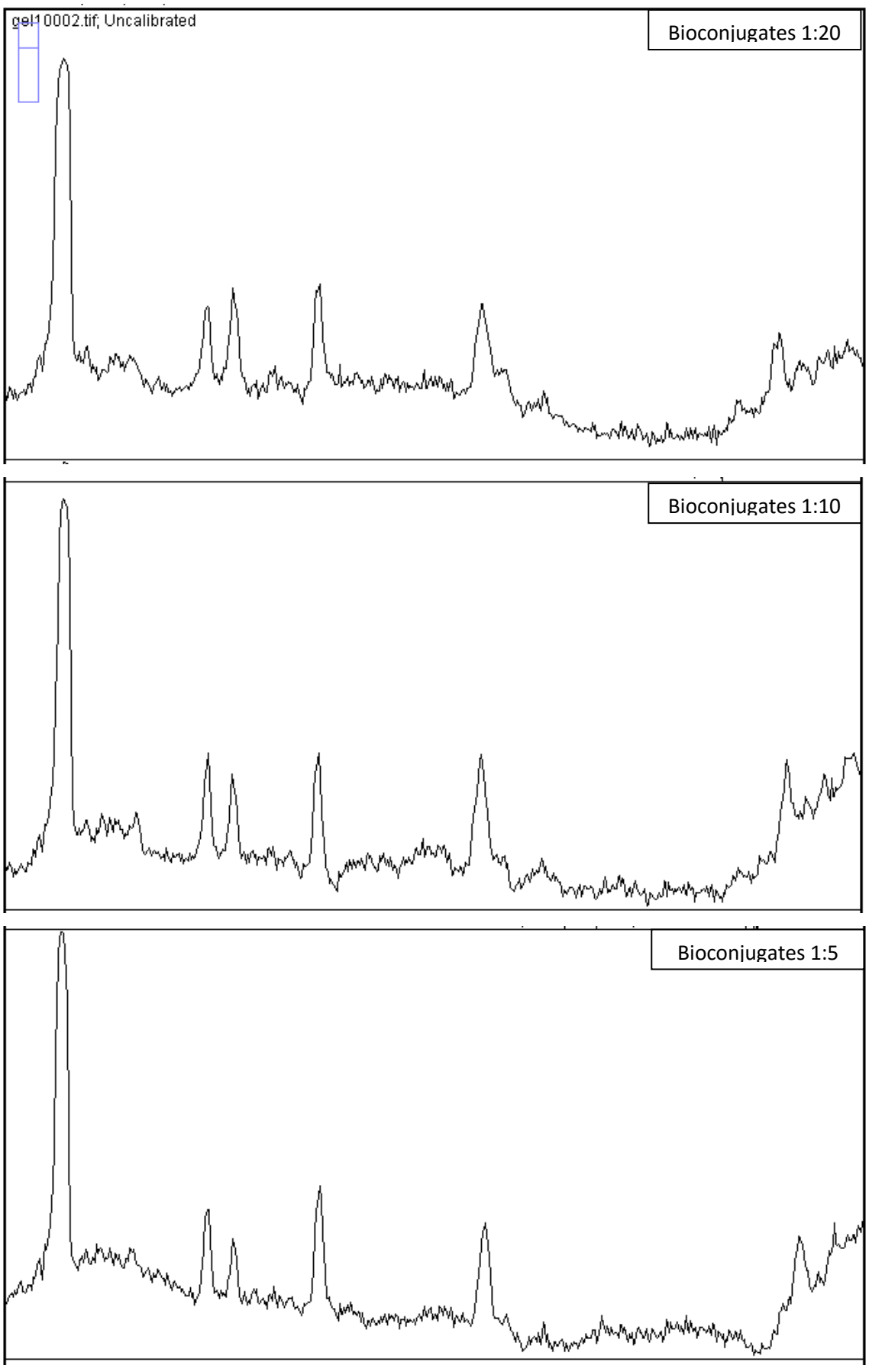

Figure 5.10.: Spectra from Sample 1, 2 and 3 that correspond to Bioconjugates at ratios of enzyme:protein 1:20, 1:10 and 1:5 respectively.

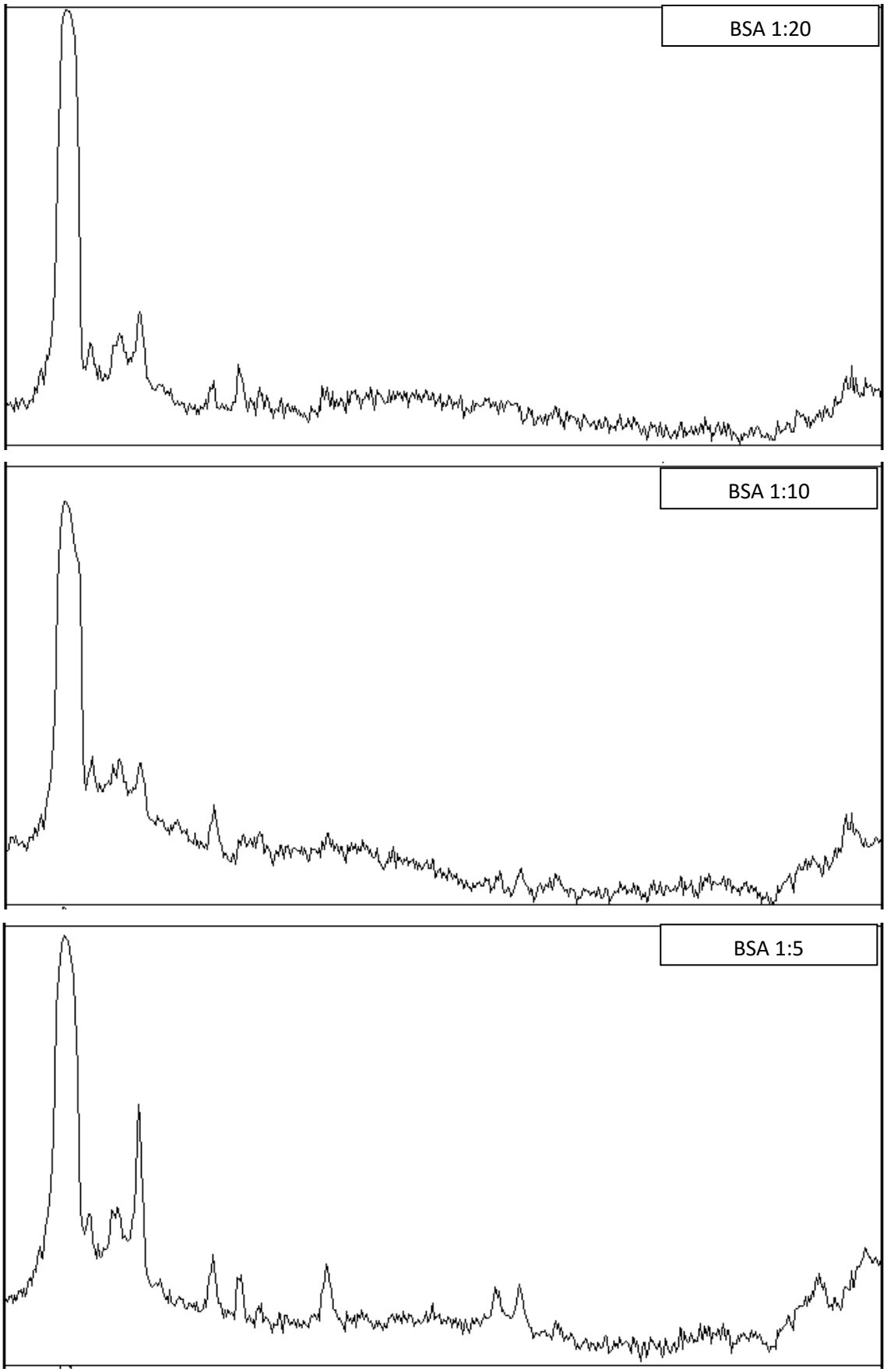

Figure 5.11.: Spectra from Sample 6, 7 and 8 that correspond to BSA at ratios os enzyme:protein 1:20, 1:10 and 1:5 respectively.

Sample 4 and 5 corresponding to Bioconjugates and BSA without trypsin were also analyzed. As it can be observed in the following spectras in Figure 5.12., both samples present peaks that correspond to electrophoresis gel bands.

In the case of sample 5, the band corresponds to the proper BSA protein. However, in the case of sample 4, an increased number of bands appear. These bands, that are usually associated to protein digestion, cannot be attributed to trypsinization of bioconjugates since sample 4 was not exposed to trypsin. For this reason, one can infer that observed peaks can correspond to possible protein fragmentation while preparing the sample for electrophoresis gel as a consequence of nanoparticle-protein interaction.

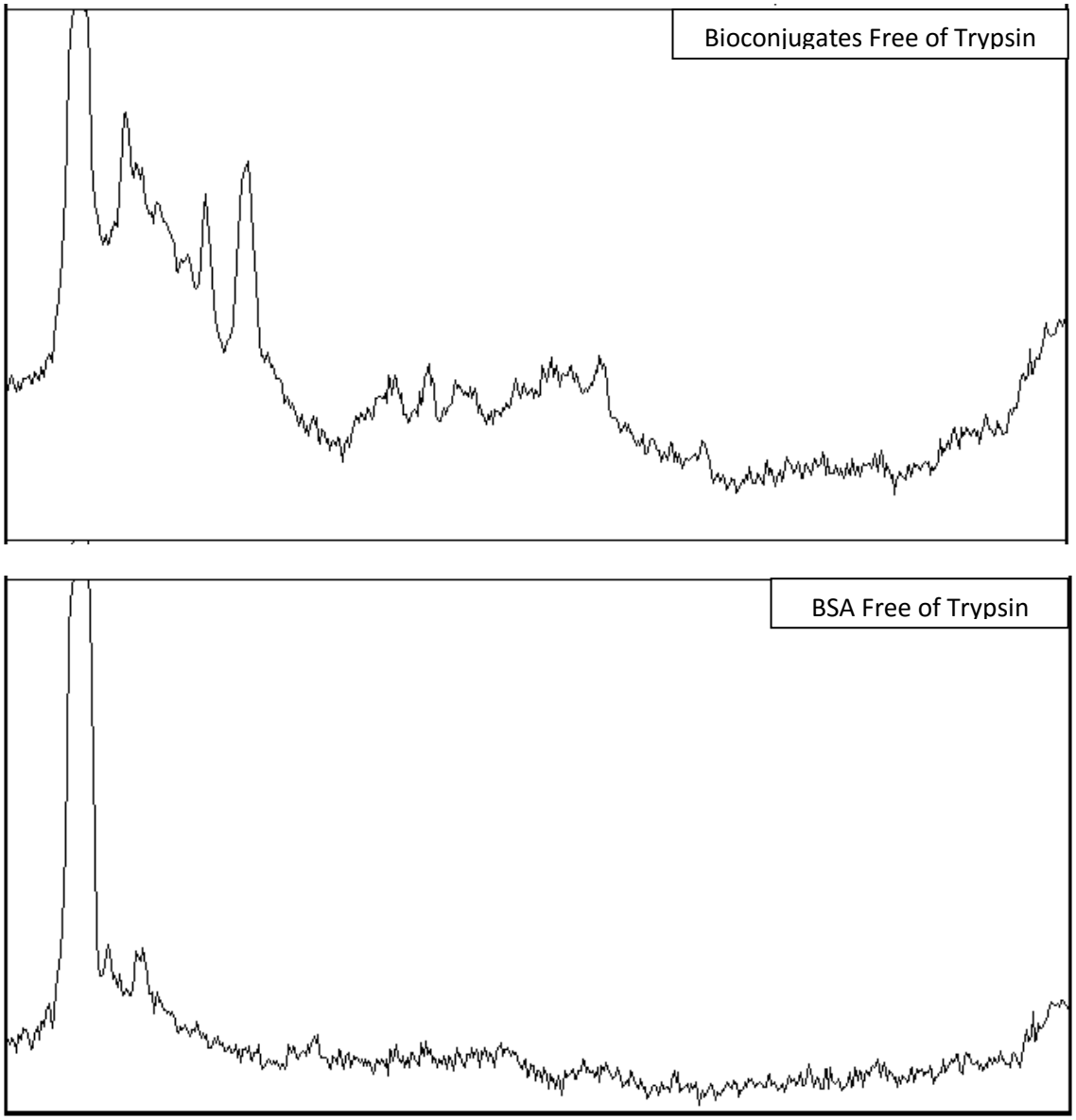

Figure 5.12.: Spectra from Sample 4 and 5 that correspond to Bioconjugates and BSA free of trypsin.

CHAPTER 6: CONCLUSIONS

CHAPTER 6: CONCLUSIONS

The gold nanoparticles synthesis inside cytoplasm was achieved by the exposure of gold precursors to HeLa cells. Once the gold precursors have internalized into the cells, they can be reduced by the internal biological environment.

Through the analysis of gold nanoparticles inside cells, different localizations of nanoparticles were observed: inside cytoplasm, inside vesicles and outside cells. These locations suggest a secretory pathway of gold nanoparticles in HeLa cells. Gold precursor's doses affect cell viability.

The composition, size and morphology of the nanoparticles generated inside cells could be determined by high resolution microscopy techniques, such as HR-TEM, ADF-STEM, EDX and SAED.

The generation of gold nanoparticles under incubation in complete cell culture medium conditions was also explored. Morphology of the resultant gold nanoparticles was characterized to be different from the one formed in cells.

The mixture of gold precursors has been tested in order to evaluate their competition in the formation of gold nanoparticles. The ratio of the precursors in the mixture was observed to be determinant in the size and aggregation state of the obtained gold nanoparticles.

The functionalization of gold nanoparticles was explored through two different methods of conjugation, in which the order of admixture between gold nanoparticles and molecules solutions determined the final conjugate state.

The time evolution of conjugates was tested in excess of molecules solution. Conjugates seem to evolve towards similar conjugation states after molecular rearrangements.

The coverage of molecules and peptides onto the gold nanoparticle surfaces was explored by reactive characterization of conjugates against aggregation, corrosion and protein corona formation.

The cellular uptake of gold nanoparticles in monocytes was different from the functionalized ones. It was observed that the time evolution of conjugates has a certain influence in cell response by the cytokine release.

Metabolization of proteins was observed to be determined by the conformational state in which proteins are present: free or adsorbed onto gold nanoparticles surfaces. Proteins have been seen to be less susceptible to digestion when they are attached onto gold nanoparticles generation the Protein Corona.

LIST OF ABBREVIATIONS

Au NPs: Gold Nanoparticles

c-CCM: Complete Cell Culture Media

DCS: Differential Centrifugal Sedimentation

DLS: Dynamic Light Scattering

DMEM: Dulbecco's Modified Eagle Medium

EDX: Energy-Dispersive X-ray Spectroscopy

FBS: Fetal Bovine Serum

FESEM: Field Emission Scanning Electron Microscopy

$HAuCl_4$: Gold(III) chloride trihydrate

HAADF: High-Angle Annular Dark Field

HeLa: Human Cervical Adenocarcinoma epithelial cells

HP: High Pressure

IL-1β: Interleukin 1beta

LP: Low Pressure

MEM: Minimum Essential Medium Eagle

MUA: 11-Mercaptoundecanoic acid

NaCl: Sodium Chloride

NaCN: Sodium Cyanide

PB: Phosphate Buffer

PC: Protein Corona

ROS: Reactive Oxygen Species

SEM: Scanning Electron Microscope

SERS: Surface-Enhanced Raman Spectroscopy

SPR: Surface Plasmon Resonance

STEM: Scanning Transmission Electron Microscope

TEM: Transmission Electron Microscope

ThioAu: Sodium Aurothioamalate Hydrate

TNFα: Tumor Necrosis Factor alpha

UV-Vis: UV-Visible

Z-Potential: Zeta-Potential